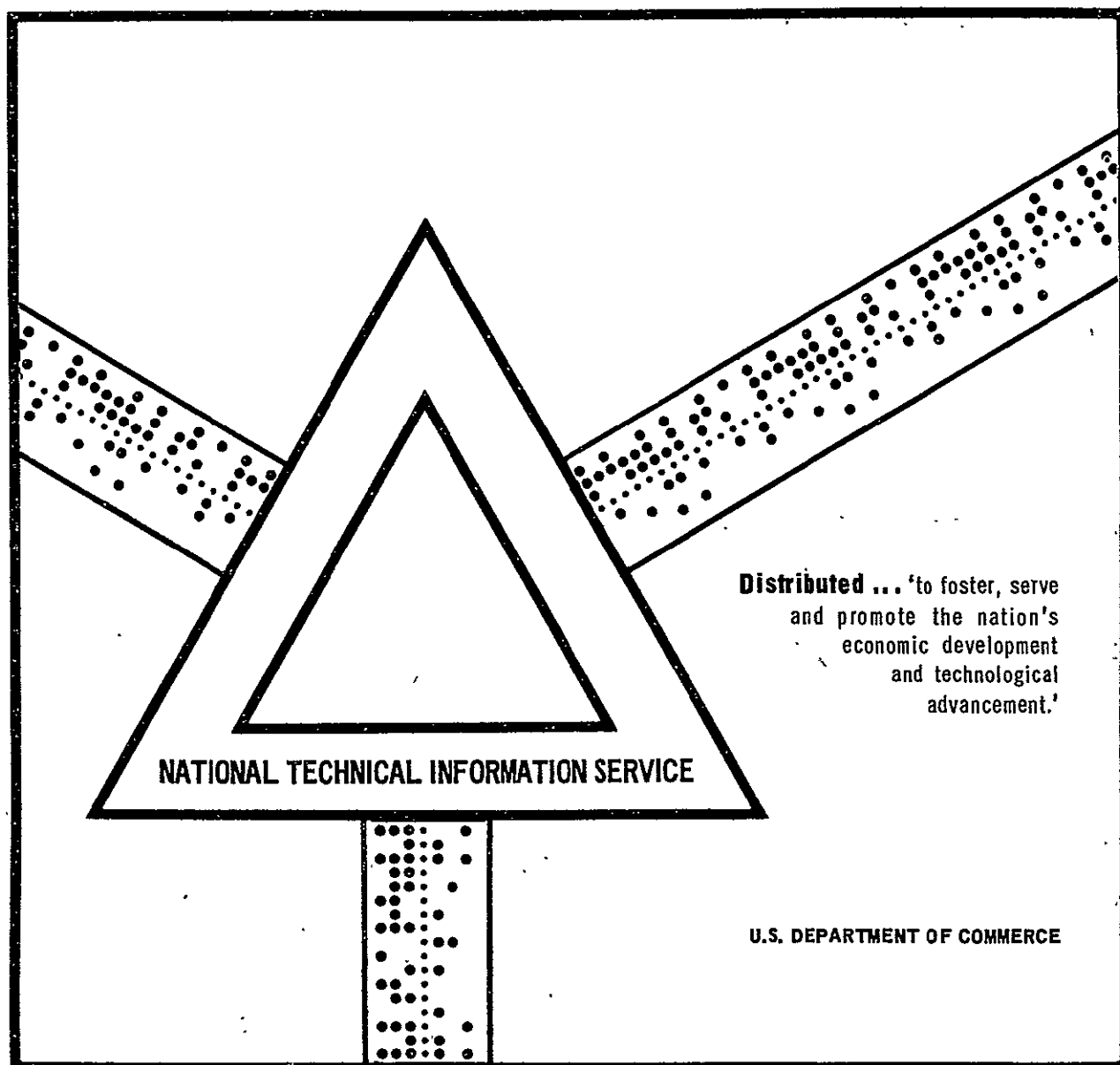


INSTRUMENTATION AND COMMUNICATION RESEARCH AT  
MSFC

George C. Marshall Space Flight Center  
Marshall Space Flight Center, Alabama

May 1971



NASA TECHNICAL  
MEMORANDUM

NASA TM X-64572

May 1971

NASA TM X-64572

INSTRUMENTATION AND COMMUNICATION  
RESEARCH AT MSFC

RESEARCH ACHIEVEMENTS REVIEW  
VOLUME IV REPORT NO. 3

N71-29319

(ACCESSION NUMBER)

74

(PAGES)

TMX 64572

(NASA CR OR TMX OR AD NUMBER)

FACILITY FORM 602

N71-29326

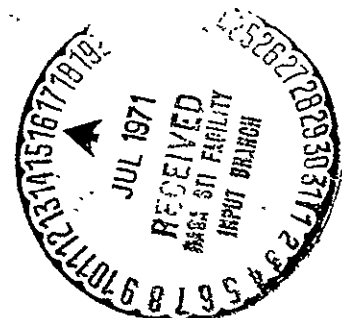
(THESE)

(CODE)

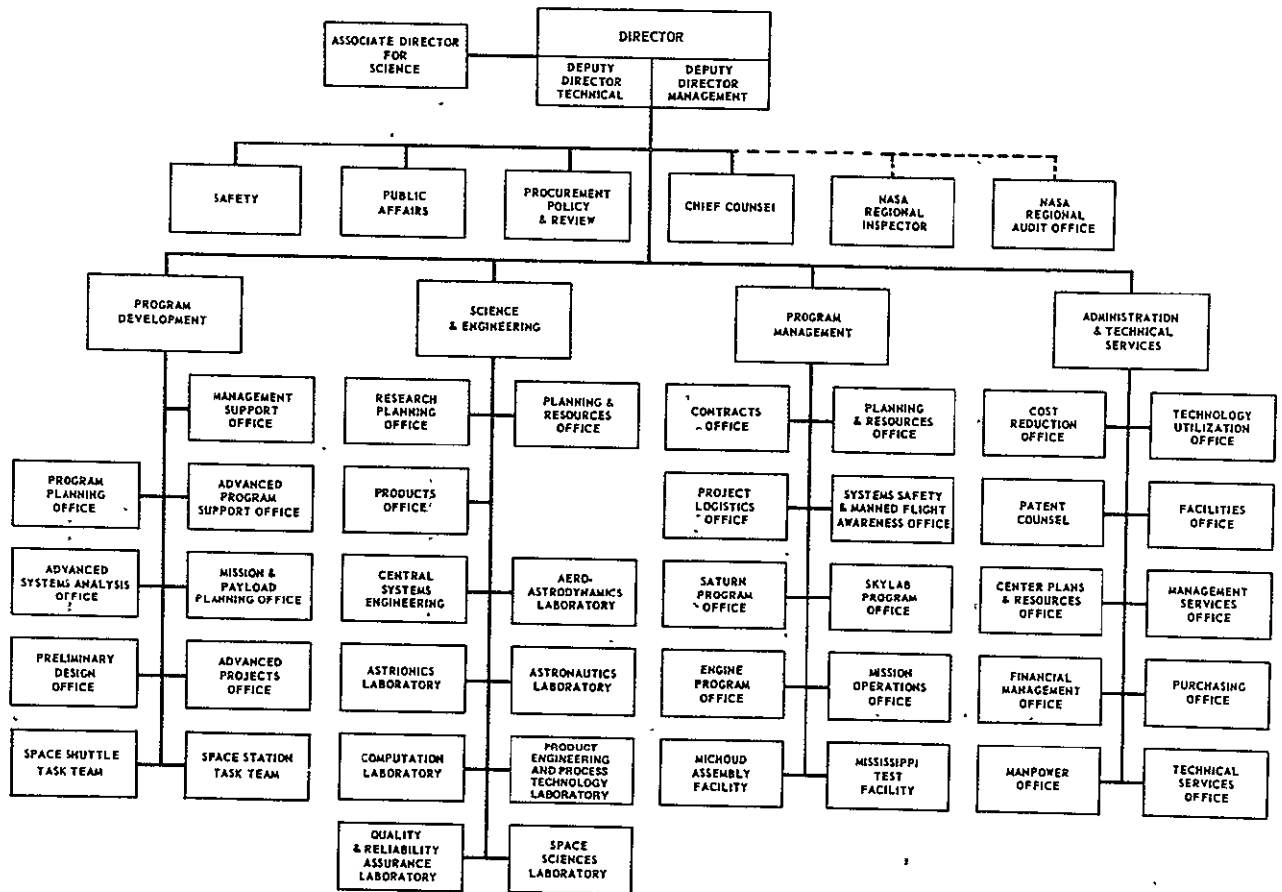
(CATEGORY)

SCIENCE AND ENGINEERING DIRECTORATE  
GEORGE C. MARSHALL SPACE FLIGHT CENTER  
MARSHALL SPACE FLIGHT CENTER, ALABAMA

Reproduced by  
NATIONAL TECHNICAL  
INFORMATION SERVICE  
Springfield, Va. 22151



# GEORGE C. MARSHALL SPACE FLIGHT CENTER



## RESEARCH ACHIEVEMENTS REVIEWS COVER THE FOLLOWING FIELDS OF RESEARCH

- Radiation Physics
- Thermophysics
- Chemical Propulsion
- Cryogenic Technology
- Electronics
- Control Systems
- Materials
- Manufacturing
- Ground Testing
- Quality Assurance and Checkout
- Terrestrial and Space Environment
- Aerodynamics
- Instrumentation
- Power Systems
- Guidance Concepts
- Astrodynamics
- Advanced Tracking Systems
- Communication Systems
- Structures
- Mathematics and Computation
- Advanced Propulsion
- Lunar and Meteoroid Physics

PREFACE

The Research Achievement Reviews document research accomplished by the laboratories of Marshall Space Flight Center. Each review covers one or two fields of research and attempts to present the results in a form readily useable by specialists, system engineers, and program managers.

Reviews of this fourth series are designated Volume IV and will span the period from May 1970 through May 1972.

In accordance with NASA policy the International System of Units (SI Units), as defined in NASA SP-7012, are used in this publication.

*The papers in this report were presented November 19, 1970*

William G. Johnson  
Director  
Research Planning Office

CONTENTS...

INTRODUCTION TO INSTRUMENTATION AND COMMUNICATION RESEARCH AT MSFC

Page

By C. T. Paludan. . . . . 1

X-RAY SOURCE FOR GRAZING INCIDENCE MIRROR TEST

Page

By C. T. Jones . . . . . 3

BIBLIOGRAPHY. . . . . 7

LIST OF ILLUSTRATIONS

Figure	Title	Page
1.	Electrical diagram of first source. . . . .	4
2.	Intensity versus energy curve for aluminum . . . . .	4
3.	First source developed . . . . .	6
4.	Jarrell-Ash source. . . . .	6
5.	Optical environmental chamber. . . . .	7
6.	Ray trace through mirrors. . . . .	7
7.	Final source . . . . .	8
8.	Test chamber . . . . .	9

A DIGITAL PRESSURE TRANSDUCER

Page

By H. S. Harman

SUMMARY . . . . . 11

INTRODUCTION. . . . . 11

TECHNICAL DESCRIPTION OF DIGITAL TRANSDUCER WITH DIGITAL ADDRESSING AND LIMIT MONITORING. . . . . 11

CONCLUSIONS. . . . . 15

# CONTENTS (Continued) . . .

## LIST OF TABLES

Table	Title	Page
1.	Guideline Specifications. . . . .	12
2.	Calibration of Digital Pressure Transducer . . . . .	17

## LIST OF ILLUSTRATIONS

Figure	Title	Page
1.	A/D converter with analog transducer . . . . .	13
2.	Digital transducer with digital addressing and limit monitoring . . . . .	14
3.	Photograph of digital transducer . . . . .	15
4.	Dimensional drawing of digital transducer . . . . .	16
5.	Photograph of digital transducer without case . . . . .	16
6.	Nonlinearity with pressure of digital pressure transducer . . . . .	18
7.	Sensitivity versus temperature and zero shift versus temperature of digital pressure transducer . . . . .	18

## INVESTIGATION OF DATA COMPRESSION TECHNIQUES ✓

By W. E. Maynard

	Page
SUMMARY . . . . .	19
INTRODUCTION. . . . .	19
ANALYSIS OF TECHNIQUES USING DETERMINISTIC SIGNALS . . . . .	20
CONCLUSIONS. . . . .	26
REFERENCES . . . . .	30

## LIST OF ILLUSTRATIONS

Figure	Title	Page
1.	Telemetry Redundancy Analyzer Facility . . . . .	20
2.	Compression ratio as a function of tolerance for a sine wave sampled at 10 000 samples per second. . . . .	21

## CONTENTS (Continued) . . .

	Page
3. Compression ratio as a function of tolerance for a sine wave sampled at 10 000 samples per second. . . . .	22
4. RMS error as a function of tolerance for a sine wave sampled at 10 000 samples per second. . . . .	22
5. RMS error as a function of tolerance for a sine wave sampled at 10 000 samples per second. . . . .	24
6. Compression ratio as a function of tolerance for a triangle wave sampled at 10 000 samples per second. . . . .	24
7. Compression ratio as a function of tolerance for a triangle wave sampled at 10 000 samples per second. . . . .	25
8. RMS error as a function of tolerance for a triangle wave sampled at 10 000 samples per second. . . . .	25
9. RMS error as a function of tolerance for a triangle wave sampled at 10 000 samples per second. . . . .	27
10. Compression ratio as a function of tolerance for a square wave sampled at 10 000 samples per second. . . . .	27
11. Compression ratio as a function of tolerance for a square wave sampled at 10 000 samples per second. . . . .	28
12. RMS error as a function of tolerance for a square wave sampled at 10 000 samples per second. . . . .	28
13. RMS error as a function of tolerance for a square wave sampled at 10 000 samples per second. . . . .	29

## AM BASEBAND TELEMETRY TECHNIQUES

	Page
By J. J. Clubb	
SUMMARY . . . . .	31
LIST OF ABBREVIATIONS. . . . .	31
INTRODUCTION. . . . .	31
APPROACH. . . . .	31
SS/FM . . . . .	32
DSB/FM . . . . .	32
CBW FM/FM. . . . .	33

# CONTENTS (Continued)

	Page
COMPATIBLE, SSB/DSB/CBW .....	33
MULTIPLEXER .....	33
DEMUTIPLEXER .....	35
OVERALL PERFORMANCE .....	41
CONCLUSIONS .....	41

## LIST OF TABLES

Table	Title	Page
1.	Equipment Specifications .....	40

## LIST OF ILLUSTRATIONS

Figure	Title	Page
1.	Multiplexer block diagram .....	34
2.	Multiplexer composite output .....	35
3.	Double sideband output from the multiplexer .....	36
4.	Single sideband output from the multiplexer .....	37
5.	FDM demultiplexer overall block diagram .....	38
6.	Demultiplexer .....	39
7.	System performance .....	41

## HIGH STABILITY FM TV TRANSMITTER WITH SAMPLED AUTOMATIC FREQUENCY CONTROL

	Page
By M. A. Honnell	
SUMMARY .....	43
INTRODUCTION .....	43
SPECIFICATIONS .....	43
SYSTEM DESCRIPTION .....	44
SWITCHING PULSES .....	46



# CONTENTS (Continued)...

	Page
ERROR SIGNAL.....	47
FREQUENCY STABILITY .....	48
CONCLUSIONS.....	49
BIBLIOGRAPHY.....	50

## LIST OF TABLES

Table	Title	Page
1.	Specifications of S-band FM TV Transmitter.....	44

## LIST OF ILLUSTRATIONS

Figure	Title	Page
1.	S-band FM television transmitter .....	44
2.	Video signal and carrier frequency deviation.....	45
3.	FM television transmitter with sampled AFC .....	46
4.	Switching pulses.....	47
5.	Discriminator output signal with reference voltage clamped to zero .....	48
6.	Video signal clamped to hold capacitor voltage .....	48
7.	Output frequency stability factor.....	48
8.	Output frequency stability factor $\delta_0$ versus open-loop gain $K_0$ .....	49
9.	Measured frequency stability .....	49

## SPACE STATION RF HAZARDS

By R. A. Inman

	Page
SUMMARY .....	51
INTRODUCTION.....	51
RF EXPOSURE STANDARDS .....	51
BIOLOGICAL EFFECTS .....	52
POWER DENSITY CALCULATIONS.....	53

# CONTENTS (Continued) . . .

	Page
POWER DENSITY VERSUS PARABOLIC ANTENNA PARAMETERS. . . . .	53
SHIELDING FROM RF RADIATION . . . . .	55
CONCLUSIONS. . . . .	55
REFERENCES. . . . .	55

## LIST OF TABLES

Table	Title	Page
1.	Examples of Allowable Exposure Times. . . . .	51
2.	Examples of Low Gain Antenna Radiation Levels at 20 W Power. . . . .	54
3.	Examples of High Gain Parabolic Antenna Radiation Levels at 20 W Power. . . . .	54

## TELEVISION RESEARCH

	Page
By C. T. Huggins	
SUMMARY . . . . .	57
INTRODUCTION. . . . .	57
ELECTRICAL CHARACTERISTICS OF PHOTO-TRANSISTOR ARRAY. . . . .	57
REAL TIME INTELLIGENCE ACQUISITION . . . . .	58
MOSAIC EVALUATION SYSTEM. . . . .	59
CONCLUSIONS. . . . .	64
REFERENCES. . . . .	65

## LIST OF ILLUSTRATIONS

Figure	Title	Page
1.	Section of mosaic with XY interconnections. . . . .	58
2.	Simplified block diagram of analog signal chain. . . . .	60
3.	Block diagram of 400-by-500 element solid-state television camera . . . . .	60
4.	400-by-500 element mosaic evaluation system. . . . .	61
5.	Probe test stand for mosaic . . . . .	61

CONTENTS (Concluded). . .

	Page
6. Probe cards in position on mosaic. . . . .	62
7. Scanning pattern of 400-by-500 element photo-transistor test set . . . . .	63
8. Miniature solid-state television camera . . . . .	64
9. Space usage of solid-state television camera. . . . .	65

# INTRODUCTION TO INSTRUMENTATION AND COMMUNICATION RESEARCH AT MSFC

By

C. T. Paludan

Research and technology efforts in support of the Skylab program have set the pace for research in instrumentation and communication in recent years. An example of this is the X-ray source, which is discussed later in this Research Achievements Review. Now that the design of flight hardware and much of the ground testing of Skylab are completed, research related to the reusable space shuttle, the space station and base, the nuclear shuttle, and experiment modules takes on a more prominent role. The conflicting requirements for more data, but simplified mission procedures, have forced innovations in the data technology fields. Some of these in the fields of data collection, data handling, and data transmission are discussed in this report.

It should be remembered that flight programs also require innovations in ground testing, with resultant instrumentation research requirements.

Just as NASA's overall space program has beneficially affected progress in fields that are not directly related to space, instrumentation and communication research also finds application in unexpected areas. Obviously, some of the Skylab and space station experiments are directly oriented toward earth problems, but it is often a nice surprise to discover that radiation effects testing for the nuclear stage can lead to new medical techniques, or that a hazardous gas monitor for the space station is of interest to antipollution researchers.

Only a sampling of the diverse research achievement in instrumentation and communication is discussed herein. To put these samples in perspective, a somewhat larger sampling is listed below without giving details. Some of these activities are well advanced, while others may be in initial stages. In several cases, work by university professors in our summer faculty program and by research fellows sponsored by the National Academy of Science is included.

1. Computer optimization of radio frequency circuits.
2. Use of the supercooled Josephson junction as a radio frequency detector.
3. Precise and absolute determination of the local acceleration of gravity with a laser interferometer.
4. Precise measurement of velocity for spacecraft docking by application of the Mossbauer effect.
5. Sensor technology for slush hydrogen.
6. Hydrogen gas monitor.
7. Zero-gravity propellant quantity determination.
8. Instrumentation for very low velocity gas flows.
9. Digital blast gauge.
10. Biomedical instrumentation and experiments.
11. Optical computer technology; use of a laser and optics to perform Fourier transformations.
12. Optical rendezvous and docking.
13. Optical data transmission between the shuttle booster and orbiter.
14. Laser altimeter for orbital calibration of metric photography.
15. Multispectral photography.
16. Thermal mapping with an electromechanical scanner.

17. Nuclear radiation technology.
18. Geographic research by man in orbit.

Some of the activities mentioned above are joint efforts involving divisions and laboratories other than the Instrumentation and Communication Division of the Astrionics Laboratory.

At MSFC we feel that good instrumentation and communication techniques are essential to every facet of a space technology program. Our research is oriented toward the national space program as

presently envisioned. Our justification was expressed by Lord Kelvin in 1848:

When you can measure what you are speaking about and express it in numbers, you know something about it; and when you cannot measure it, when you cannot express it in numbers, your knowledge is of meagre and unsatisfactory kind. It may be the beginning of knowledge, but you have scarcely in your thought advanced to the stage of a science.

# X-RAY SOURCE FOR GRAZING INCIDENCE MIRROR TEST

By

C. T. Jones

N71-29320

In 1968 the Radiation Section of the Measuring Branch of Astrionics Laboratory was assigned the task of providing an X-ray source to check out the S-056 X-ray telescope. It was determined that the use of an isotope source would require a liquid or a foil-covered vapor deposit of some substance and that the X-ray emission of soft X-ray producing elements would be greatly attenuated by foil or liquid containers. Therefore, it was evident from the beginning that an isotope source would be unsatisfactory in accomplishing the objective; hence, it was necessary to develop an acceptable source. The S-056 X-ray telescope is an Apollo Telescope Mount (ATM) experiment that is designed to study the sun's energy from a wavelength of 200 to 2000 pm (2 to 20 Å). A source was designed, developed, and tested that met the requirements of the experiment engineer. Areas to be discussed herein include requirements, theory of operation, design, and use of an X-ray source for this unique application.

The theory of producing X-rays is not new technology, but the application and flux characteristics are innovations in X-ray technology. In 1895 Roentgen first produced X-rays by passing an electric discharge through a highly evacuated tube and detected these unknown rays with a paper screen covered with crystals of platinum barium cyanide. He found that X-rays are a byproduct of the collision of electrons with an element. More work by other groups showed that the energy of X-rays depends upon the type of target used. The electrons from the cathode, interacting with the electrons in the plate, emit X-rays; and the energy of these X-rays depends upon whether the interactions are with the K-shell or L-shell electrons. The energy of K-alpha radiation from aluminum is about  $2291 \times 10^{-19}$  J (1430 eV), because that is the excitation voltage of the aluminum K-shell electrons. This energy level corresponds to a wavelength of 830 pm (8.3 Å). Since the S-056 experiment will study energy in the 200- to 2000-pm (2- to 20-Å) range, this element provides a proper wavelength for testing.

Electrons passing through a potential of a few hundred volts cause an emission of continuous radiation. When the voltage is increased to 1430 V, characteristic radiation from the K-shell electrons of aluminum is generated. This voltage varies with the atomic number of the plate element. X-rays produced at less than  $1.6 \times 10^{-14}$  J (100 keV) are said to be soft X-rays, and the characteristic radiation from aluminum is ultrasoft. This radiation is so soft that a few centimeters of air will easily attenuate its strength. This is one of the primary reasons for working in a vacuum; the other is that the filaments for electron sources must operate in a vacuum to keep them from burning to destruction.

Figure 1 shows simply how the electrical parameters are arranged to produce X-rays. The filament is heated by a low voltage power supply, and a high positive potential is applied to the aluminum plate. When the electrons interact with the electrons in the plate elements, characteristic radiation as well as some continuous radiation is emitted.

Figure 2 shows a plot of intensity versus energy of characteristic radiation and continuous radiation. As the voltage increases, the characteristic radiation remains stationary and the continuous radiation shifts to higher energies. One does, however, reach a maximum level that is practical for the ratio of K-alpha radiation and continuous spectrum radiation.

When the requirements were first presented, it was determined that a point source at an infinite distance (e.g., 100 m) was needed to align the mirrors in the X-ray region. Immediately, parallel efforts were begun to develop a source and conduct a literature search for a commercial product. The source had to be extremely intense so that short exposures could be taken without undue interference from vibration. The in-house effort to build a source was performed strictly on an experimental basis.

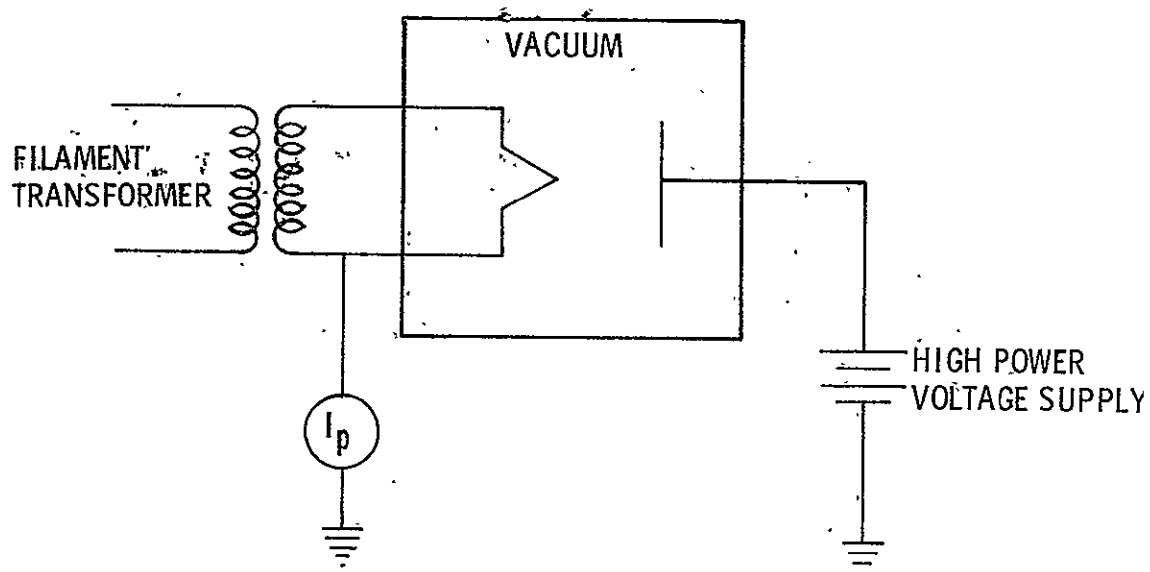


Figure 1. Electrical diagram of first source.

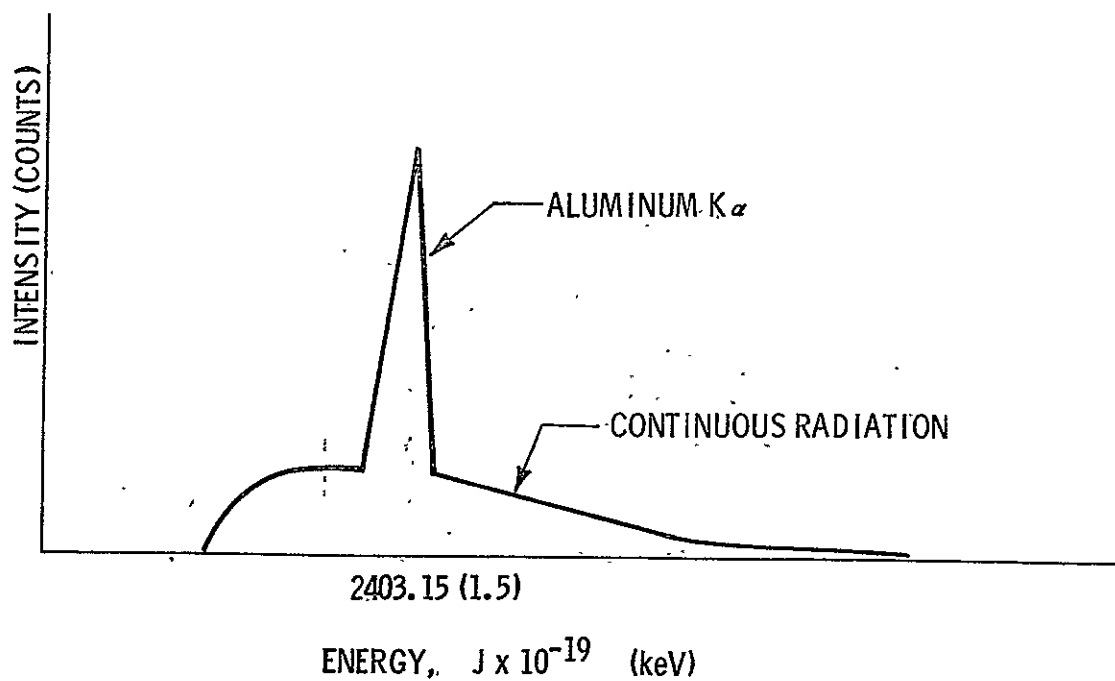


Figure 2. Intensity versus energy curve for aluminum.



Figure 3 shows the first source developed. A stainless steel housing was fabricated to house the plate and filament and was made vacuum tight. A thin aluminum foil was placed over the window so that measurements could be taken with an ionization chamber. The aluminum plate was mounted on a piece of Kel-F on one end of the housing, and the filament of an 866 vacuum tube was mounted on a piece of Kel-F on the opposite end of the housing. The source emitted X-rays, but it became too hot and did not generate enough X-rays. The ratio of heat input to X-ray output was much too great.

A literature search disclosed that Jarrell-Ash, Inc. marketed a microfocus X-ray source, which is shown in Figure 4. The main features of the Jarrell-Ash source were that the targets could be changed and the source was water-cooled. A unit was purchased and testing was conducted using aluminum targets. This source was very intense and short exposure times were taken with this instrument. The ratio of heat input to X-ray output was low, which was another good feature of this source.

However, the testing philosophy of the telescope mirrors changed and, consequently, the source requirements changed. A point source at an infinite distance was no longer needed, but rather an intense broad source was desired. In addition to being broad, the source had to be uniform over the entire emission area. The mirrors were now going to be tested in a front-to-front configuration with one set of mirrors collimating the X-rays and the other set being tested. Figure 5 shows the mirror system in the optical environmental chamber. As shown, the source is now positional just behind the resolution target that, in turn, is positioned at the focal plane of the collimating telescope.

For front-to-front testing, a new design for the X-ray source was necessary. The source needed to be large enough to illuminate the resolution target with X-rays from all angles and uniform in its emission. A low ratio of heat input to X-ray output was necessary to prevent undue heating of the telescope assembly. Another reason for a broad source was that the resolution targets could be changed to different sizes so that resolution studies could be made.

The in-house development proceeded. The next source was 8.9 cm in diameter with a square emitting

area of  $6.3 \text{ cm}^2$ . The source was made from aluminum, and the inside was machined so that it would be water cooled. Above the square emitting surface were 10 rows of tungsten filaments in the vertical and 10 rows in the horizontal. This source proved to be intense, but the ratio of the heat input to the X-ray output was too great, even with water cooling. Since the water lines were copper, it was necessary to have the plate at ground potential for safety. In addition to having a high heat input, many of the X-rays were being wasted.

Figure 6 shows how energy is received at the mirrors and the origin of the energy. As shown, only a circular band of energy was being used by the mirrors; therefore, the development of a circular source was begun. A block of aluminum 8.9 cm by 11.4 cm and 2.9 cm thick was fabricated with a 0.5-cm hole in the center. A ceramic tube was used as the insulating material for the high voltage connector that passed through its center. Inside the block of aluminum, a cooling cavity was machined to help control the heat input to the vacuum system and experiment. Fill and drain outlets were installed for the coolant. Approximately 1.9 cm above the plate, a circular filament holder was positioned with insulating ceramic standoffs. Around the filament plate, which was made of copper, were positioned 16 screws to hold the filaments. This gave the source a spoked-wheel filament pattern. When a pinhole picture was taken of this arrangement, however, the source was found to be uniform all the way around the circle. On the outside of the filament plate was a grid plate that assisted in controlling the electrons being boiled off the tungsten filaments. The final configuration for the source is shown in Figure 7.

The test fixture used throughout the development of this source is shown in Figure 8. The resolution chart used during the tests is shown in the foreground. The large tube housed some 7.62 cm diameter stainless steel mirrors, and the rear housing contained a camera for resolution and alignment studies.

This source is capable of producing an ultrasoft X-ray flux of approximately  $1 \times 10^9$  photons/cm<sup>2</sup> s. The unit was successfully tested in the optical environmental chamber and was used extensively in X-ray imaging studies of the ATM S-056 experiment optical system.



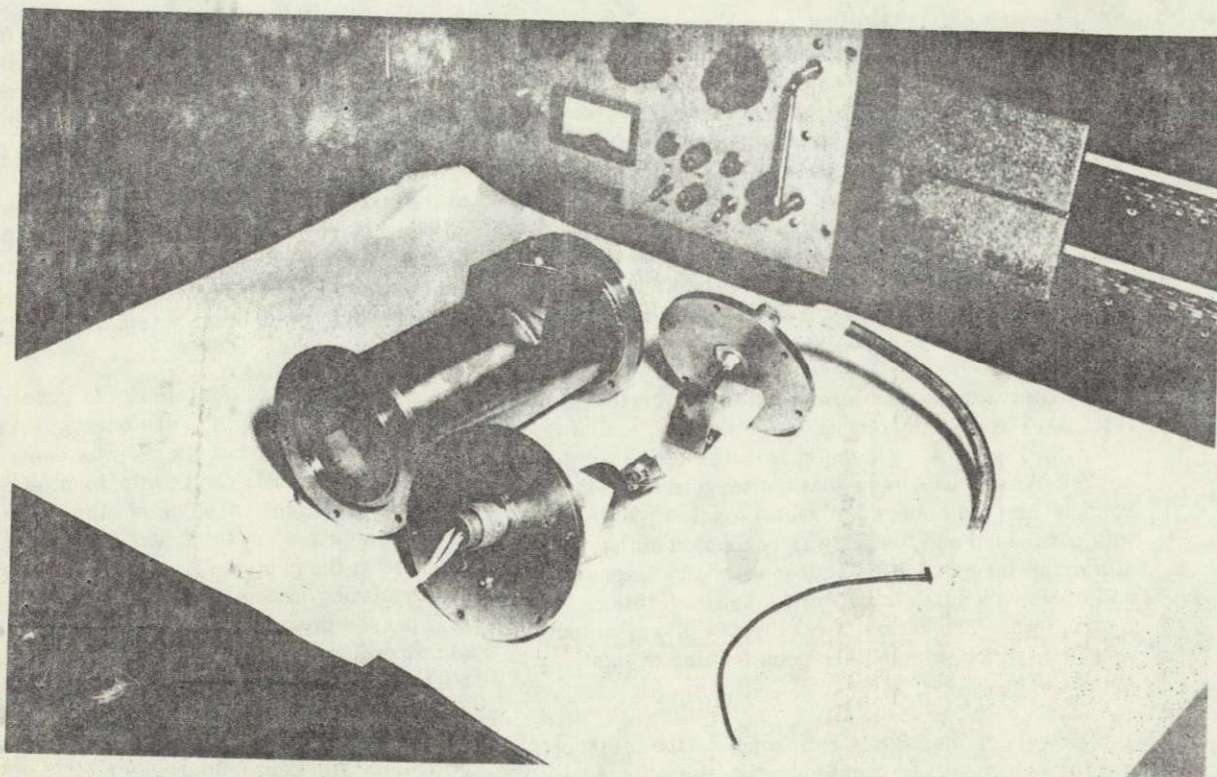


Figure 3. First source developed.

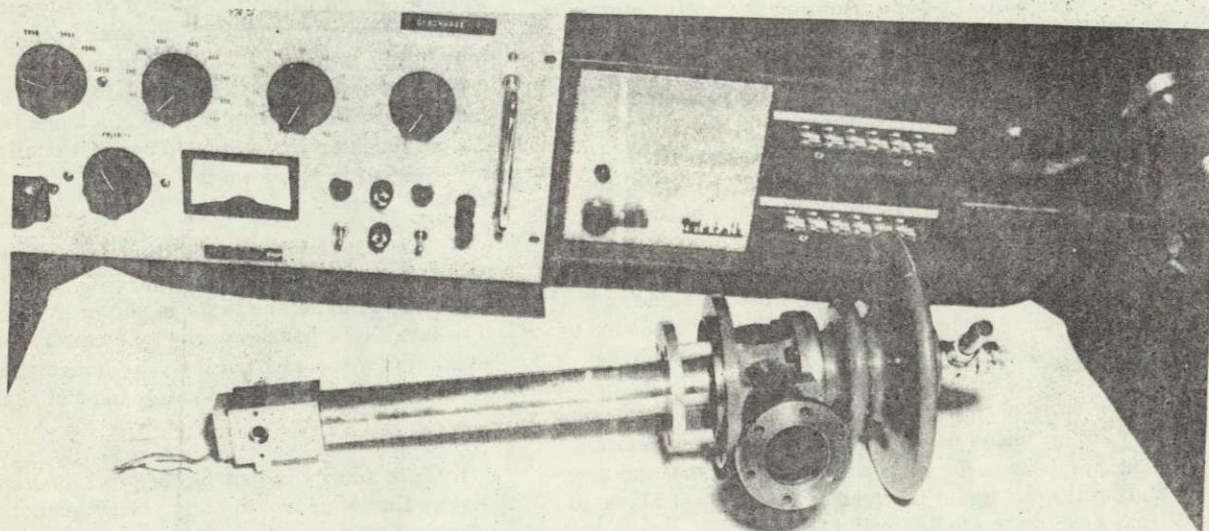


Figure 4. Jarrell-Ash source.



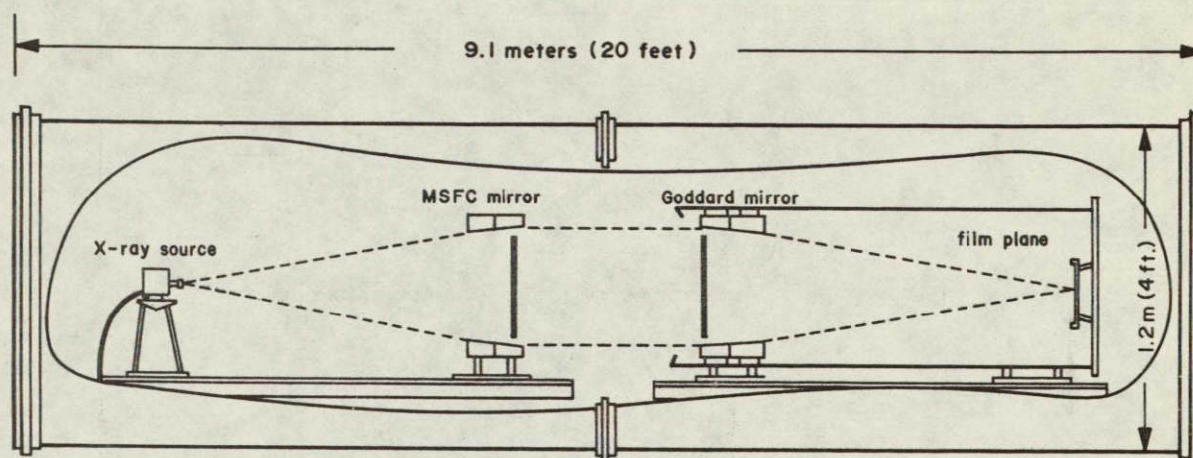


Figure 5. Optical environmental chamber.

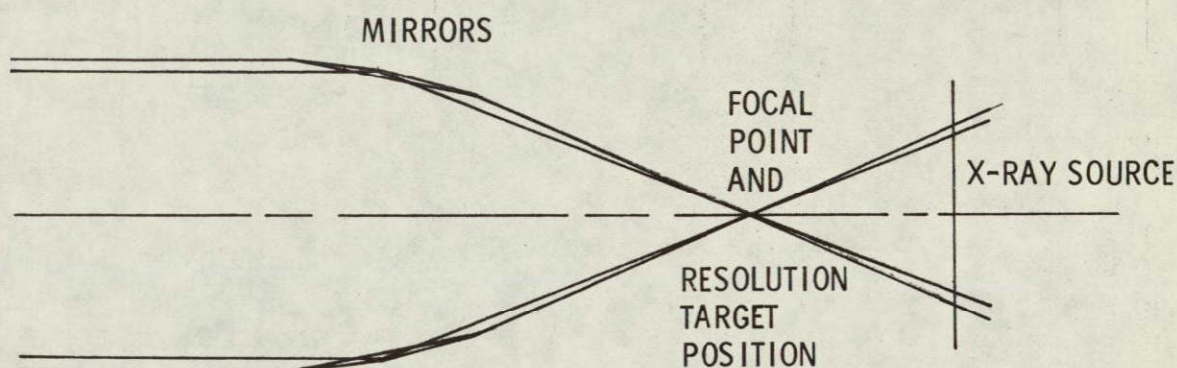


Figure 6. Ray trace through mirrors.

## BIBLIOGRAPHY

Compton, Arthur H.; and Allison, Samuel K.: X-Rays in Theory and Experiment. Second edition, D. Van Nostrand Company, Inc., Princeton, N. J., 1963.





Figure 7. Final source.



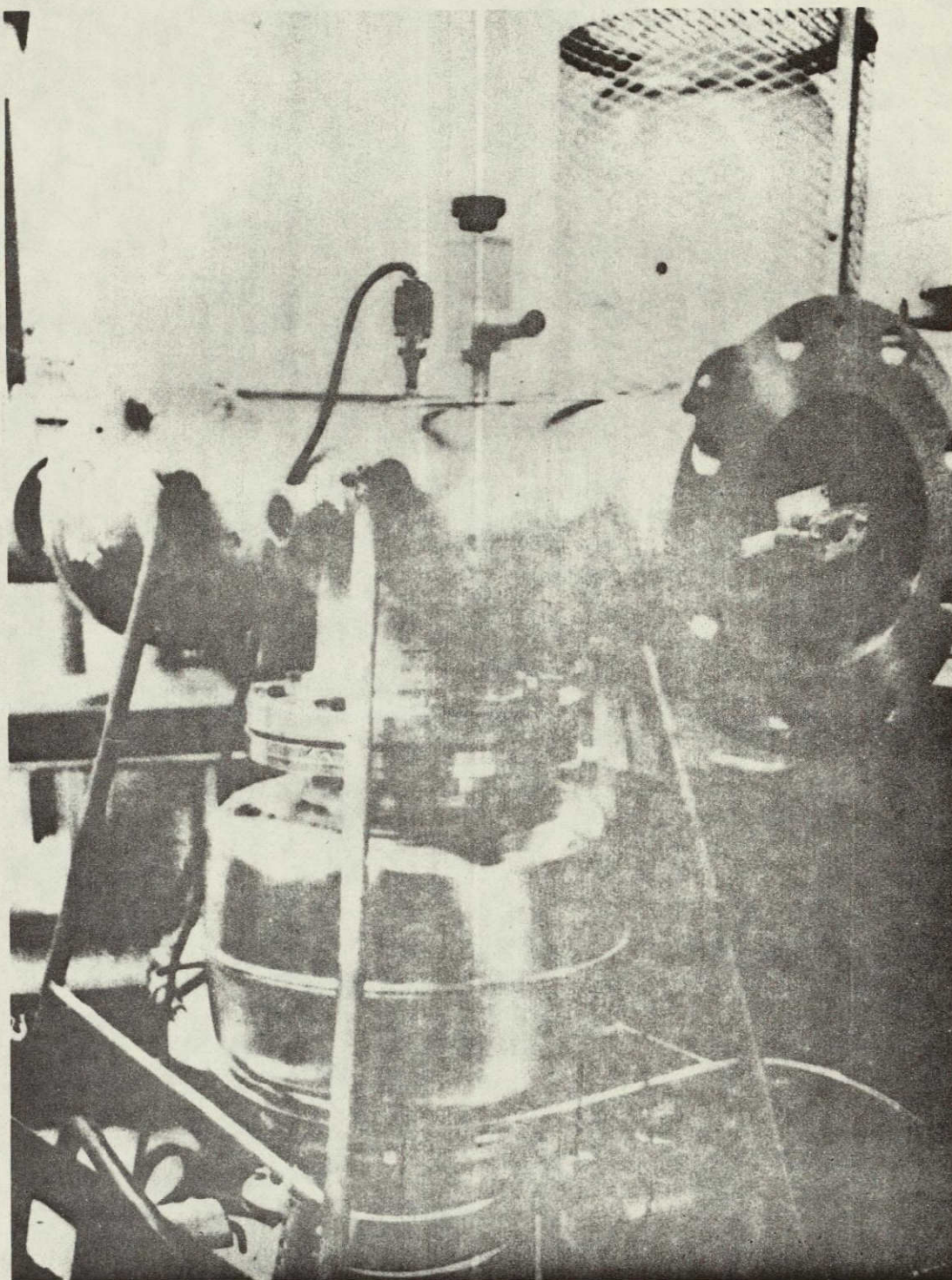


Figure 8. Test chamber.



# A DIGITAL PRESSURE TRANSDUCER

By

H. S. Harman

N71-29321

## SUMMARY

A digital pressure transducer, its operational features, and its performance against guideline specifications are discussed. Performance meeting the guideline specifications was achieved.

## INTRODUCTION

NASA has always realized the need for a practical, reliable digital pressure transducer and, therefore, has sponsored a number of studies and research and development contracts in this area, all of which have been somewhat encouraging in their results. Earlier efforts produced a digital force balance transducer that had a high resolution and accuracy. In this transducer, pressure displacing a bellows or diaphragm was sensed starting an up-down counter; the resulting digital number was presented in parallel for display and also was converted to an analog value of current for forcing the sensing bellows back to its initial position electromagnetically. The unique feature of this system was that the digital conversion was in the force feedback loop. The bellows or diaphragm was always at the zero or near-zero position, which reduced hysteresis. This transducer was useful for air data and laboratory applications but was sensitive to acceleration, vibration, and temperature extremes. Because of its electromechanical structure, temperature and acceleration compensation of this system was extremely difficult and impractical. Another research and development effort was initiated toward a more direct conversion from pressure to a digital output. In this effort, pressure acting directly on a birefringent material was studied as a possibility, but this was not successful because of material creep effects, which caused hysteresis and nonrepeatability. The comparatively recent availability of high performance monolithic and hybrid circuit modules for analog to digital (A/D) conversion changed NASA's research and development

approach to the digital transducer problem. To meet the environmental requirements of liquid rocket propulsion systems, such as those encountered on the Saturn V and those anticipated on the space shuttle engine and vehicle, a transducer must meet the minimum specifications shown in Table 1. A contract was awarded to Metrophysics, Inc., Santa Barbara, California, with these specifications as a guideline and with a scope of work specifying the use of a state-of-the-art low level deposited film transducer as a force summing device and a state-of-the-art miniature analog-to-digital converter. The primary research and development objective was to design a 10-bit serial output digital transducer meeting these specifications.

## TECHNICAL DESCRIPTION OF DIGITAL TRANSDUCER WITH DIGITAL ADDRESSING AND LIMIT MONITORING

The digital transducer consists of five functional parts; the analog transducer, the A/D converter, the address detector, the calibration check circuit, and the limit monitor. The digital transducer communicates over four lines with the receiving (or control) station. These four lines are the address line, the digital signal output line, the limit line, and the alarm line. The first 3 of these lines can be shared by as many transducers as the drive capability of the receiving station allows, while the alarm line can only be shared by 10 transducers as explained later.

The analog element is a bridge-type transducer producing a 30-mV full scale output signal. One leg of the transducer bridge can be shunted by fixed resistors for calibration check.

The A/D converter (Fig. 1) operates on the principle of successive approximation. It provides the excitation voltage for the transducer bridge through an electronic switch. The excitation voltage is scaled down by a voltage divider, buffered by the reference



TABLE 1. GUIDELINE SPECIFICATIONS

1. Range: 0 to 15 N/cm <sup>2</sup> to 0 to 5000 N/cm <sup>2</sup>	14. Weight: Approximately 0.25 kg
2. Maximum overload: 150 percent of rated range	15. Electrical connection: Case-mounted electrical receptacle DR 60853-12-8P
3. Pressure media: Fluids compatible with types 17-4PH and 17-7PH stainless steel	16. Identification: The model designation, serial number, range, maximum excitation, and manufacturer are engraved on each unit.
4. Excitation: 28 Vdc $\pm$ 1 Vdc	17. Dimensions: 4 cm in diameter by 7.5 cm in length
5. Digital output: 10-bit serial, nonreturn to zero, most significant bit first. A logic "1" corresponds to a maximum of +25 V, 7 mA maximum. Other logic levels are available.	18. Calibration: 6 wire shunt calibration
6. Resolution: 0.1 percent full scale (FS)	19. Clock signal: Up to 10 kHz, 0.1 ms minimum pulse width, 0 to +5 V amplitude into 10 k $\Omega$
7. Nonlinearity: 0.3 percent FS	20. DC reset: +5 V into 5 k $\Omega$
8. Hysteresis: < 0.1 percent FS	21. Conversion rate: Up to 1000 words (= conversions) per second
9. Zero balance: < 2 percent FS	22. Calibration check: Command 0 to +28 V (supply voltage)
10. Temperature range: -54 to +74°C	23. Shock: 1000 g's (1 ms duration)
11. Thermal sensitivity shift: < 0.002 percent/°C	24. Acceleration: 50 g's, 5 = 3000 Hz
12. Thermal zero shift: < 0.002 percent FS/°C	25. Acoustic noise: 165 dB
13. Pressure connection: 7/16-20 external fitting per MS 33656-E4	

amplifier, and applied to the ladder switches in the steering network. This voltage serves as reference voltage of the A/D converter and, because it is proportional to the excitation voltage, makes the conversion accuracy independent of supply voltage changes.

The floating output of the transducer bridge is applied to a special differential comparator in which the feedback signal from the ladder network is subtracted from the bridge output signal. The difference of these two signals is then amplified by the high gain amplifier and applied to the steering network. The

polarity of this signal during each of the 10 clock pulses of one conversion decides whether "0's" or "1's" are produced at the digital output.

The bridge excitation voltage and the reference voltage of the ladder switches are on during the duration of each clock pulse and are off between clock pulses. During the off-period, the bridge voltage and reference voltage go to zero. The differential comparator puts out a zero signal and the zero restorer, and forces the output of the high gain amplifier to zero. In this manner zero drift of the amplifier is effectively eliminated.



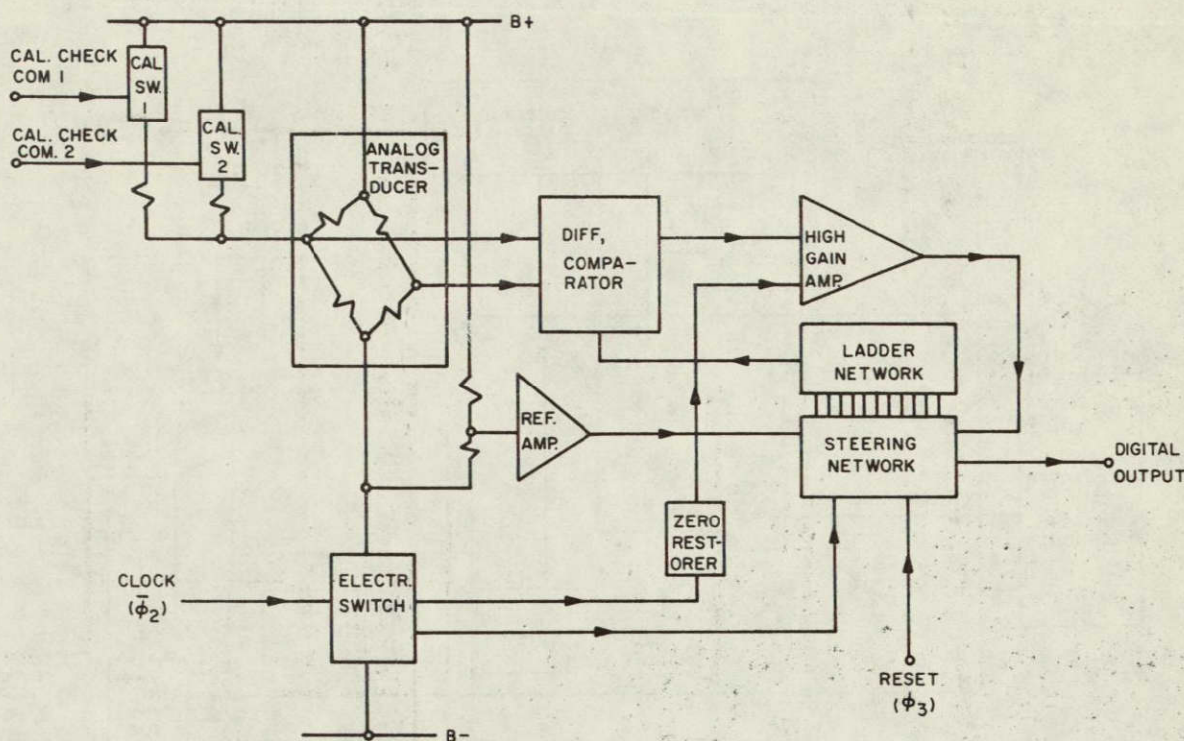


Figure 1. A/D converter with analog transducer.

At the end of one conversion, which coincides with the end of an address word, the steering network is reset by a pulse  $\phi_3$  from the clock circuits.

The address detector consists of three parts; the clock, the address register, and the address decoder (Fig. 2).

To understand the function of the address detector, the address format is explained. An address word comprises 10 bits. The first five bits are used for the address proper. Bits 6 and 7 are used for calibration check and bits 8 and 9 are used for limit loading. Bit 10 is used solely for end-of-address identification. The "1's" and "0's" differ in their length. The length of a "0" corresponds to one-fourth of a bit period, the length of a "1" corresponds to one-half of a bit period, and the end of address pulse equals three-fourths of a bit period. The presence of a pulse even during the transmission of a "0" makes it possible to synchronize the transducer circuits without the aid of an additional clock line.

The clock circuit derives the internal clock and synchronization signals from the leading edges of

the address pulses. The address signal is shifted bit by bit into the address register when clock  $\phi_1$  makes a transition from negative to ground. This transition occurs during the second quarter of the bit period. During this time, only "1" pulses are present and shifted as "1's" into the register; "0" pulses last only one-fourth of a bit period and have decayed to zero when the positive transition of the clock pulse occurs. A "0" is then shifted into the address register.

Clock pulse  $\phi_3$  is derived from the end of the address signal and occurs once every 10 bits. It synchronizes the A/D converter, the address decoder, the calibration check command circuits, and the steering gates of the limit monitor.

Assume that a transducer has received its address. The address register is filled with the address word and the address decoder, and upon receiving clock pulse  $\phi_3$ , puts out a "1" enabling G1. The digital output signal from the A/D converter can pass G1 and appears on the output signal line. The address decoder stays in its "1" state until the next address has been shifted into the address register. If this address is not the transducer's address, then the



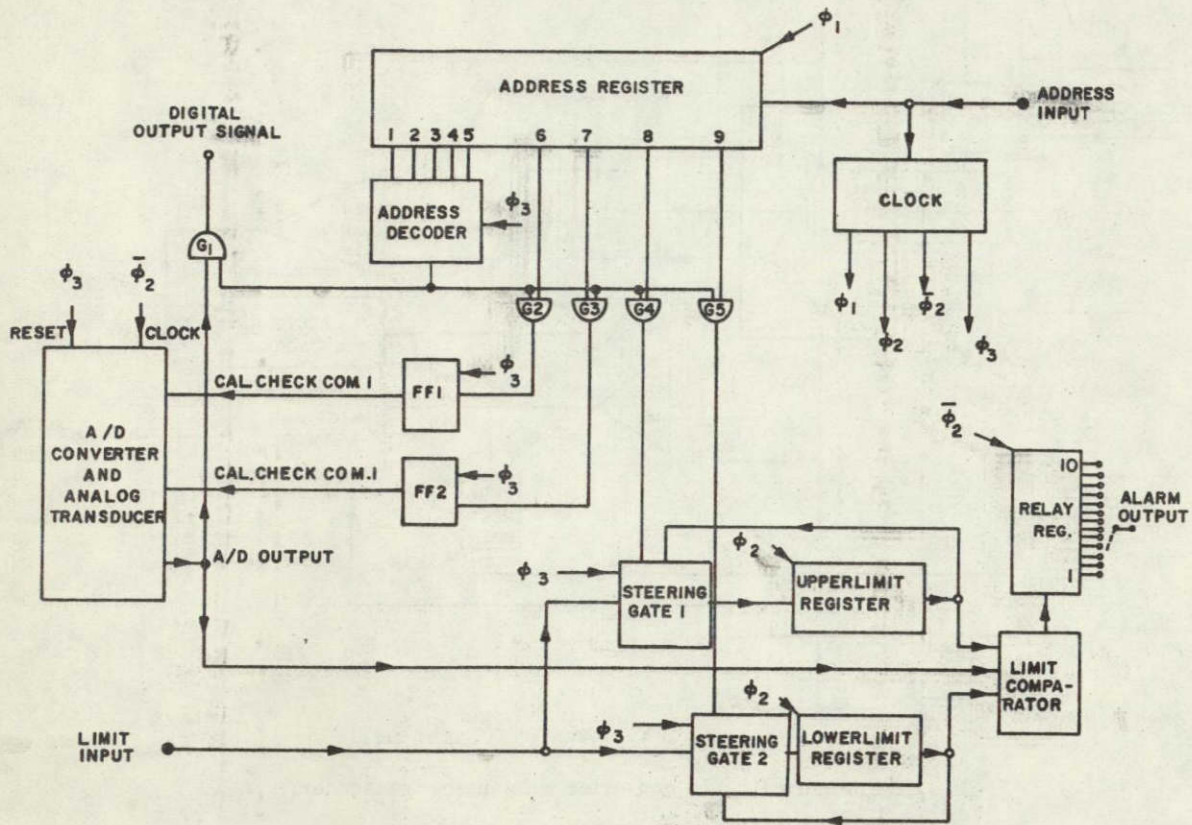


Figure 2. Digital transducer with digital addressing and limit monitoring.

output of the decoder is set to "0" by  $\phi_3$  and G1 is closed.

In a similar manner the calibration check command signals are obtained. With the proper address in the address register and bit 6 or 7, a "1" gate, G1 or G2, is enabled setting flip-flop FF1 or FF2. The corresponding shunt calibration switches are then turned on and the transducer bridge is unbalanced. The digital output signal corresponding to the unbalanced state of the bridge can now pass G1. After 10 clock pulses when  $\phi_3$  reappears and some other address is in the address register, FF1 or FF2, respectively, is reset and the calibration switches are turned off.

The limit monitor consists of two recirculating registers, two steering gates, a comparator, and a delay register. Each register can hold a limit of 10 bits in length. In the normal mode the limits are continuously recirculated through the steering gates and compared to the output of the A/D converter. If

the signal from the A/D converter is greater than the upper limit, the limit comparator will place a "1" into the delay register at the end of the address word that coincides with the end of a conversion. Similarly, a "1" is placed into the delay register if the signal is smaller than the lower limit. The "1" travels through the register and appears at each of the 10 outputs in sequence. If, for instance, the alarm output is connected to stage 3 of the delay register, then a "1" will appear on the alarm line during the third bit period following the end of the address pulse on the address line. The receiving station (control circuit) will then detect the location in time of this "1" and be able to identify the transducer in which an alarm condition exists. Other transducers in the system have their alarm output connected to the other stages of their delay registers and can also be identified by the position in time of their alarm signals. Up to 10 transducers can share a common alarm line without loss of identification by coinciding alarm pulses. Note that a transducer does not need to be addressed to produce an alarm



signal; it will do so at any time whether addressed or not.

The limits stored in the limit register can be changed in the following manner. The upper limit is changed by addressing the transducer with an address that has a "1" in position 8. At the end of the address, when the address decoder goes to "1", G4 puts out a "1" setting the steering gate 1 to the limit loading mode. In this mode the upper limit register is connected to the limit input line and recirculation is interrupted. A limit word is now shifted into the register. After the last bit of the limit word, the steering gate is set back by  $\phi 3$  to the recirculating mode. The limit monitoring function is not interrupted during a limit loading cycle and an alarm signal might be produced.

The lower limit is changed the same way as the upper limit with the exception that the address word must have a "1" in position 9 instead of position 8.

## CONCLUSIONS

The configuration of the digital transducer (Figs. 3, 4, and 5) meets the guideline specifications. Performance as presented in Table 2 and Figures 6 and 7 exceeds specification requirements. The overall performance of this transducer makes it an excellent candidate for future applications on the space shuttle, the space station, and in associated development work.



Figure 3. Photograph of digital transducer.



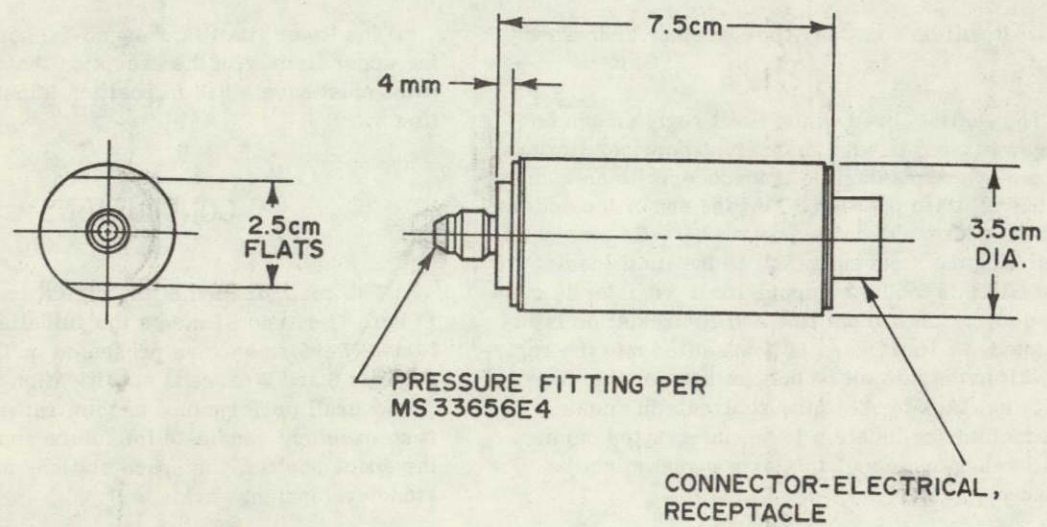


Figure 4. Dimensional drawing of digital transducer.

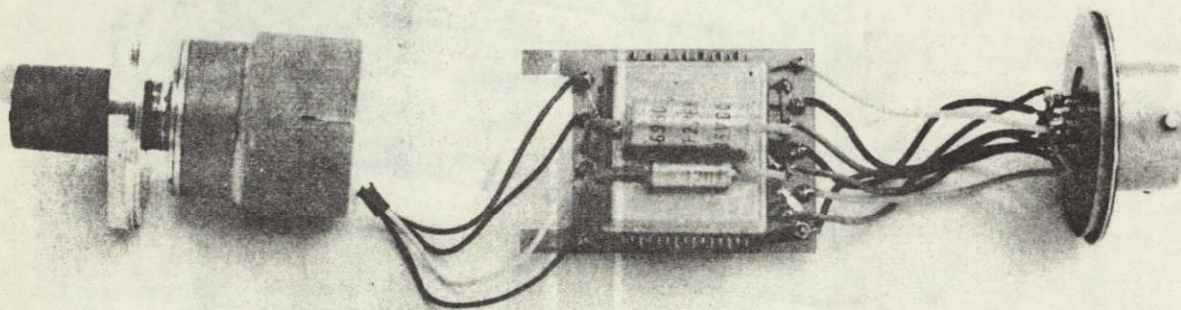


Figure 5. Photograph of digital transducer without case.



TABLE 2. CALIBRATION OF DIGITAL PRESSURE TRANSDUCER

## a. Temperature, +30°C

N/cm <sup>2</sup>	Reading <sup>a</sup> No. 1		Reading No. 2		Ideal	$\Delta$ From Linearity				Repeatability, R2 - R1	
	Up	Down	Up	Down		Up	Down	Up	Down	Up	Down
0	0.5	0.5	0.5	0.5	0.5	0	0	0	0	0	0
2	125	125	125	125	125.4	-0.4	-0.4	-0.4	-0.4	0	0
4	250	250.5	249.5	250.5	250.4	-0.4	+0.1	-0.9	+0.1	-0.5	0
6	375	375.5	375	375.5	375.3	-0.3	+0.2	-0.3	+0.2	0	0
8	500	501.5	500	501.5	500.3	-0.3	+1.2	-0.3	+1.2	0	0
10	624.5	625	624	625	625.2	-0.7	-0.2	-1.2	-0.2	-0.5	0
12	750	751	750	751	750.1	-0.1	+0.9	-0.1	+0.9	0	0
14	875	875	875	875	875.1	-0.1	-0.1	-0.1	-0.1	0	0
16	1000	1000	1000	1000	1000	0	0	0	0	0	0

## b. Temperature, -55°C

N/cm <sup>2</sup>	Reading No. 1		Reading No. 2		Ideal	$\Delta$ From Linearity				Repeatability, R2 - R1	
	Up	Down	Up	Down		Up	Down	Up	Down	Up	Down
0	3	3	3	3	3	0	0	0	0	0	0
2	127	127	127	127	128.1	-1.1	-1.1	-1.1	-1.1	0	0
4	252	253	252.5	254	253.3	-1.3	-0.3	-0.8	+0.7	+0.5	+1
6	377	379	378	379	378.4	-1.4	+0.6	-0.4	+0.6	+1	0
8	503	504.5	504	505	503.5	-0.5	+1	+0.5	+1.5	+1	+0.5
10	627	628.5	627	629	628.6	-1.6	-0.1	-1.6	+0.4	0	+0.5
12	753	753.5	753	755	753.8	-0.8	-0.3	-0.8	+1.2	0	+1.5
14	878.5	879	879	879	878.9	-0.4	+0.1	+0.1	+0.1	+0.5	0
16	1004	1004	1004	1004	1004	0	0	0	0	0	0

## c. Temperature, +74°C

N/cm <sup>2</sup>	Reading No. 1		Reading No. 2		Ideal	$\Delta$ From Linearity				Repeatability, R2 - R1	
	Up	Down	Up	Down		Up	Down	Up	Down	Up	Down
0	1	1	1	1	1	0	0	0	0	0	0
2	125.5	126	125.5	126	125.8	-0.3	+0.2	-0.3	+0.2	0	0
4	250.5	252	250.5	252	250.5	0	+1.5	0	+1.5	0	0
6	375	376	375	376	375.3	-0.3	+0.7	-0.3	+0.7	0	0
8	500	501.5	500	501.5	500	0	+1.5	0	+1.5	0	0
10	624	625	624	625	624.8	-0.8	+0.2	-0.8	+0.2	0	0
12	749	750	749	750	749.5	-0.5	+0.5	-0.5	+0.5	0	0
14	874	875	874	874	874.3	-0.3	+0.7	-0.3	+0.2	0	-0.5
16	999	999	999	999	999	0	0	0	0	0	0

a. Calibration check reading: 750.



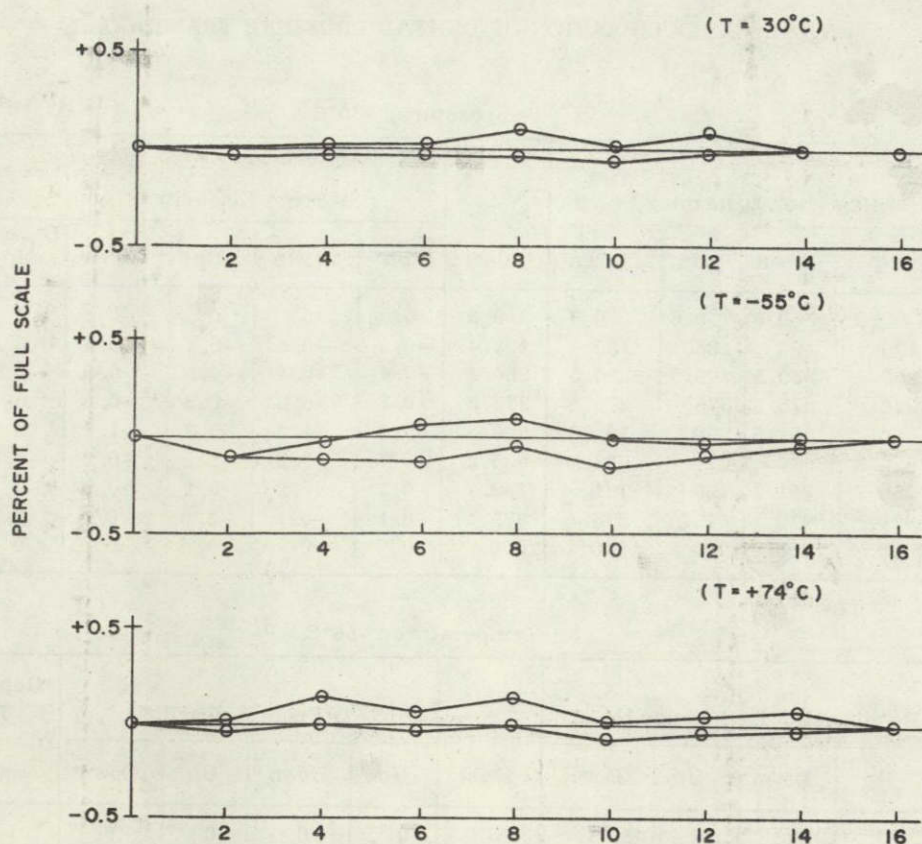


Figure 6. Nonlinearity with pressure of digital pressure transducer.

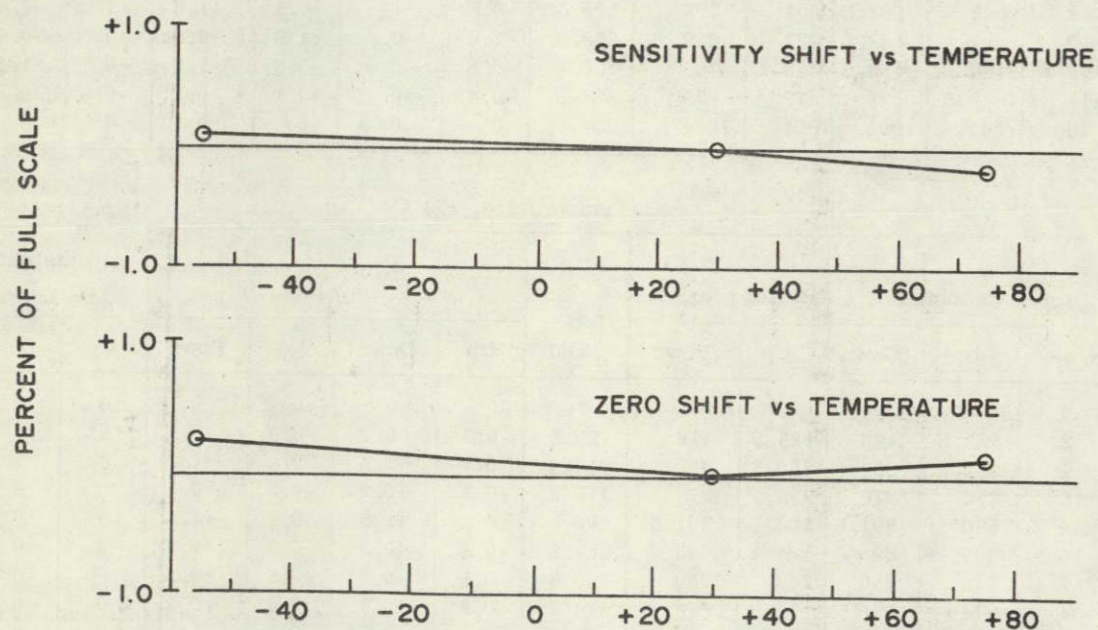


Figure 7. Sensitivity versus temperature and zero shift versus temperature of digital pressure transducer.



# INVESTIGATION OF DATA COMPRESSION TECHNIQUES

By

W. E. Maynard

N71-29322

## SUMMARY

The results of a study of five different data compression techniques are presented. The performance of each technique was analyzed for input data models consisting of three known deterministic signals. The basic operation of each technique was established, and some knowledge of their relative effectiveness was determined.

## INTRODUCTION

A vast amount of space flight data is being generated by today's data transmission systems. The amount will surely increase with the arrival of scheduled deep space probes and extended orbital flights. Some of the data are highly redundant; that is, the data remain constant or change at a constant rate for long periods of time. Prior investigators have shown that it is possible to remove this redundancy by transmitting only significant samples [1]. Redundant data are determined by an arithmetic process or technique. This process, known as data compression, allows the same information to be transmitted with little or no error.

The technique is the heart of any data compression system. Numerous techniques exist, but the following five have shown the most promise:

1. ZFN — Zero order, fixed corridor, non-redundant sample transmitted.
2. ZVA — Zero order, variable corridor, artificial preceding sample transmitted.
3. FFP — First order, fixed corridor, preceding sample transmitted.
4. FVP — First order, variable corridor, preceding sample transmitted.
5. FVA — First order, variable corridor, artificial preceding sample transmitted.

These techniques have been in existence for some time [2]. The purpose of this study was to determine if any, or all, of these techniques lend themselves to a practical and beneficial application in present and future data transmission systems.

To accomplish this, it was necessary to implement these techniques in a system where they could be studied exhaustively. This was made possible by the acquisition of the Telemetry Redundancy Analyzer (TRA) [3].

The TRA allows any one of the five techniques to be selected. The same data can, in turn, be applied to each of the techniques, while the tolerance is varied from 0 to 1.275 V. Up to 99 999 data samples can be analyzed for any given study or run. The TRA outputs the nonredundant samples (NRS, sometimes referred to as transmitted samples) and the mean square error ( $D^2/N$ ). Root-mean-square (rms) error can be calculated from the value of  $D^2/N$ , and the amount of compression can be expressed in terms of compression ratio (CR), which is defined as:

$$CR = \frac{\text{total number of samples}}{\text{number of nonredundant samples}}$$

The capability and flexibility of the TRA has been increased by the addition of peripheral equipment (Fig. 1). The TRA compresses, reconstructs, and analyzes the data. The remainder of the equipment takes actual or simulated data, conditions and formats these data into a form that the TRA can accept, and then prints or records the results of the TRA analysis.

It was necessary to establish the operation of the TRA and the implementation of the techniques. This was done by analyzing known deterministic signals. The signals were a 150-Hz, 1-V, peak-to-peak sine wave, triangle wave, and square wave. These signals were sampled at 10 000 samples per second for a total of 10 000 samples.

Data compression techniques are not used on deterministic signals for any practical data transmission system because the two unknowns, frequency and amplitude, can be determined in a more efficient



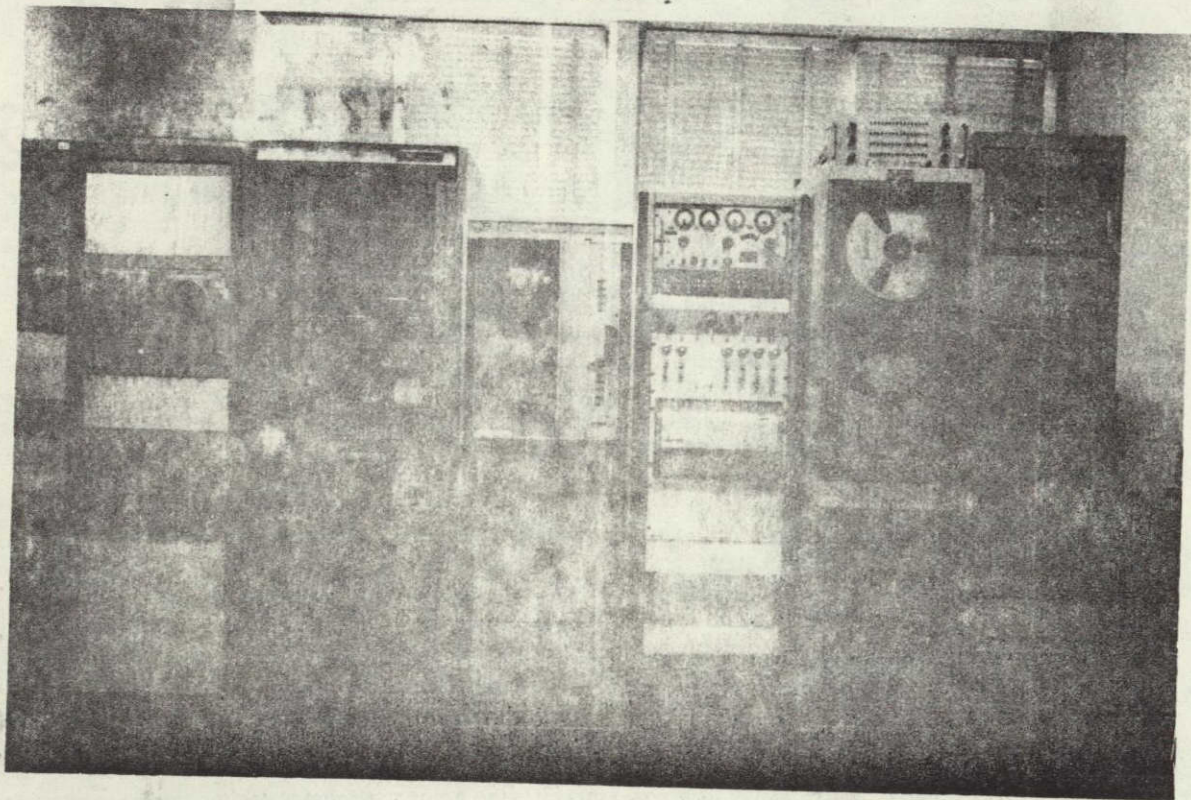


Figure 1. Telemetry Redundancy Analyzer Facility.

manner. However, since the results can be predicted for these signals, the operation of the techniques can be established to provide a medium for comparing the relative effectiveness of the techniques and to expose any peculiarities they might have.

The ability of a technique to remove redundancy is measured in the amount of error for a given CR. This is illustrated throughout this paper by plotting CR as a function of tolerance and rms error as a function of tolerance. Tolerance is expressed in percent of 5 V, and the error is represented as a percentage of the full scale rms voltage input.

## ANALYSIS OF TECHNIQUES USING DETERMINISTIC SIGNALS

### Sine Wave

Some of the individual traits of the techniques are evident when CR as a function of tolerance is considered (Fig. 2). The CR remains constant for a

noticeable increase in tolerance and then rapidly changes to a new value where it again remains constant. There is some similarity among the techniques in that they level off and reach a plateau at the same value of CR. However, they do not all reach the same plateau for the same value of tolerance.

At a sampling ratio of 10 000 samples per second, there are 66.6 samples per cycle of data. For a tolerance of 0 percent, all of these samples are transmitted samples (NRS); but as the tolerance is increased, more and more of these samples are considered as redundant samples and are not transmitted. The plateaus become significant as the number of NRS decreases. The arithmetic process of the techniques essentially divides the cycle of data into corridors and considers one sample of each corridor as an NRS. An increase in tolerance will allow more redundant samples but does not increase the number of corridors, thereby keeping the same number of NRS and the same CR. However, the number of corridors and NRS changes as the tolerance is increased sufficiently but tends to stabilize at an even number since the waveshape is uniform.

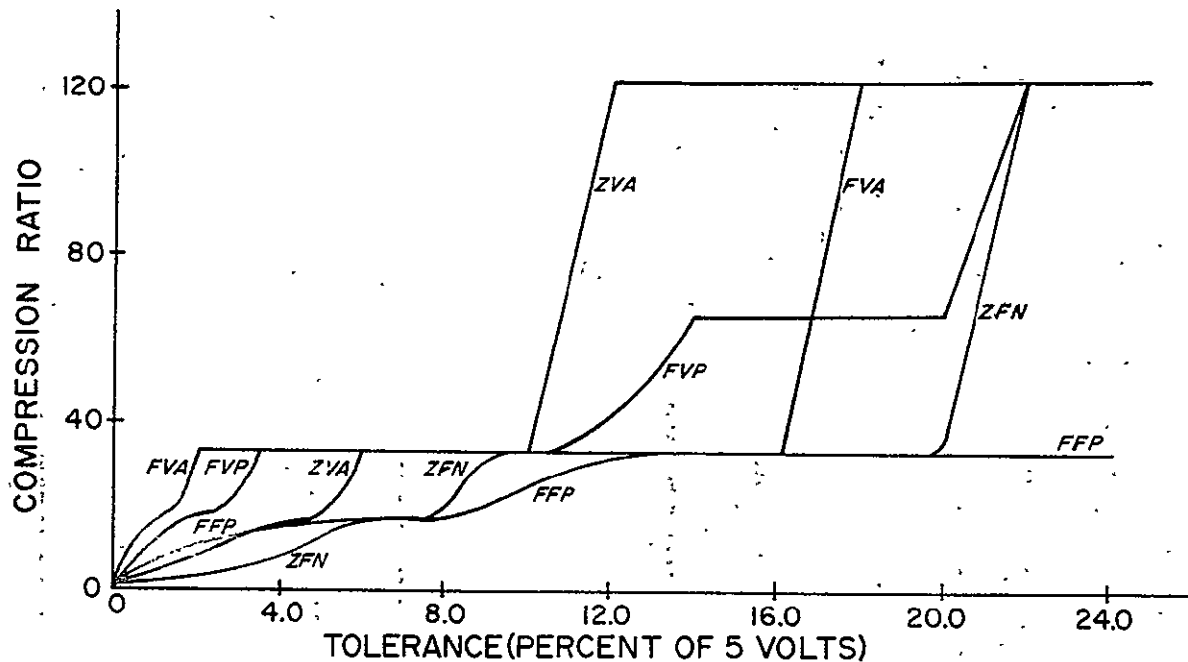


Figure 2. Compression ratio as a function of tolerance for a sine wave sampled at 10 000 samples per second.

One would expect the CR to reach a maximum of 10 000, which would occur when the tolerance completely encompasses the signal and produces only one NRS. This is not the case, however, because of a limitation of the TRA. The TRA must truncate after 127 successive redundant samples have been received and then establish a new NRS and corridor. This limitation will allow only 81 NRS and a maximum CR of 123:5.

Some observations from Figure 2 worth noting are:

1. The ZVA technique reaches the first plateau much sooner than the ZFN because of the variable corridor of the ZVA technique. Its corridor can, effectively, be larger than that of the ZFN technique for the same tolerance selection. More compression is achieved with the ZVA technique.

2. The FFP technique never reaches maximum CR because of its corridor construction, where the first two data samples are required to establish the fixed corridor. This corridor can never encompass the entire signal; therefore, at least two NRS per cycle will always exist.

3. The FVP and FVA techniques, like the ZVA technique, have variable corridors that allow them to have, effectively, a larger corridor than the tolerance selection.

4. The techniques where the artificial preceding sample is transmitted allow more compression.

To determine the relative effectiveness of the techniques, the same data are redrawn (Fig. 3) for a more practical range of tolerances. The results are:

1. More compression can be achieved with the first-order techniques because they are derived from the principle of slope and the sine wave has a slope, to some degree.

2. The ZVA technique becomes superior to the FFP technique at a tolerance of 3 percent.

3. The ZFN is a poor performer.

The rms error for a given tolerance (Fig. 4) is equal in importance to the amount of compression at a given tolerance. The maximum error will occur

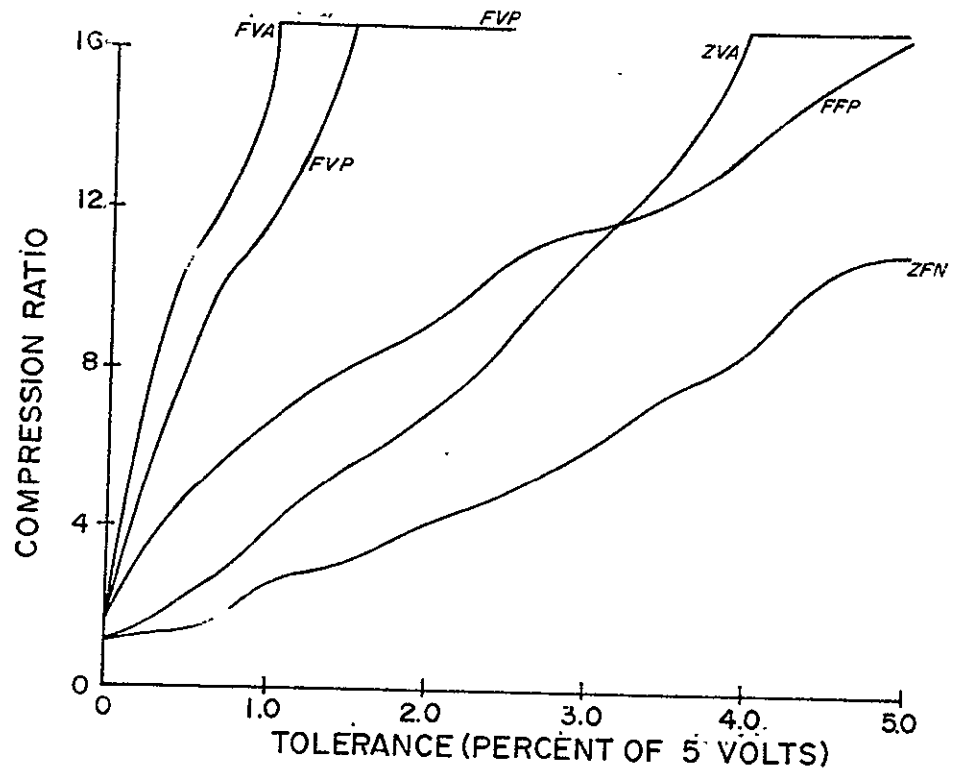


Figure 3. Compression ratio as a function of tolerance for a sine wave sampled at 10 000 samples per second.

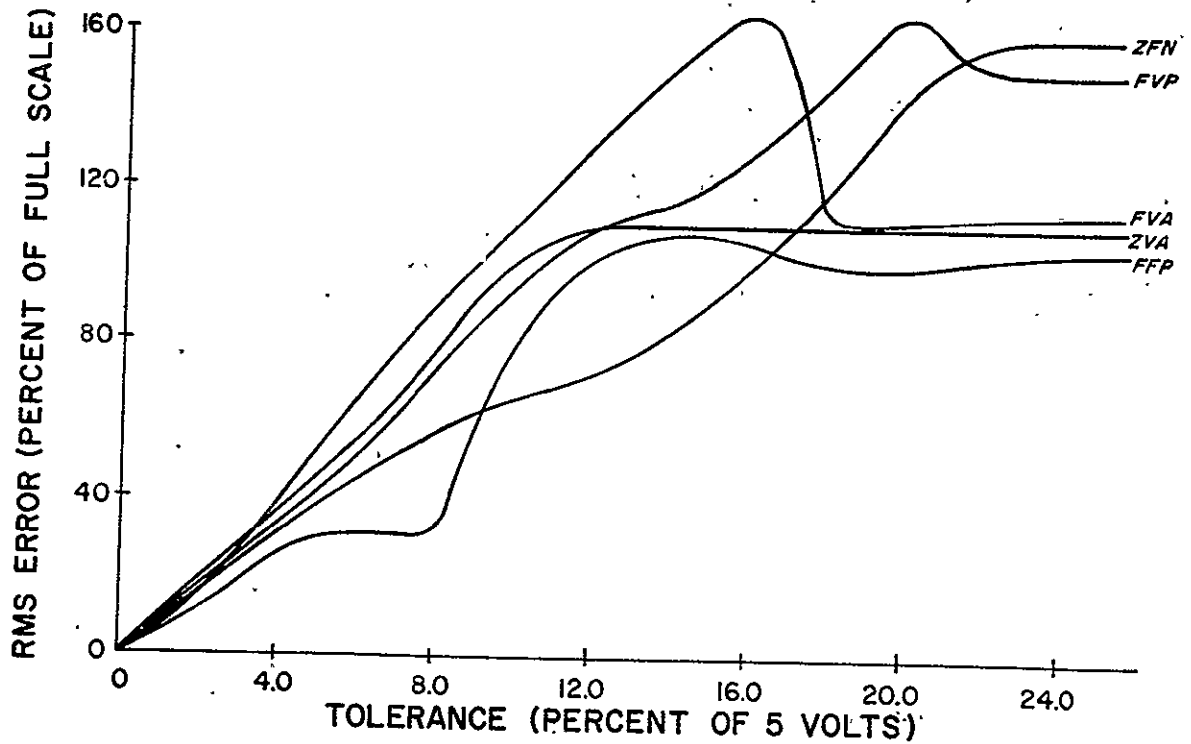


Figure 4. RMS error as a function of tolerance for a sine wave sampled at 10 000 samples per second.



when the tolerance completely encompasses the data source, giving one NRS. If the NRS is located at a peak of the sine wave, the maximum error will be:

$$\% \text{ maximum rms error} = \frac{\sqrt{\frac{1}{2\pi} \int_0^{2\pi} \left(\frac{1}{2} \sin t + \frac{1}{2}\right)^2 dt}}{0.3535} \times 100 = 173\%$$

If the NRS is located at the midpoint of the wave, the maximum error will be:

$$\% \text{ maximum rms error} = \frac{\sqrt{\frac{1}{2\pi} \int_0^{2\pi} \left(\frac{1}{2} \sin t\right)^2 dt}}{0.3535} \times 100 = 100\%$$

It can be seen that the rms error continues to increase as the tolerance is increased, even during the periods in which the CR remained constant. This occurs because the sizes of the corridors within a cycle do not remain equal as the tolerance is increased; that is, there will be more redundant samples in one corridor than another, thus creating a greater error. An exception occurs when the tolerance is increased to a point where the minimum possible number of NRS occurs. At this point, the NRS becomes stable and the rms error remains constant. Since the FFP technique does not allow the minimum number of NRS, it will never reach maximum error. Also, the ZVA technique will never reach maximum error. A tolerance greater than 0.500 V will create the condition of minimum NRS for this technique. Under the condition of minimum NRS, the techniques using the artificial preceding sample as the transmitted sample will have the least error. This results because the adjustment is toward the center of the waveshape. Techniques with fixed corridors, ZFN and FFP, have periods in which the error remains constant. All of the techniques exhibit this to a degree, and it occurs at the same point in which the CR remains constant.

The same data are redrawn (Fig. 5) so that a comparison can be made within a practical tolerance band. The FFP technique has the least error, and the techniques with the adjusted preceding sample have the largest error.

Considering both CR and rms error, the FVA and FVP techniques are definitely superior to the other three. The FVA technique has the best performance at low tolerances, but the FVP technique becomes superior at a tolerance of about 4 percent.

## Triangle Wave

The response of the techniques to a triangle wave is similar to that of a sine wave. This can be seen from the plot of CR as a function of tolerance (Fig. 6). Once again, for the same reasons as stated before, the CR reaches plateaus. All peculiarities mentioned before apply for the triangle wave.

The same data are redrawn (Fig. 7) so that comparisons can be made for a more practical range of tolerances. The performance of the zero-order techniques is almost unchanged, while that of the first-order techniques is improved. The FFP technique is noticeably improved at the lower tolerances, which is expected since the triangle has a well defined slope.

RMS error as a function of tolerance (Fig. 8) is also very similar to that of a sine wave; however, the errors are larger. It can be shown that the maximum theoretical error will occur when there is only one NRS. If that sample occurs at the peak, the error will be:

$$\% \text{ maximum rms} = \frac{\sqrt{\frac{1}{4} \left[ 2 \int_0^2 \left(\frac{1}{2} t\right)^2 dt \right]}}{0.287} \times 100 = 200\%$$

If the NRS occurs at the midpoint of the waveshape, the error will be:

$$\% \text{ maximum rms error} = \frac{\sqrt{\frac{1}{4} \left[ 4 \int_0^1 \left(\frac{1}{2} t\right)^2 dt \right]}}{0.287} \times 100 = 100\%$$

The fixed corridor of the FFP technique follows the slope of the triangle waveshape much closer; consequently, it no longer has periods in which the rms error remains constant. Otherwise, the techniques exhibit the same characteristics with one important exception: technique FVA began to oscillate. This is a result of the implementation, which may or may not be true for all implementations. For a well defined slope, all samples will be redundant except the first one. With each redundant sample, the corridor is updated, or decreased, until the upper and lower limits of the corridor essentially overlap. Thus, when an NRS occurs, the midpoint of the corridor of the preceding sample is

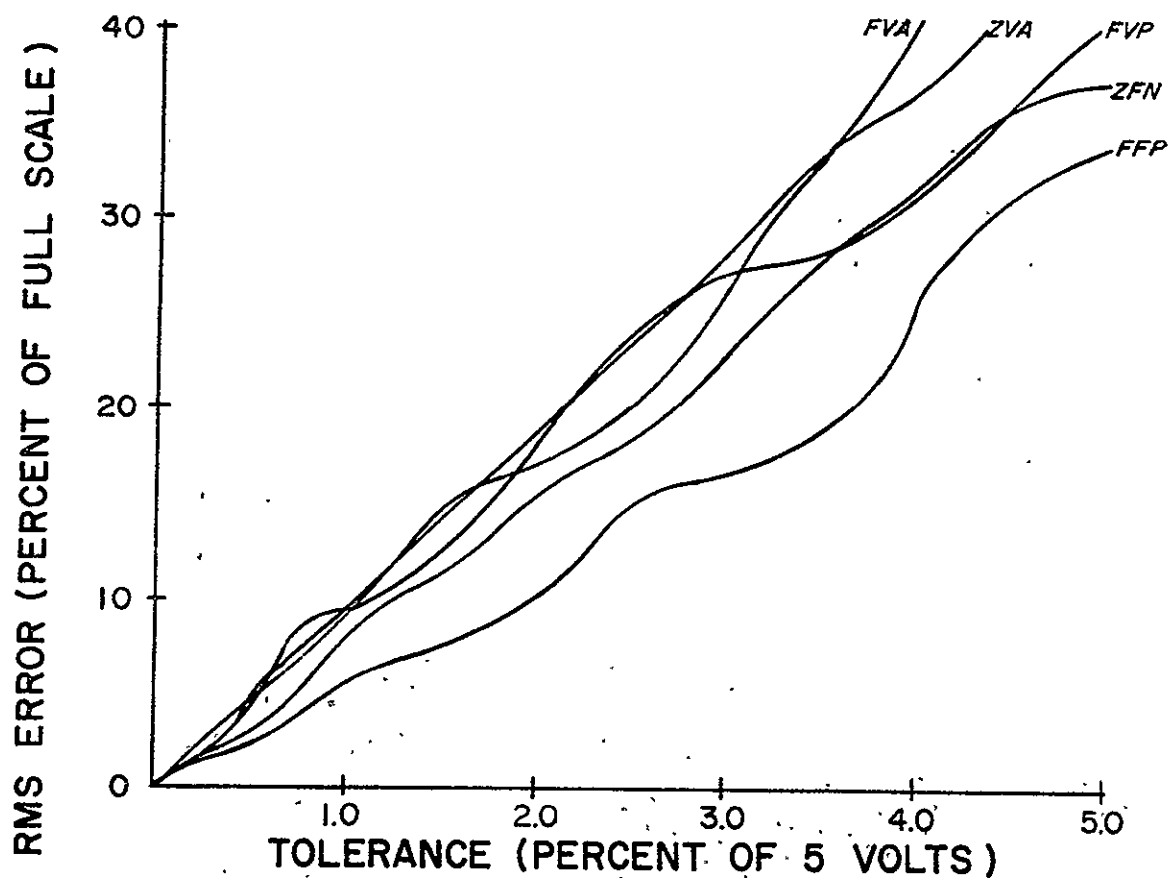


Figure 5. RMS error as a function of tolerance for a sine wave sampled at 10 000 samples per second.

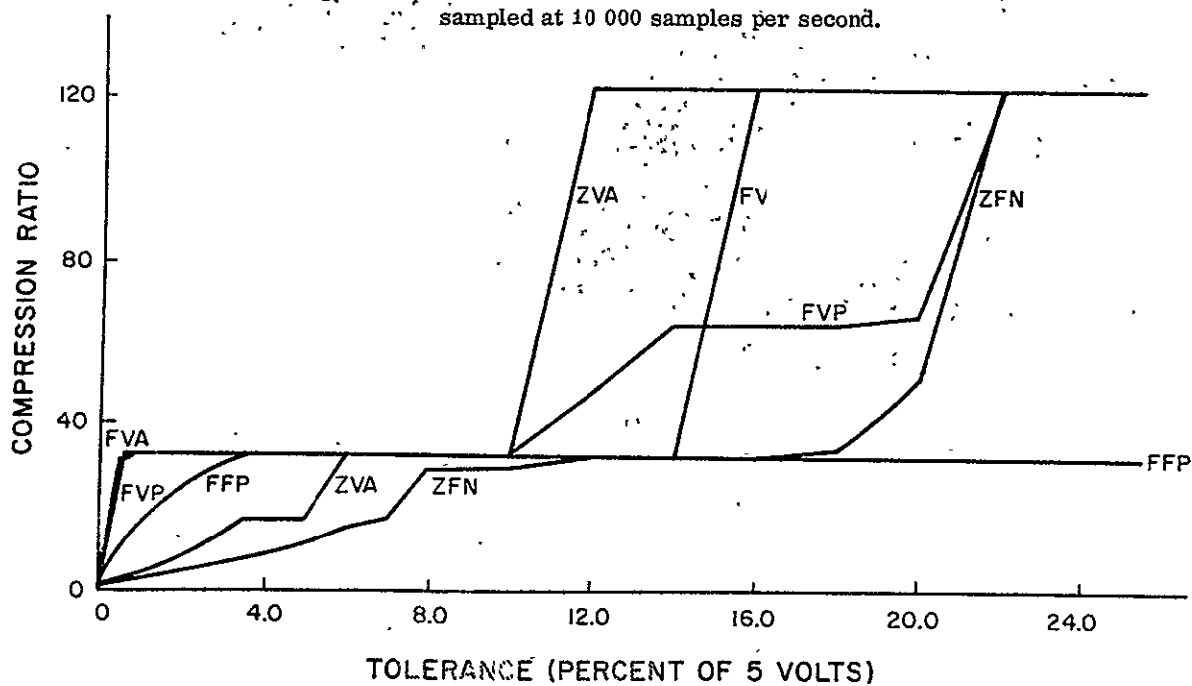


Figure 6. Compression ratio as a function of tolerance for a triangle wave sampled at 10 000 samples per second.

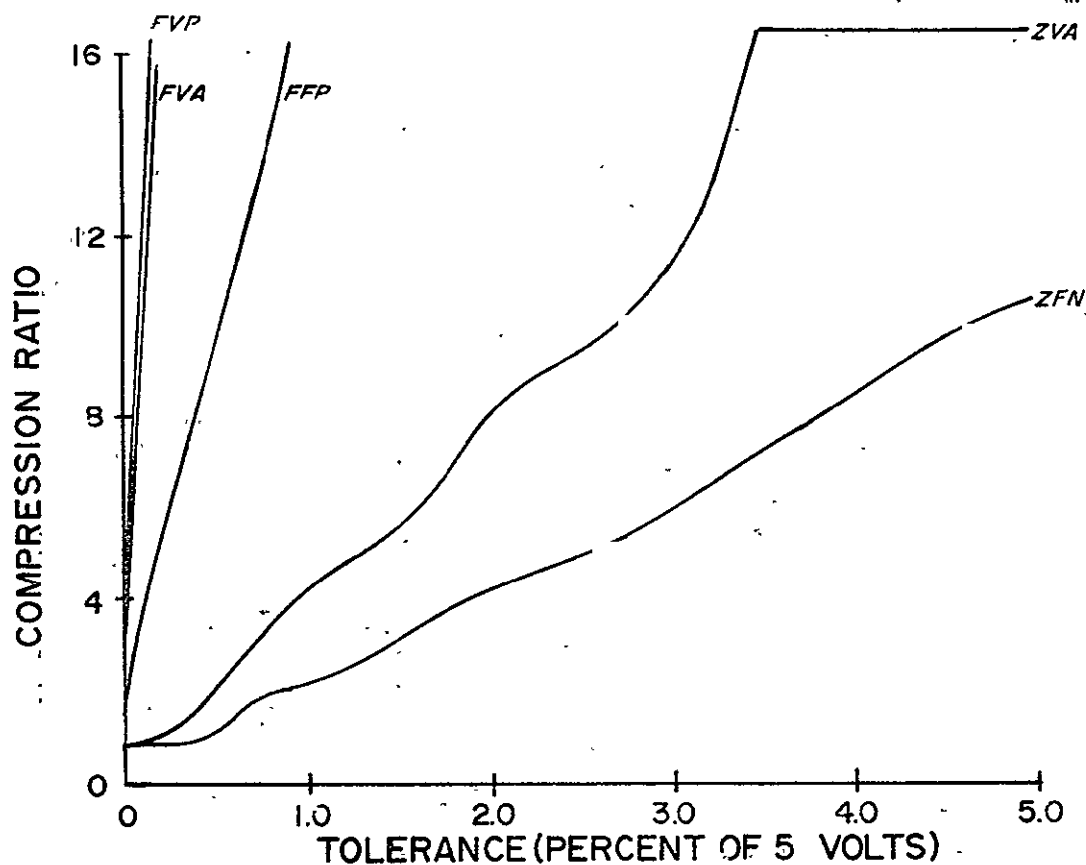


Figure 7. Compression ratio as a function of tolerance for a triangle wave sampled at 10 000 samples per second.

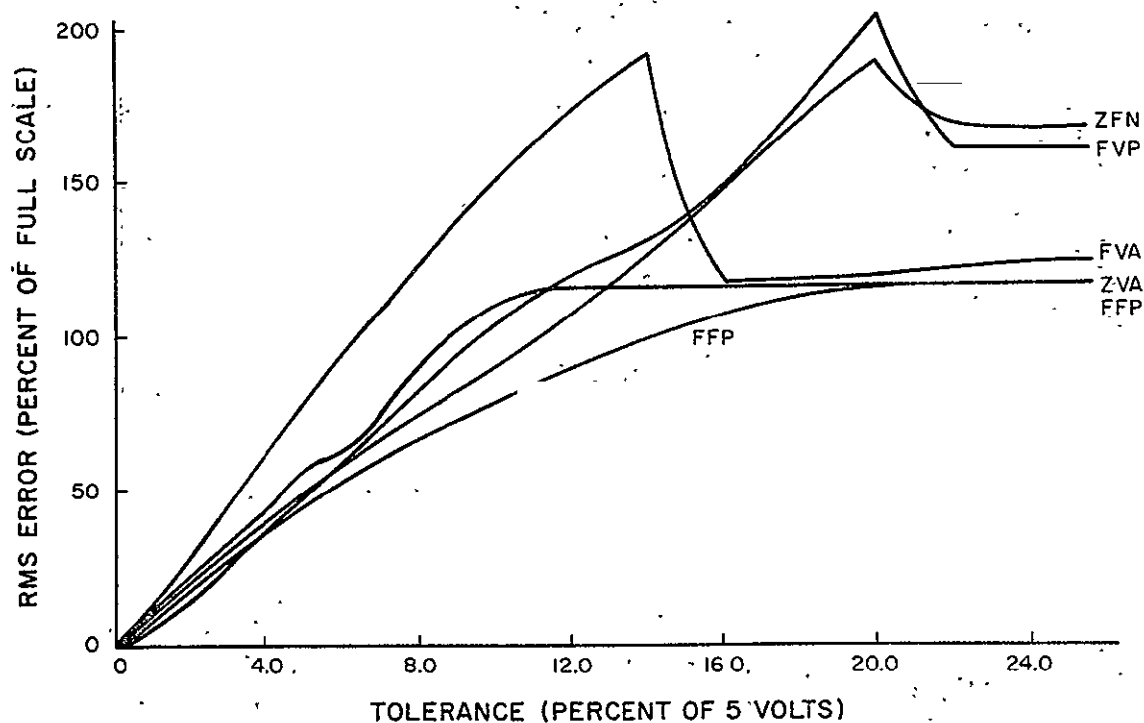


Figure 8. RMS error as a function of tolerance for a triangle wave sampled at 10 000 samples per second.

calculated for the transmitted sample. At this point, the arithmetic process breaks into oscillations. Thus far, oscillations have been detected only in the FVA technique.

The same data are redrawn (Fig. 9) at lower tolerances. In comparison, the FVA and FVP techniques have more error and the FFP technique has less error than they did for the sine wave. Otherwise, the results are the same.

Consolidating the CR and rms analyses shows which techniques are best for this type of data. The zero-order techniques are poor performers. The FFP technique does not excel at low tolerances but improves to equal performance with the FVP technique at a tolerance of 0.150 V. The FVA technique has the best performance at extremely low tolerances but is quickly surpassed by the FVP technique at a tolerance of 0.050 V. Overall, the FVP technique is superior. The oscillations of the FVA technique could prove to be a serious disadvantage in using this technique. This is based on the fact that many practical measurements, such as pressure and temperature, would fit this type of data model.

## Square Wave

Results from the plot of CR as a function of tolerance (Fig. 10) for a square wave differ radically from those obtained previously. Again, CR values reach plateaus, and the same explanation holds true. However, the fixed corridor of the FFP technique now allows it to encompass the entire wave shape, thus giving the maximum value of CR. All techniques quickly reach maximum CR since the bi-level wave is highly redundant. The difference here is that the zero-order techniques perform better than the first-order techniques.

The data are redrawn (Fig. 11) to illustrate this better. For the same value of tolerance, the zero-order techniques give the largest CR. In fact, all of the techniques give a comparatively larger value of CR. This is attributed to the data remaining constant for half of the time.

A study of the rms error over the full tolerance range (Fig. 12) shows, in comparison, a much smaller error for a given CR. Maximum error will again occur when there is only one NRS. When this

sample occurs at the peak, the maximum error will be:

$$\% \text{ maximum rms error} = \frac{\sqrt{\frac{1}{2} \int_0^1 (1)^2 dt}}{0.5} \times 100 = 141\%$$

This is the only value considered, since there is slight probability a sample will occur anywhere else.

The characteristics of a square wave do not allow maximum error to be achieved by any of the techniques. Minimum NRS is quickly achieved, and approximately half of the samples taken contribute no error.

The relative effectiveness of the techniques can be realized from the redrawn data (Fig. 12). All of the techniques give only a small error for the first 4 to 5 percent of tolerance. At this point, the techniques with variable corridors begin to increase rapidly in error. The ZFN and FFP techniques offer a very low error over a large tolerance range.

In conclusion, considering both CR and rms error, the ZVA and ZFN techniques give the best performance. However, the FVP and FFP techniques are equal to their performance at low tolerance in rms error, but provide only half as much CR. In general, technique FVA is a poor performer.

## CONCLUSIONS

Three significant conclusions resulted from this study. First, the telemetry redundancy analyzer facility can determine which of the five data compression techniques is best for any type of data. The same methods used on the simulated data could be used to determine the effectiveness of the techniques on data being generated by present and future data transmission systems.

Secondly, the five techniques implemented in the facility have been defined; i. e., their operation has been established. It is now possible to predict some, if not all, of the peculiarities of the technique. Whether these peculiarities will present advantages or disadvantages can be determined only with further study. For example, the oscillations that occurred

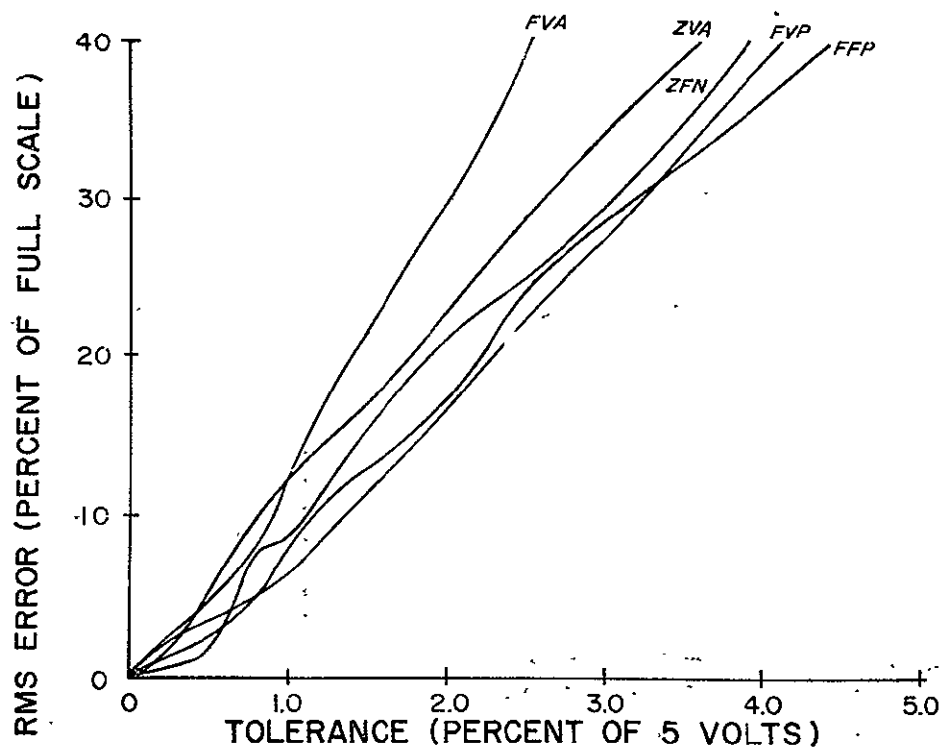


Figure 9. RMS error as a function of tolerance for a triangle wave, sampled at 10 000 samples per second.

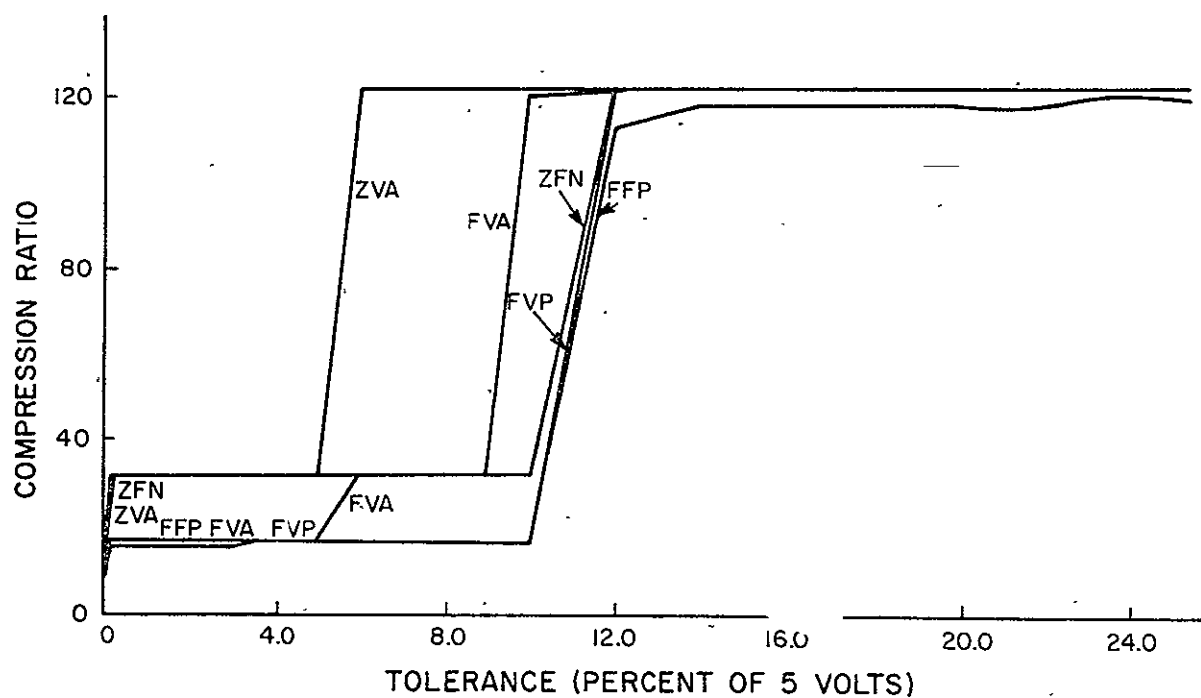


Figure 10. Compression ratio as a function of tolerance for a square wave, sampled at 10 000 samples per second.

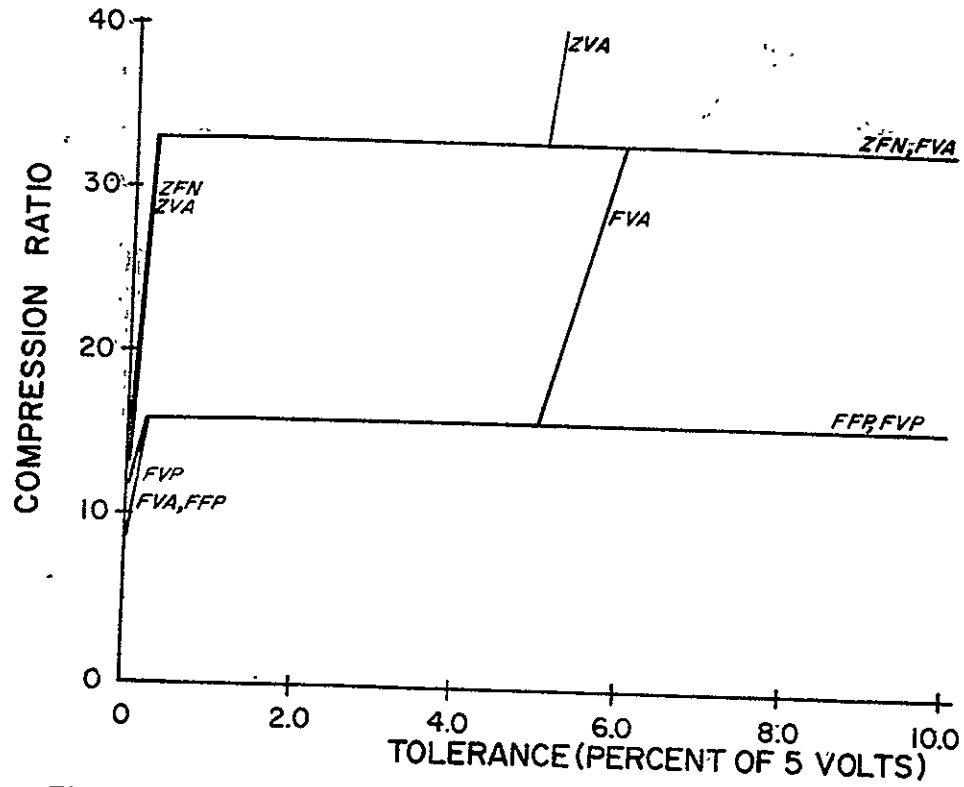


Figure 11. Compression ratio as a function of tolerance for a square wave sampled at 10 000 samples per second.

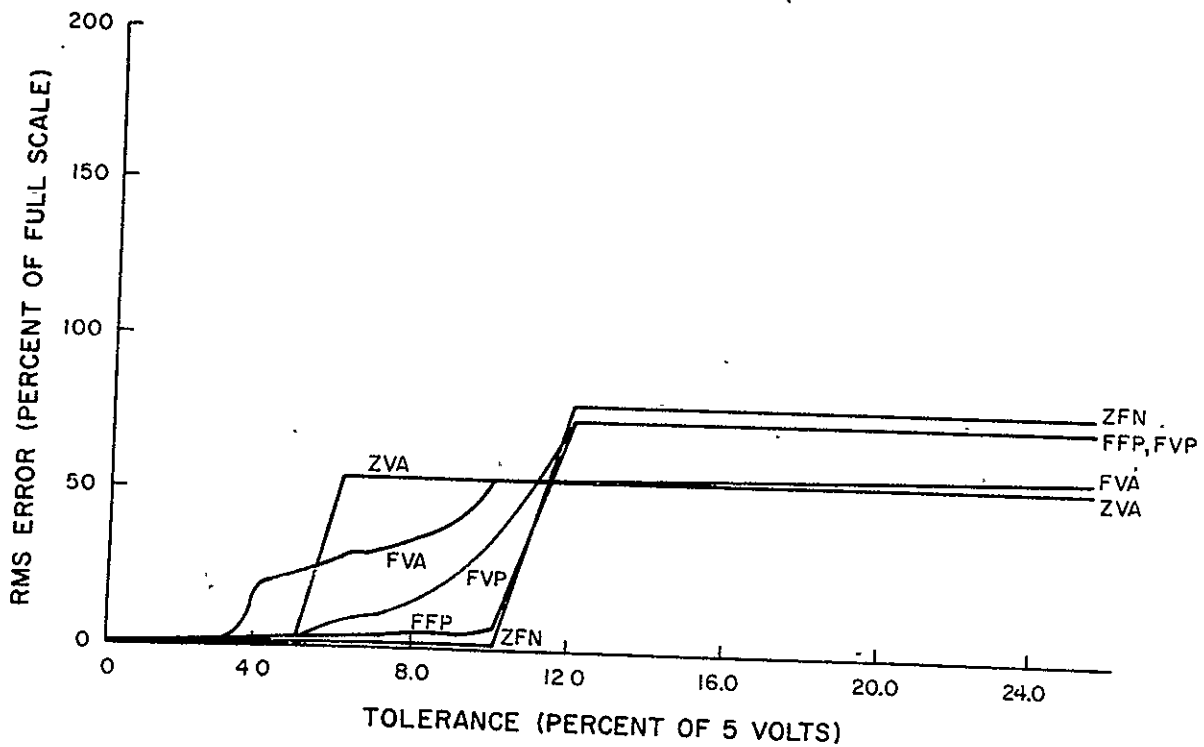


Figure 12. RMS error as a function of tolerance for a square wave sampled at 10 000 samples per second.

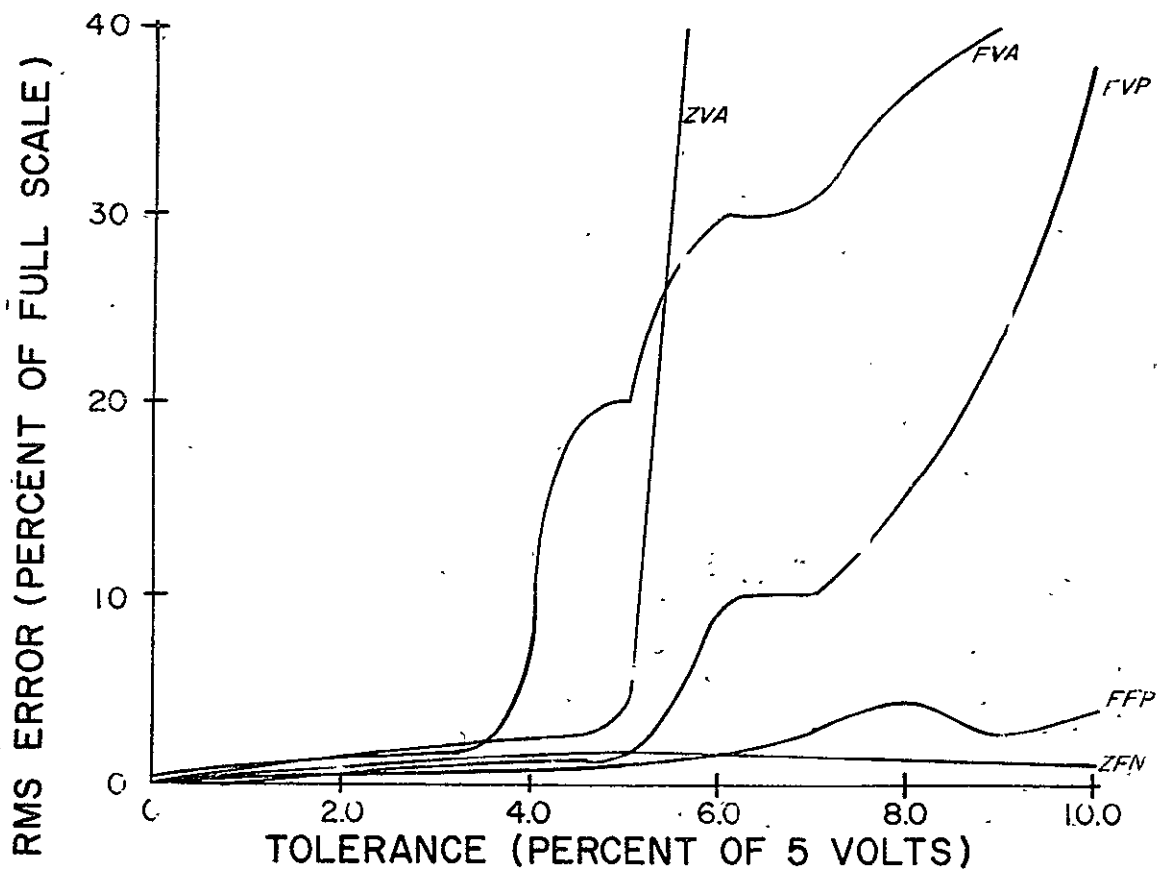


Figure 13. RMS error as a function of tolerance for a square wave sampled at 10 000 samples per second.

with the FVA technique are a disadvantage. Only further study will show if this technique should be rejected. Not all of the peculiarities can be attributed to the techniques. For example, the TRA must truncate after 127 successive redundant samples have been received.

Finally, knowledge gained here is instrumental in establishing whether data compression techniques offer any practical and beneficial use in data transmission systems. Certainly, no conclusions may

be drawn as to which technique is superior since deterministic signals would not be found in any practical situation. It should also be noted that the data were vastly oversampled. In spite of this, the techniques have demonstrated that they are capable of removing redundancy from data. At least one of the techniques, FVP, has demonstrated that it has promise. This does not imply that the others do not, since the results can, at best, be termed preliminary. As expected, one technique is not best for all types of data.

## REFERENCES

1. Frost, W. O.: Considerations in the Design of a Self-Adaptive Data Acquisition System. Masters Thesis, University of Alabama, 1969.
2. Haskew, R. J.; and Simpson, R. S.: A Study of Redundancy in Saturn Flight Data. University of Alabama, Bureau of Engineering Research, Technical Report No. 9, MSFC Contract NAS 8-20172, August 1966.
3. Telemetry Redundancy Analyzer System. Radiation Incorporated, MSFC Contract NAS 8-18011, Huntsville, Alabama, April 1967.



# AM BASEBAND TELEMETRY TECHNIQUES

By

J. J. Clubb

N71-29323  
INTRODUCTION

## SUMMARY

Techniques and circuits used to design a highly flexible telemetry system are discussed. This single sideband/double sideband/constant bandwidth compatible system conforms to Inter-Range Instrumentation Group (IRIG) standards.

## LIST OF ABBREVIATIONS

<u>Abbreviation</u>	<u>Meaning</u>
AGC	automatic gain control
AM	amplitude modulation
CBW	constant bandwidth
DSB	double sideband
DSB/FM	double sideband modulation of an FM carrier
FDM	frequency division multiplexer
FM	frequency modulation
PLL	phase-locked loop
QDSB	quadrature double sideband
RC	resistance capacitance
rf	radio frequency
SSB	single sideband
SSB/FM, SS/FM	single sideband modulation of an FM carrier

As early as 1966, the telemetry community was confronted with the critical problem of perfecting techniques to transmit shock, vibration, and acoustic information. Although moderately small quantities of wideband data channels had been a typical measuring requirement for more than a decade, the need for better methods to transmit these measurements had increased enormously. In addition to greatly increased numbers of channels, the users were also requesting that the performance be improved to provide dc response and waveform reproduction and to allow cross-correlation from channel to channel.

Some of the items responsible for these increases are the following: the physical size of space vehicles such as the Saturn requires a large number of dynamics measurements; the tremendous cost of building a large, complex space vehicle dictates that there be very few developmental launches; and very early in almost any program, man will probably be a passenger. Consider also the catastrophic effects that a vehicle failure can have on an entire program. For these reasons, the vibration and acoustic parameters of the vehicle must be defined as early and as completely as possible. To accomplish this, as many measurements as possible must be made on each flight. The effort described here deals with the study and development of hardware to meet the known and projected requirements for wideband data using AM baseband techniques.

## APPROACH

The first step in solving this problem was to determine the techniques that could potentially provide the desired performance. A study revealed that three techniques had good possibilities in this

area:

1. SS/FM — single sideband suppressed carrier amplitude modulation on a frequency modulated carrier.
2. DSB/FM — double sideband suppressed carrier amplitude modulation subcarriers on a frequency modulated carrier.
3. CBW FM/FM — constant bandwidth FM/FM arrangements of FM/FM channels with uniform response.

Each of these techniques has certain capabilities and limitations that will be described in more detail.

### SS/FM

Since telemetry equipment using the SS/FM technique has been utilized in recent years in the Saturn and certain Titan programs, early efforts were spent in determining any possible limitations and how SS/FM might be improved to the point of meeting the increased requirements.

The early equipment was designed primarily to provide data for power spectral density analysis and consequently was a nonphase coherent system. The phase response of individual channels and the uniformity of phase characteristics between channels were not adequate for measurements requiring waveform reproduction or cross-correlation analysis. Another problem was poor low frequency response along with large passband ripple. These deficiencies were primarily the result of implementation and component limitations rather than inherent shortcomings in the SS/FM technique.

An ideal SS/FM channel would provide dc channel response with a carrier component of fixed phase carrying the dc information. However, the technology for generating and detecting such a signal does not now exist, and dc response for SS/FM will probably not be achieved in the near future. Technology has progressed to the point where a considerable improvement over the earlier SS/FM system is possible. Although dc response could not be accomplished, channels having low passband ripple, uniform channel-to-channel phase response, and a low frequency response of 10 Hz were achieved.

Even though dc response was not possible for SS/FM, this technique was not completely rejected because it has two very favorable characteristics. In a typical measuring program for half or more of the total wideband channels, the user's only interest is power spectral density and SS/FM is ideally suited to provide this. The other factor is rf bandwidth utilization efficiency. In most measuring programs, the wideband data occupy 90 percent or more of the total rf bandwidth required to transmit all of the measurements. The availability of rf spectra is now limited and probably will become a critical problem in the future. Therefore, any system must have good bandwidth utilization efficiency. SS/FM has a two to one advantage over most other techniques. For these reasons, SS/FM was not completely discarded as a candidate.

### DSB/FM

For some applications, low frequency response and in many cases dc response along with good waveform reproduction are rigid requirements. Wideband data channels having dc response along with excellent phase characteristics can be achieved by the DSB/FM technique. As in SS/FM, dc information is provided by a carrier of fixed phase. In contrast to SS/FM, the generation and detection of this type of signal are well within the present state of the art.

A DSB/FM channel occupies twice the frequency space required for an SSB/FM channel. Therefore, with DSB/FM the data bandwidth accommodated is halved, or else only half as many channels can be handled per system.

A variation in the DSB/FM technique that will increase the bandwidth utilization efficiency is QDSB/FM. In QDSB/FM two data channels modulate carriers of the same frequency but differing in phase by 90 degrees. This allows two channels to occupy the frequency space normally occupied by one. Demodulation of a QDSB/FM signal is much more difficult than demodulation of a normal DSB/FM signal because any deviation from the 90-degree phase difference of the reinserted carriers will result in increased channel intermodulation. However, intermodulation distortion of less than 1 percent has been achieved for QDSB/FM.

## CBW FM/FM

Constant bandwidth is a variation of the familiar FM/FM technique, and this discussion covers AM baseband techniques. CBW FM/FM will not be discussed further except to point out that it has certain advantages in some cases and disadvantages in others.

## COMPATIBLE SSB/DSB/CBW

From the preceding discussion, note that each technique offers features that are advantageous to the data user but neither technique provides all of the transmission capabilities and characteristics that one might prefer. For a given wideband data application, assuming equal availability of equipment, the user's selection of a technique would likely vary with the specific requirements and data characteristics. If the user was primarily interested in power spectral density, he would probably choose SSB/FM to minimize rf power and spectral requirements. On the other hand, if the measurement required dc response and phase correlation over a relatively wide frequency range, the user might select DSB/FM. If the user's primary interest was medium response channels to reproduce waveforms with low distortion and a high signal-to-noise ratio, then CBW FM/FM might be a better choice.

An optimum system would allow the user to select the type of channel that best suited his needs. Toward this goal, a hybrid system that allows each channel to use either of the techniques has been developed. This hybrid concept permits a flexible intermixing of SSB, DSB, or CBW subcarriers on an rf link.

## MULTIPLEXER

The major problems involved in the design of AM baseband equipment are: (1) subcarrier summing; (2) automatic gain control and correction; and (3) derivation and reconstruction of carriers. These problems are almost the same for either SSB or DSB. It is only necessary to either use or bypass sideband filtering in the multiplex operation and make minor changes in the demultiplexer equipment to accommodate either type of channel. Since DSB occupies twice the bandwidth of SSB, the data bandwidth must be

halved, alternate channels must be deleted, or the QDSB technique must be used for DSB channels.

The hybrid baseband system was designed to achieve compatibility with existing as well as contemplated telemetry standards. Compatibility was accomplished through judicious arrangements of interchangeable "plug in" assemblies of "universal" circuit designs.

As is the usual case, there were two similar but distinct problem areas in designing equipment for this system: a multiplexer operation where many signals are combined for transmission as one composite signal, and a demultiplexer operation where the components of the composite signal are separated and the original signals are recovered. The multiplexer will, in almost all cases, be used in an airborne application; therefore, size, weight, power consumption, and intended environment must be major considerations during the design. For the demultiplexer these were only minor considerations since it is usually ground-based in a controlled environment.

The multiplexer shown in Figure 1 is typical of an airborne unit for use with wideband data.

The multiplexer will accept up to 24 data channels plus a special service channel. The multiplexer is capable of SSB operation or DSB operation. Channel frequency allocations are every 4 kHz from 4 kHz to 104 kHz with 64 kHz and 68 kHz used for pilot and reference tones. The channels illustrated in Figure 2 allow data frequencies of 10 Hz to 2000 Hz on all 24 channels during SSB operation, dc to 1000 Hz on all 24 channels or dc to 2000 Hz on 12 channels during DSB operation, or any compatible combination thereof.

The channels can be combined in any manner at either combiner A or combiner B; however, the pilot tone always goes to combiner A and the reference tone to combiner B. The output of combiner A is passed through an AGC circuit before being passed on to combiner B. The two paths allow portions of the data to bypass the AGC loop if desired. The pilot tone serves as an amplitude and frequency reference for the demodulation process in the demultiplexer. The reference tone serves to remove ambiguities inherent in the carrier synthesis operation.

The multiplexer is a phase coherent system; therefore, all channel, pilot, and reference frequencies are developed in 26 separate voltage-controlled crystal oscillators that are phase-locked to components of a harmonic spectrum that is derived from an extremely stable master oscillator.

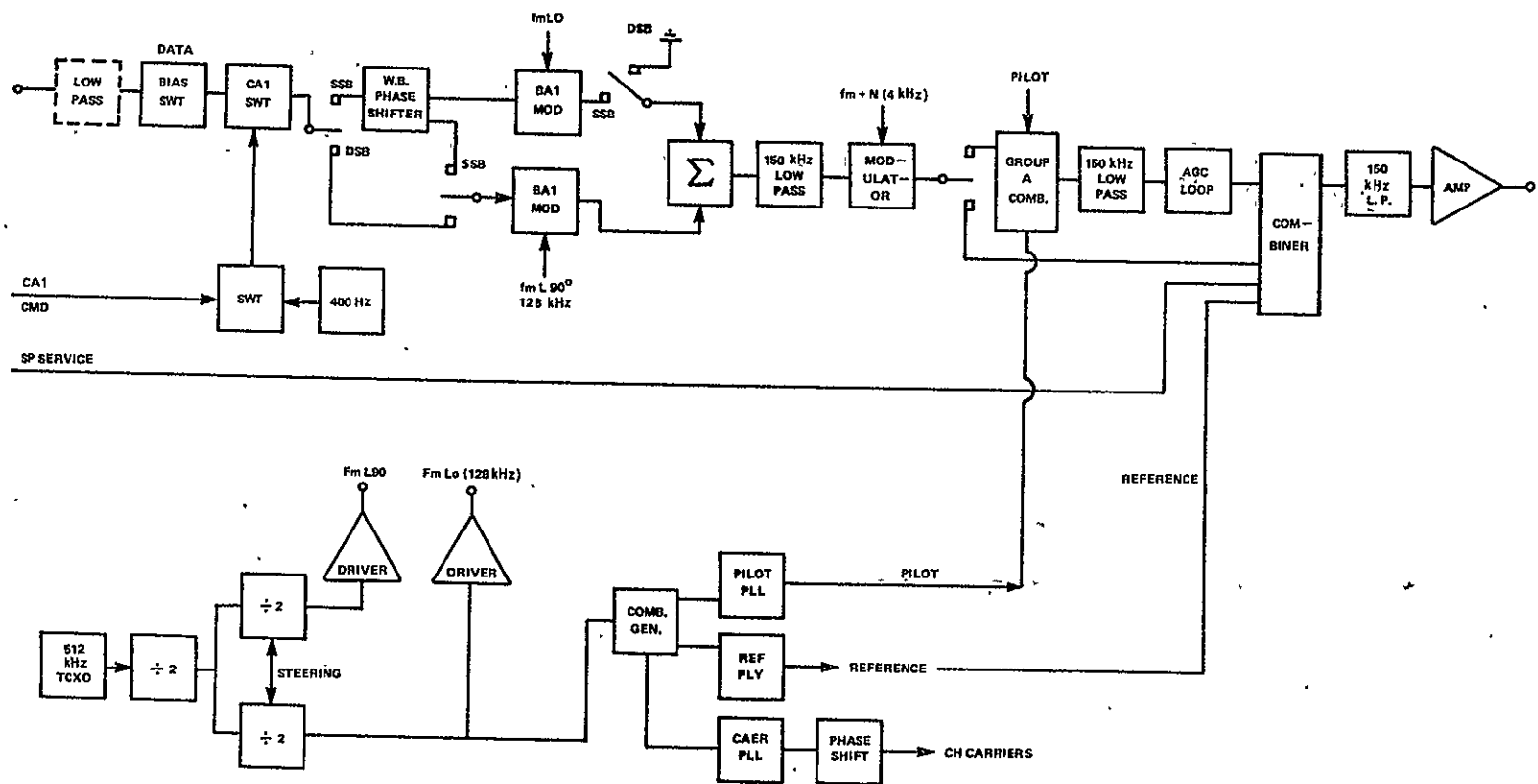


Figure 1. Multiplexer block diagram.

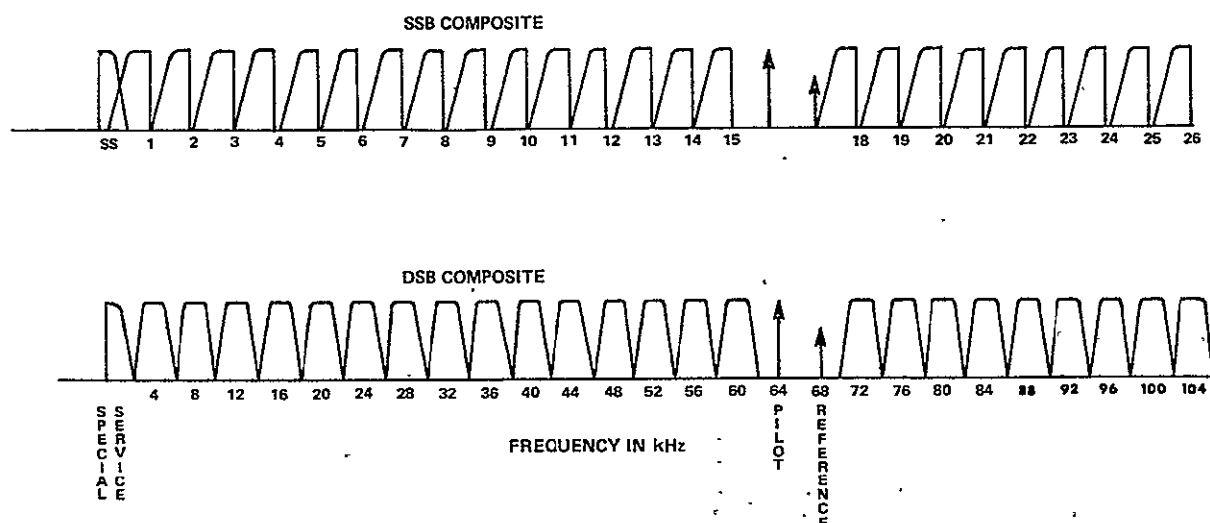


Figure 2. Multiplexer composite output.

A channel unit consists of input buffer stages, a wide-band phase-shifter, three balanced modulators, a summing amplifier, and a low-pass filter. Provisions are contained so that any channel may be switched to either SSB or DSB. Provisions are also contained for changing the channel units to accept signals riding on either a 0 Vdc or 2.5 Vdc reference level. All channel units use a double-frequency translation modulation technique that makes each channel unit frequency independent and eases the filter design problems.

The multiplexer achieves a carrier and null signal suppression of 50 dB for both SSB and DSB operation and 50 dB of sideband suppression in the SSB mode (Figs. 3 and 4). The amount of sideband suppression achieved during SSB operation is determined by the accuracy with which quadrature is achieved. For the case of the data frequencies, the frequency can range from 10 Hz to 2000 Hz. A quadrature accuracy of  $90 \pm 0.16$  degrees is necessary at all frequencies to obtain a sideband suppression of 50 dB. The circuit selected to accomplish this is a 10-pole RC wideband phase-difference network.

## DEMULTIPLEXER

A multiplexer is usually designed to a fixed set of requirements to fulfill a particular mission. The demultiplexer, however, should be a universal type having parameters that may be easily selected to be compatible with many different multiplexers. In almost any working application of such a system,

there will be a tape recorder in the interface between the multiplexer and the demultiplexer. The recorder will impact dynamic time base errors on everything in the composite signal. This one factor alone greatly increases the demands placed upon the demultiplexer performance.

The circuitry used to separate the pilot tone from the composite signal, in this case a phase-locked loop, must be able to accurately track as the pilot frequency is disturbed by speed errors in the tape recorder. This suggests a loop with a relatively wide bandwidth, but the loop bandwidth should be restricted to prevent noise in the baseband around the pilot frequency from disturbing the loop. These requirements are in conflict, and the design of the pilot extraction circuits was one of the most difficult problems that had to be solved.

Another difficult problem was matching the time delay through the different paths that the carrier information and the data information must travel. As Figure 5 illustrates, it was necessary to process the composite signal in parts to equalize the delay. The low frequency portion is up-converted before being subjected to filtering. The frequency is then corrected in later operations for the low frequency portion of the composite signal.

Figure 6, an expanded version of Figure 5, illustrates the various options that the demultiplexer provides to the user. This system is versatile enough that it will be suitable for all except the very specialized or unusual multiplexers. Table 1 contains a list of the important parameters for this system.

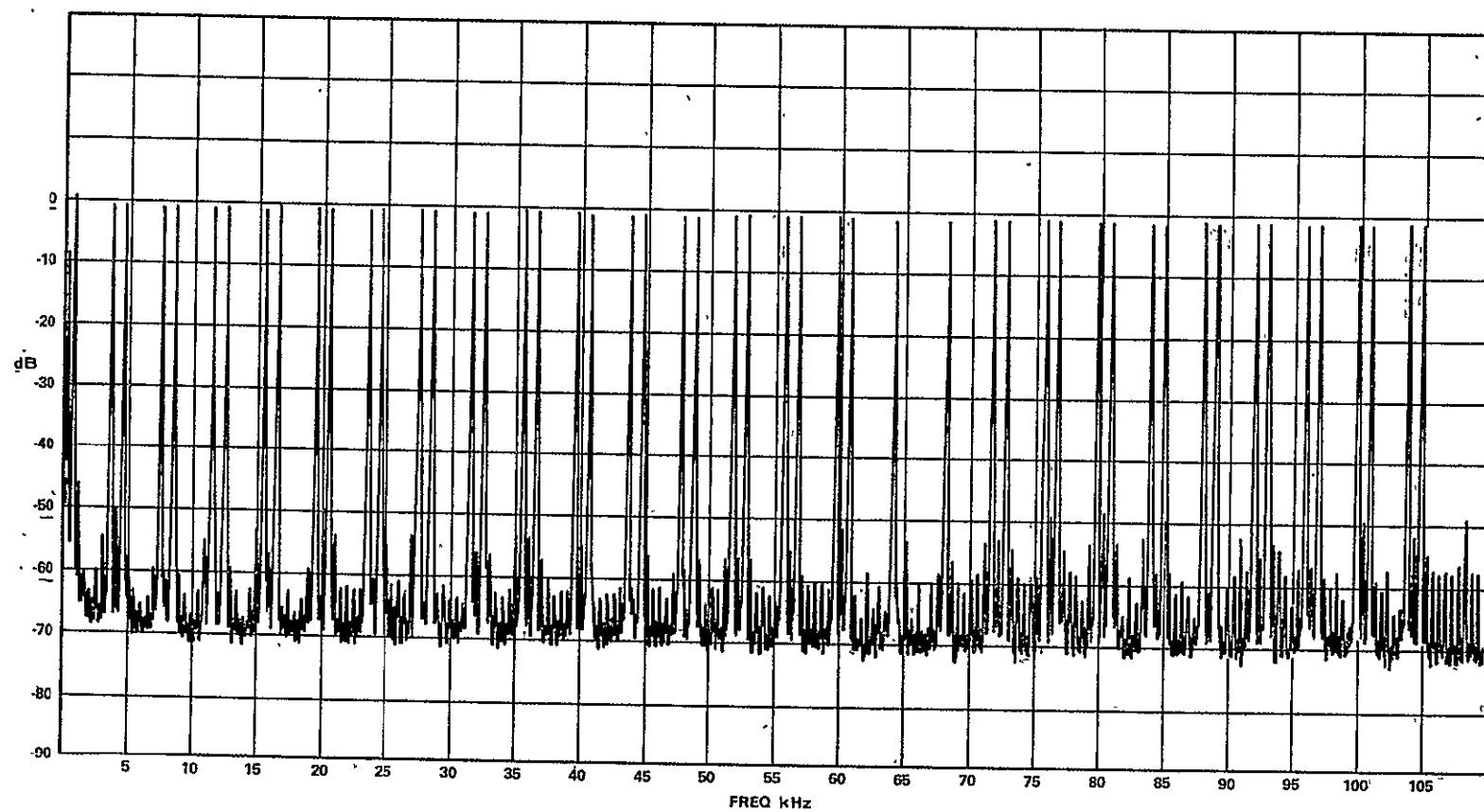


Figure 3. Double sideband output from the multiplexer.

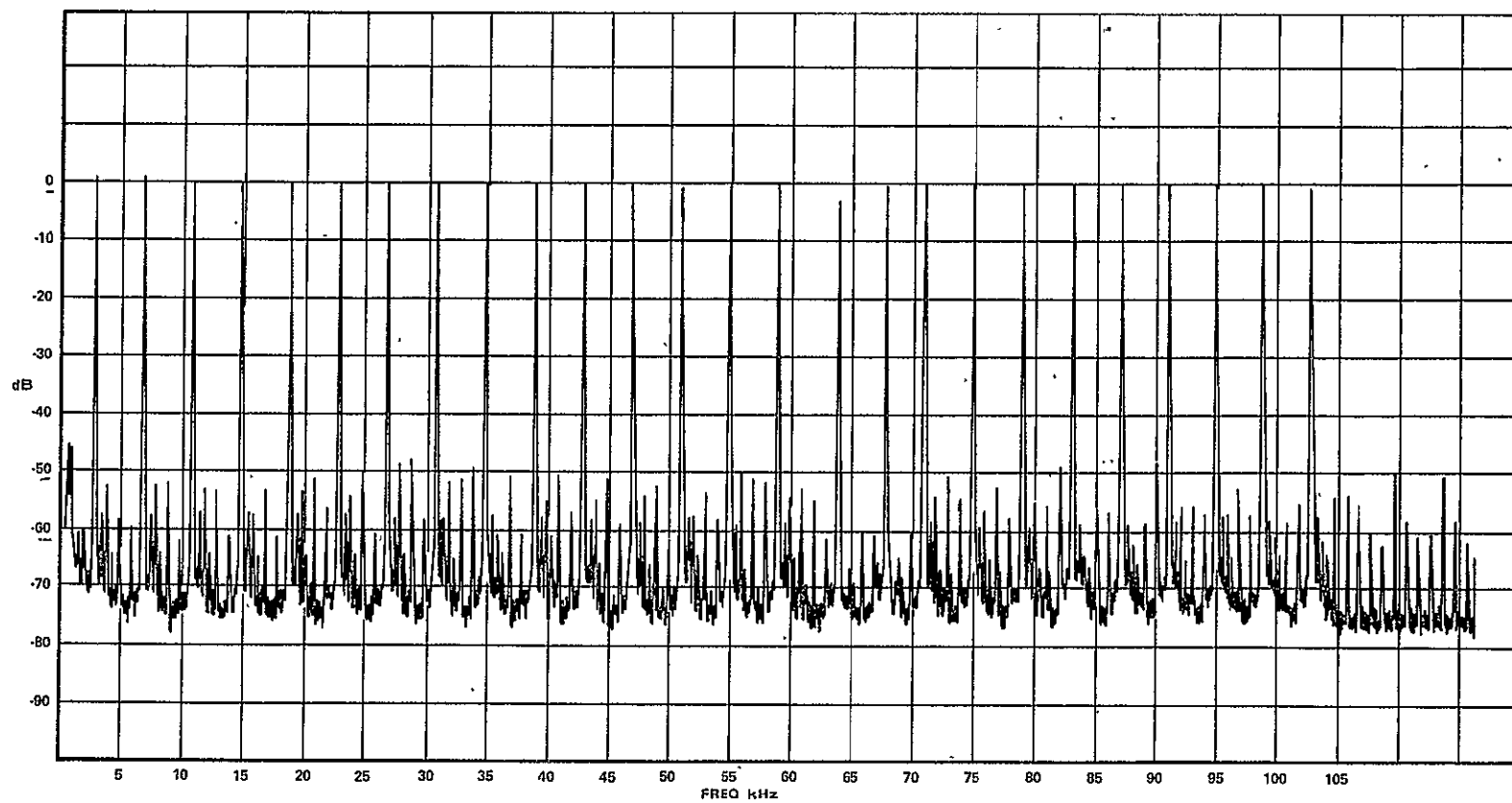


Figure 4. Single sideband output from the multiplexer.

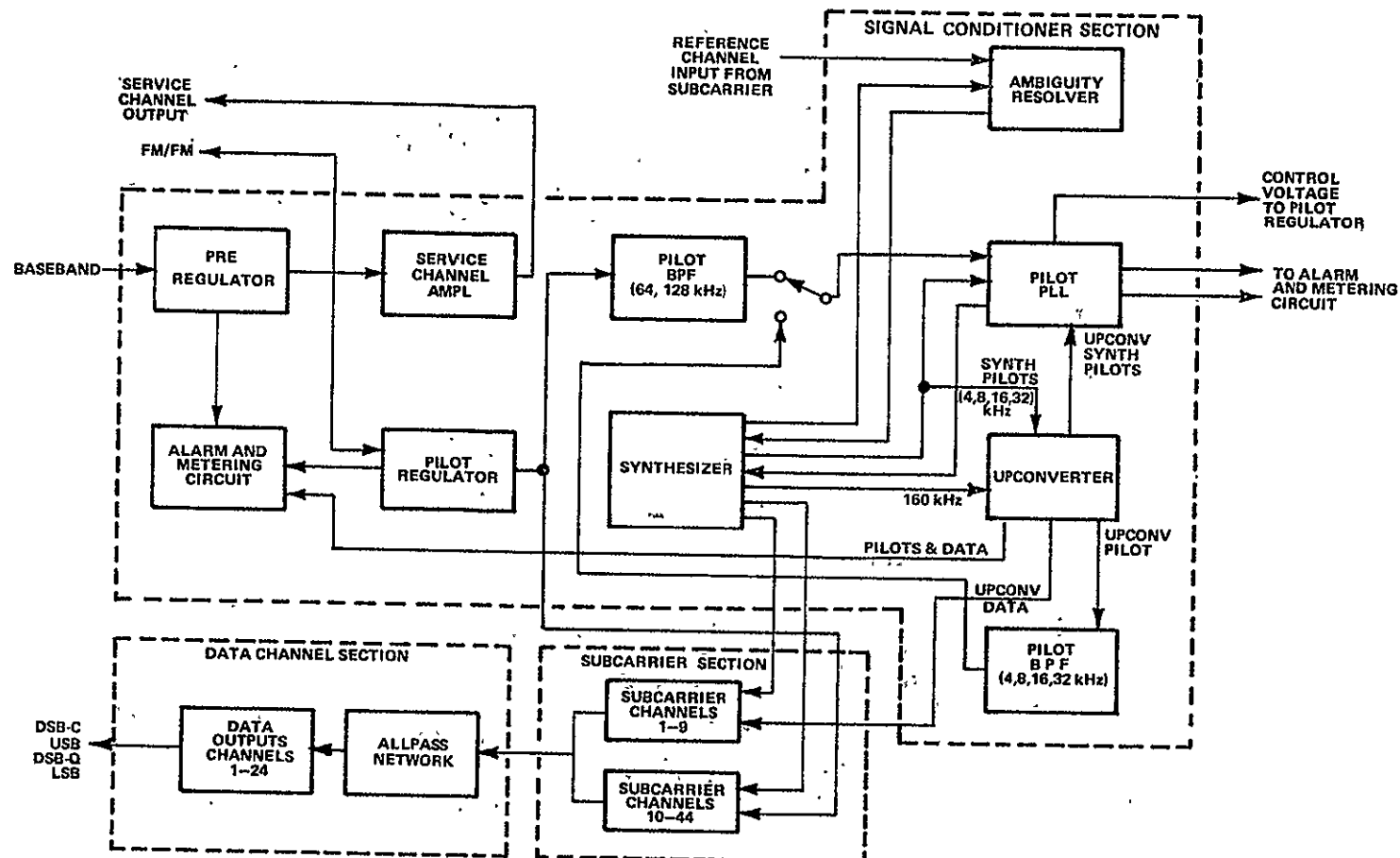


Figure 5. FDM demultiplexer overall block diagram.



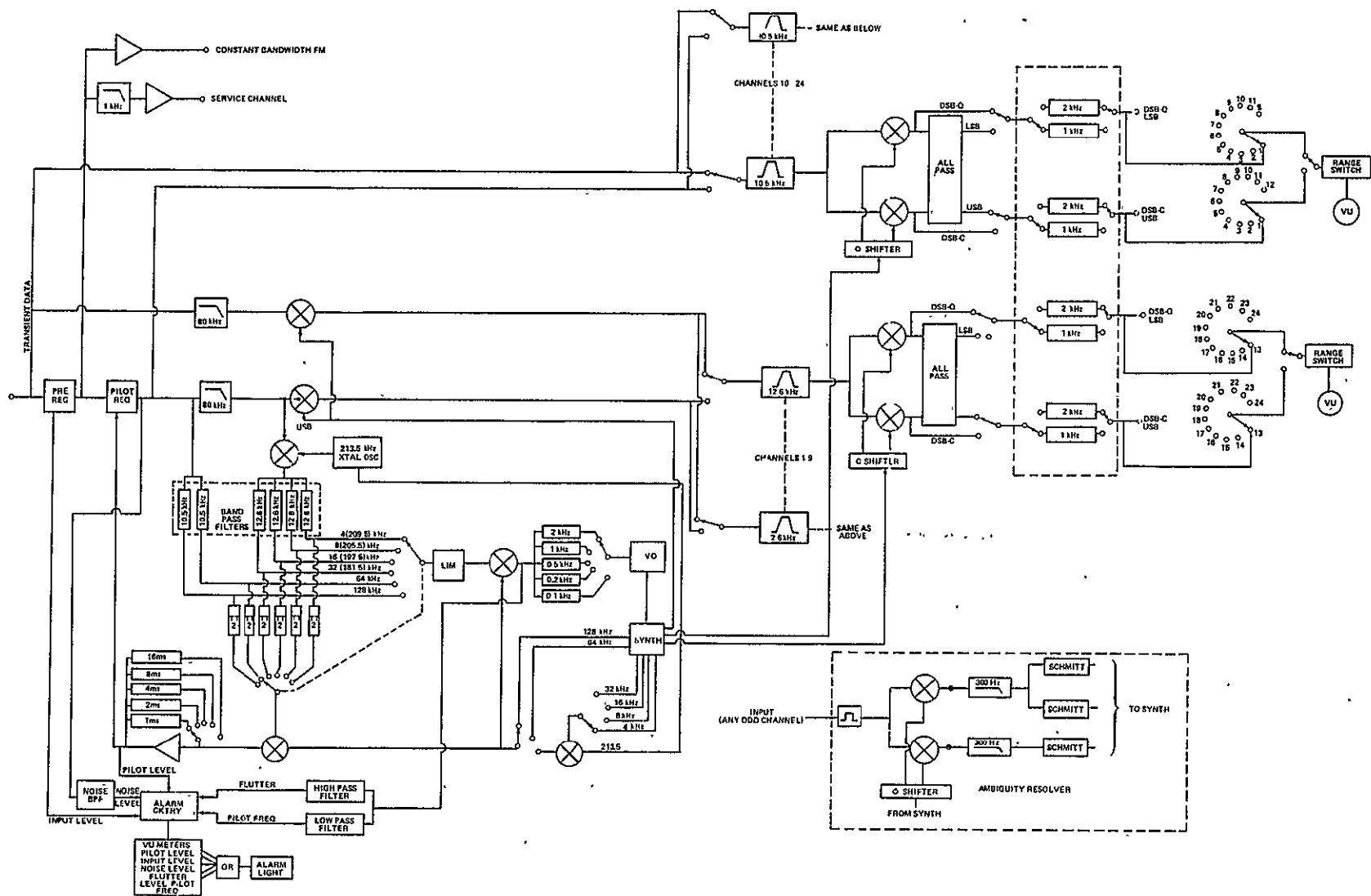


Figure 6. Demultiplexer.

TABLE 1. EQUIPMENT SPECIFICATIONS

Item	Specification
<u>Data Input</u>	
Frequency	10 Hz to 176 kHz
Impedance	Greater than 10 K
Input level	0.24 to 4 V rms
<u>Common Equipment</u>	
Preregulator attack and recovery time	0.4 s (attack), 0.9 s (recovery)
Pilot regulator output (AGC)	$\pm 0.25$ dB for 26 dB change in input level
AGC attack and recovery time	Selectable from 1, 2, 4, 8, or 16 ms, $\pm 10$ percent
Subcarrier generation	44 subcarriers accommodating 4 kHz to 176 kHz in 4-kHz steps
Subcarrier phase	0 to 360 deg
Subcarrier ambiguity remover	Operable with reference tone on any odd harmonic of 4 kHz
Pilot frequencies	4, 8, 16, 32, 64, or 128 kHz
Pilot PLL bandwidth control	Front panel selectable: 50, 100, 250 Hz or 500 Hz closed loop half bandwidth
Alarm Function	Generates alarm in event that one or more of the following conditions are obtained: <ul style="list-style-type: none"> <li>S/N ratio below prescribed level</li> <li>Flutter (on pilot) in excess of 1 percent</li> <li>Pilot level not within <math>\pm 0.5</math> percent of prescribed level</li> <li>Input level below 0.25 V rms</li> <li>Pilot frequency in excess of <math>\pm 1</math> percent</li> </ul>
<u>Channel Units</u>	
Channel output quality (24 channels)	No more than 0.3 percent degradation referred to full scale
Subcarrier capability	Each channel capable of handling QDSB or SSB
Subcarrier modulation mode	DSB - 0 deg and DSB - 90 deg simultaneously available, or upper and lower sideband

TABLE 1. (Concluded)

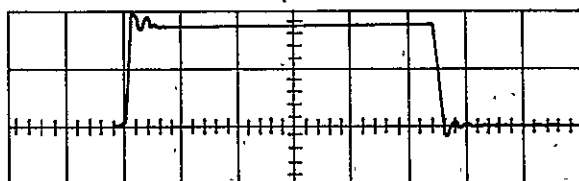
Item	Specification
Phasing network frequency range	10 Hz to 3 kHz
Rejection level	More than 50 dB
Filter output	Flat to 0.1 dB over full range, dc to 1 kHz and dc to 2 kHz
Rolloff	36 dB/oct
Output	14 V peak-to-peak across 300 $\Omega$
Time correlation (channel-to-channel)	Within 5 $\mu$ s at any frequency
Linearity	Within 0.1 dB over a 50 dB change in input
Intermodulation (each channel)	50 dB down from full scale mid-frequency response with all other channels loaded to full response individually
Total error	Less than 0.5 percent referred to full scale with all other channels loaded half scale with noncoherent noise
Tape recorded data input	System meets detail design requirements when using data subjected to perturbations induced by tape recorder WOW and flutter for rates equal to or below 500 Hz
Temperature range through which equipment is operable	+ 15 to 35°C

## OVERALL PERFORMANCE

The complete system has been extensively tested both with and without a tape recorder in the interface between the multiplexer and the demultiplexer. The tests demonstrated that this system has good dc response, excellent phase characteristics, and faithful waveform reproduction. To illustrate the performance, various frequency square waves were applied to the input and photographs were made of the corresponding output. Figure 7 is the output for a 50-Hz square wave input. Figure 7 shows the overall system performance very well and demonstrates that the working system does meet the original design goals.

## CONCLUSIONS

The initial goals of this work have been met successfully in that techniques to transmit wideband data have been perfected. Solutions to the major



SQUARE WAVE RESPONSE

50-Hz SQUARE WAVE INPUT SIGNAL APPLIED TO A DOUBLE SIDEBAND CHANNEL

Figure 7. System performance.

problems were found, and actual equipment was built and tested as a means of verifying acceptable performance using present state-of-the-art components.

A system of this type is well suited for aerospace applications where shock, vibration, or acoustic types of data must be efficiently processed.

PRECEDING PAGE BLANK NOT FOLLOWS

# HIGH STABILITY FM TV TRANSMITTER WITH SAMPLED AUTOMATIC FREQUENCY CONTROL

By

M. A. Honnell\*

N71-29324

## SUMMARY

An S-band frequency-modulated (FM) television transmitter designed to drive a traveling-wave-tube amplifier is described. It provides an 18-MHz peak-to-peak deviation at video frequencies up to 10 MHz. A frequency stability of  $\pm 0.001$  percent is achieved by alternately sampling the voltage-controlled oscillator (VCO) signal during the backporch interval of the video signal and a crystal-controlled reference signal at intervals between the sync pulse.

## INTRODUCTION

During the past several years the Instrumentation and Communication Division of the Astrionics Laboratory has supported the successful development of L- and S-band frequency-modulated television transmitters with video bandwidths exceeding those of commercial TV broadcasting systems and with power outputs up to 5 W. These transmitters were used for such tasks as the viewing of the panel deployment on the Pegasus, the viewing of liquid hydrogen in orbit, and the study of radar altimeter pulses reflected from the ocean.

The TV transmitters developed for these missions used open-loop systems with voltage-controlled oscillators carefully temperature-compensated for the required frequency stability. This compensation process is slow, and the open-loop system provides no protection against frequency drift caused by aging effects. The major advantages of the open-loop designs employed are (1) circuit simplicity, (2) wide frequency deviation, and (3) direct current response.

A better solution of the frequency-control problem is obtained by up-converting the VCO signal by mixing it with a crystal-controlled high frequency signal. This system also suffers from aging drifts and presents modulation linearity problems when wide frequency deviation is required.

A sampled automatic frequency control (AFC) system is capable of providing good frequency stability and permits wide frequency deviation with good linearity. Furthermore, in an FM TV transmitter, good low frequency response may be obtained by clamping the video-modulated signal to a fixed reference frequency. The price paid for this performance is one of greatly increased circuit complexity. The availability of integrated circuits to perform amplifying and logic functions led to the decision to utilize a sampled AFC system in the S-band FM television transmitter shown in Figure 1.

The upper part of the gold-plated aluminum case contains the radio-frequency (rf) circuits, a switching-logic section, the sampled AFC system, and a crystal-controlled reference signal source. The lower part of the case contains the dc-to-dc converter. Individual compartments are provided for critical circuit modules. Coaxial transmission lines are used for all radio-frequency and switching signal interconnections. The dc supply voltages are distributed through multisection rf filters to each individual circuit module.

## SPECIFICATIONS

The transmitter specifications tabulated in Table 1 require an easily achievable S-band power input of 80 mW to drive a traveling-wave-tube amplifier.

\* The author wishes to acknowledge that Dr. W. E. Faust and Dr. Harry L. Deffebach as graduate students under the author's supervision developed the transmitter for NASA project NAS8-11184.

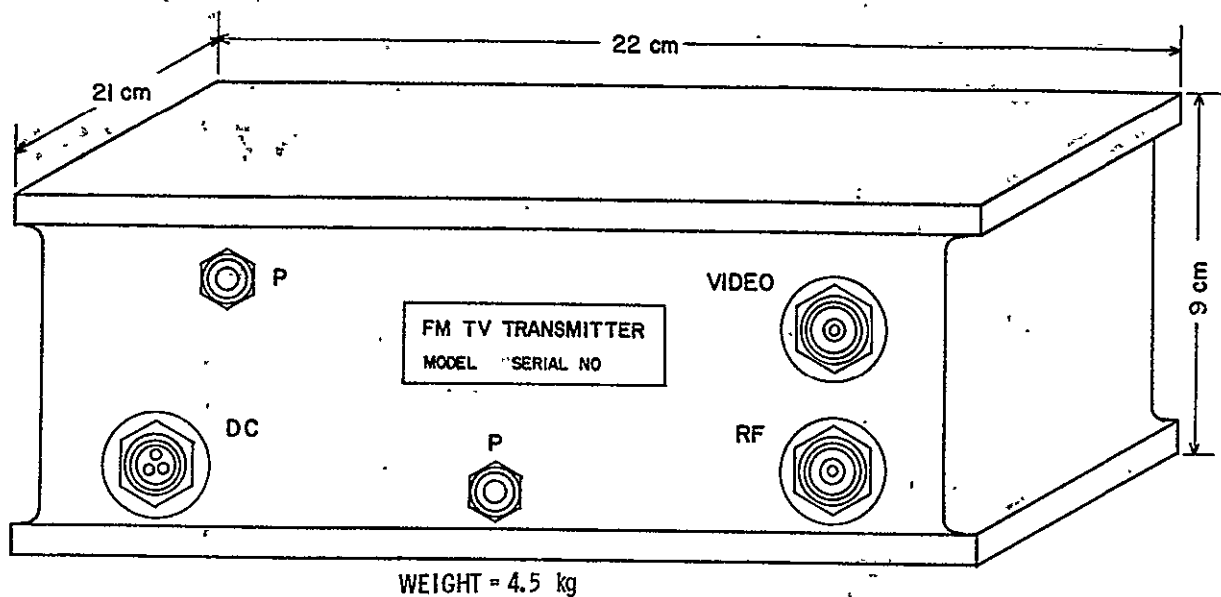


Figure 1. S-band FM television transmitter.

TABLE 1. SPECIFICATIONS OF S-BAND FM TV TRANSMITTER

Video input impedance	75 $\Omega$
Video input signal (negative, sync tip)	1.4 V peak-to-peak
Video bandwidth ( $\pm 1$ dB)	10 MHz
Vertical field frequency	60 Hz, 2/1 interlace
Horizontal scan frequency	15 750 Hz
Modulation — FM	18 MHz peak-to-peak
Backporch frequency	2250 MHz
Frequency stability limit	$\pm 0.01$ percent
Rf bandwidth ( $\pm 1$ dB)	20 MHz
Rf power output	80 mW
Rf output impedance	50 $\Omega$
Power input	28 Vdc, 600 mA
Case	Pressurized
Dimensions	9 by 21 by 22 cm
Weight	4.5 kg

The input video signal has the same scanning standards as used in television broadcasting. The specifications of 18 MHz peak-to-peak deviation for modulation frequencies up to 10 MHz and a frequency stability limit of  $\pm 0.01$  percent are particularly difficult to meet.

An appreciation of the problem involved may be obtained by looking at the video input signal for one horizontal line shown in Figure 2. It is noted that the backporch (BP) is clamped to 0 V. To transmit this signal in a minimum bandwidth, the BP of the frequency-modulated signal is clamped to the 2250 MHz carrier reference frequency. The instantaneous frequency excursion is 5.15 MHz downward and a maximum of 12.85 MHz upward, corresponding to a maximum white signal.

This is achieved by sampling the signal at the output of the VCO during the BP interval and comparing the frequency of this signal with a sample of a crystal-controlled frequency. The BP of the modulating video signal is then clamped to the error signal with the proper polarity to correct the VCO frequency during this interval.

## SYSTEM DESCRIPTION

A simplified block diagram of the system is shown in Figure 3. Solid-state circuit devices are used throughout.

The FM signal section along the top of Figure 3 receives a 1.4-V peak-to-peak video signal for maximum deviation. This signal is amplified to 1.8 V peak-to-peak to deviate the frequency of the VCO 1.8 MHz peak-to-peak. The output of the VCO

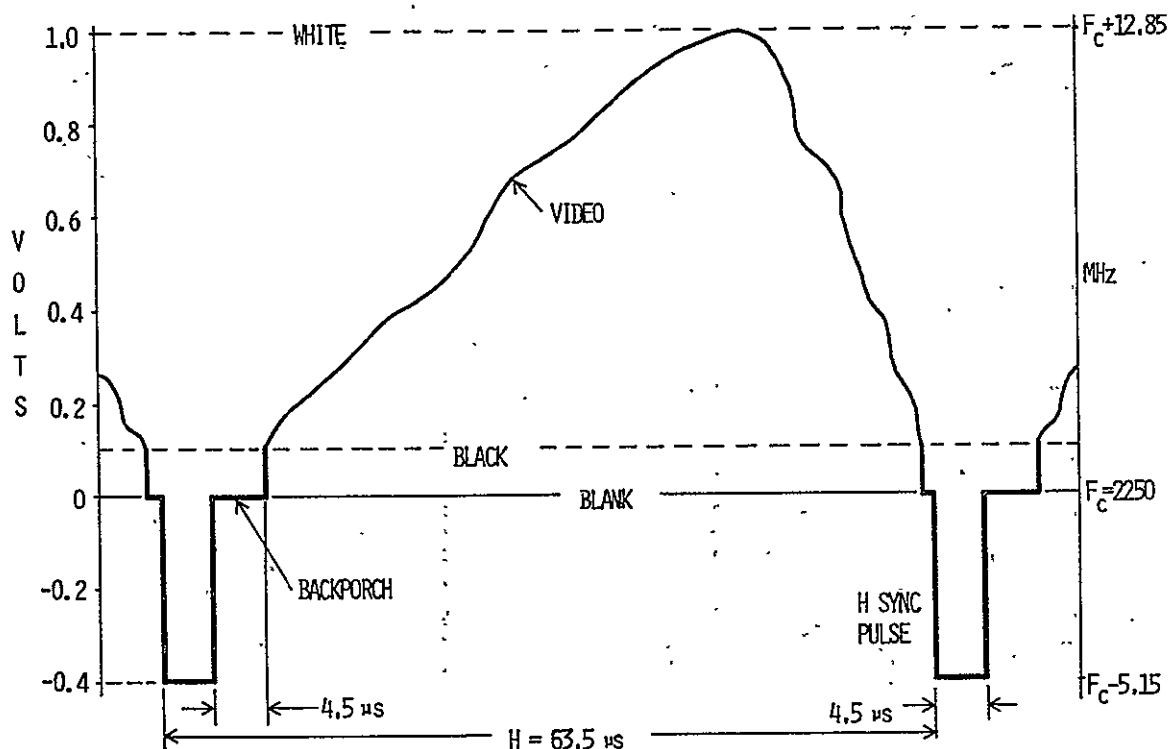


Figure 2. Video signal and carrier frequency deviation.

is amplified to a 3-W level at 225 MHz which is used to drive a times-ten frequency multiplier utilizing a step-recovery diode. The frequency deviation at this point is 18 MHz peak-to-peak. The 2250-MHz output is passed through a bandpass filter to reduce spurious sideband frequencies.

Along the right side of Figure 3 is a 45-MHz crystal-controlled reference signal source followed by a times-four transistor frequency multiplier and a 180-MHz amplifier. The 180-MHz output is heterodyned with a 225-MHz signal from the amplifier following the VCO to produce a signal of 45 MHz plus the frequency error. A diode switch alternately gates this signal and the 45-MHz reference signal through a two-stage limiter to the discriminator.

The 45-MHz VCO signal is sampled by a diode rf switch for approximately half a horizontal sync period (33  $\mu$ s) with the midpoint of the sample centered on the BP of the video signal. The 45-MHz reference signal is sampled for the remainder of the horizontal period (30  $\mu$ s) and is centered at  $H/2$ .

A second sampling diode switch follows the discriminator to sample the discriminator output signal from the VCO for 3.5  $\mu$ s during the BP interval and the signal from the reference oscillator for 7  $\mu$ s centered at  $H/2$ .

The second sampling switch serves as a time-domain filter and removes transient and beat-frequency signals produced in the rf switch circuit. Video modulation from the VCO signal is also removed by this switch.

The output from the switch is a pair of pulses centered at BP and at  $H/2$  whose amplitudes are proportional to the frequencies of the VCO and of the reference oscillator. The difference in the amplitudes of these pulses is proportional to the error in the VCO frequency. Because the discriminator output signal is later clamped, the discriminator zero produces only a second-order effect.

The train of pulses from the switch is amplified by a large factor and is then fed to a clamping circuit.

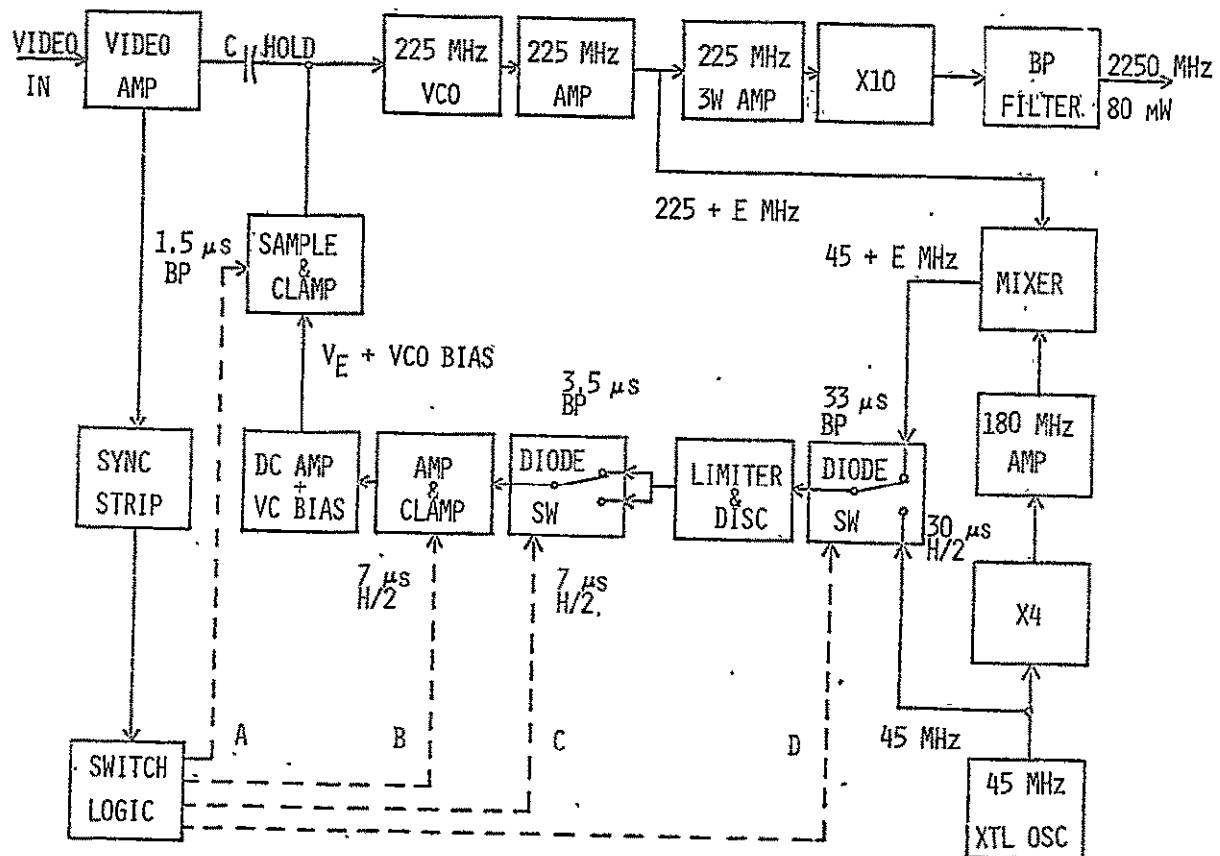


Figure 3. FM television transmitter with sampled AFC.

where the peak of the 7- $\mu$ s reference pulse is clamped to 0 V. The peak voltage of the VCO pulse is now directly proportional to the error in the VCO frequency. This waveform is amplified by a dc amplifier and has a dc voltage added to it to bias the varactor in the VCO circuit to the desired operating point.

The error sampling occurs in the sample-and-clamp circuit that samples the sum of the error signal and the VCO bias for 1.5  $\mu$ s during BP and clamps the BP of the incoming video waveform to this voltage. The hold capacitor C charges to the peak value of this voltage during BP intervals and discharges with a time constant of approximately 30 H. The error voltage is of the proper polarity to correct the frequency of the VCO. The AFC loop reduces the effect of varactor bias drifts.

## SWITCHING PULSES

The sync stripper circuit develops a pulse signal by stripping the horizontal and vertical synchronizing pulses from the incoming video signal as shown in Figure 4. The stripped pulses are fed to the switching logic network, which sets up the proper switching pulses for the sampling switches. The logic network also provides the appropriate sampling signals during the vertical synchronizing pulse intervals.

Figure 4 shows the 30- $\mu$ s rf sampling pulse, the 7- $\mu$ s reference oscillator clamping pulse, the 3.5- and 7- $\mu$ s discriminator output sampling pulses, and the 1.5- $\mu$ s error sampling and clamping pulse.

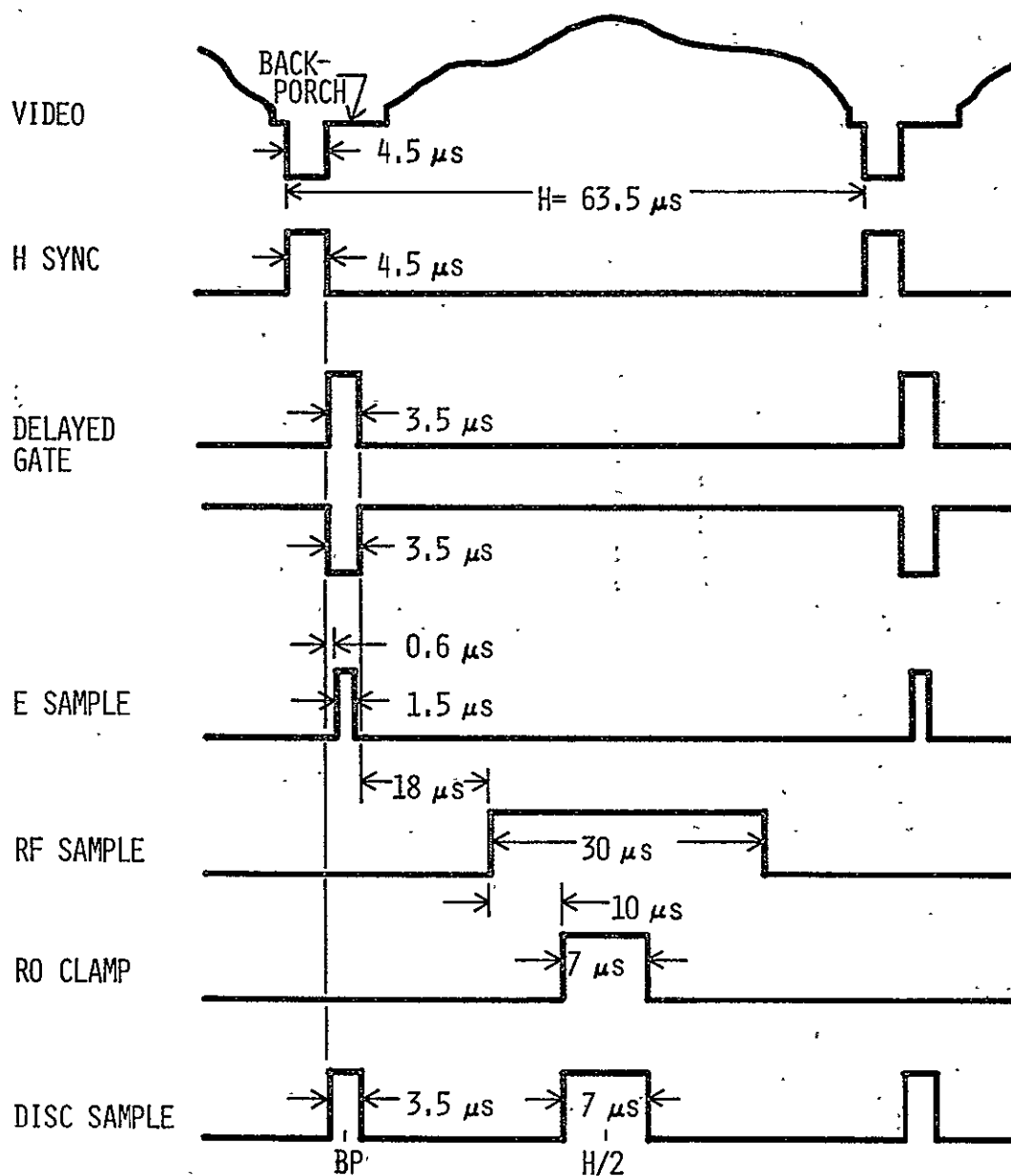


Figure 4. Switching pulses.

Note that it is possible to reference the transmitter frequency to the tip of the sync pulse rather than to the BP.

## ERROR SIGNAL

To reduce the drift of the discriminator zero away from the 45-MHz reference frequency, negative temperature coefficient capacitors are connected in parallel with the inductors in the discriminator

circuit. The zero, however, rarely coincides with the reference frequency. A typical error signal at the output of the discriminator with both the VCO and reference frequencies higher than the discriminator zero has the shape shown in Figure 5. This particular signal is shown after the reference pulse at  $H/2$  has been clamped to zero. Other pulse combinations are possible.

The uppermost diagram in Figure 6 shows the incoming video signal clamped to 0 V. The hold capacitor in the sampling circuit at the output of the



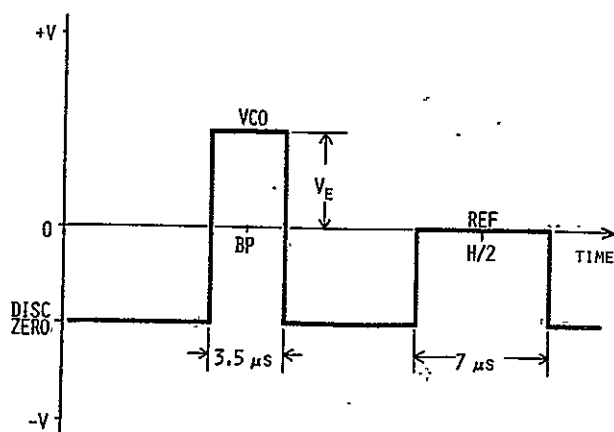


Figure 5. Discriminator output signal with reference voltage clamped to zero.

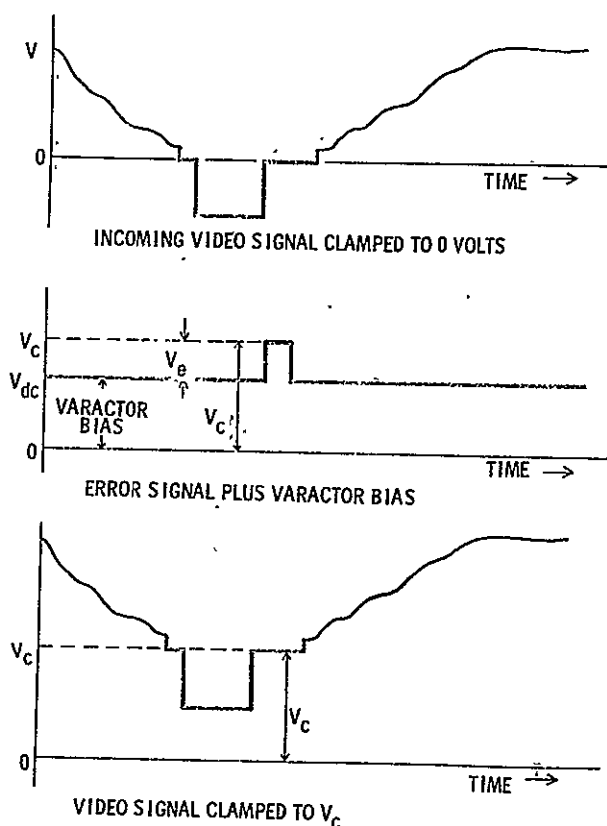


Figure 6. Video signal clamped to hold capacitor voltage.

video amplifier is charged to the voltage  $V_C$ , which is the sum of the error voltage  $V_E$  and the varactor bias voltage. The lower diagram shows the voltage applied to the varactor in the VCO circuit. This voltage decays exponentially with a time constant of approximately 30 horizontal sweep periods so that it decays a negligible amount until the next sample is taken. The long time-constant of the hold circuit is used to prevent the frequency correction from taking place at too rapid a rate to minimize picture distortion.

## FREQUENCY STABILITY

An equation for the output frequency stability factor derived from a mathematical model of the FM TV transmitter is presented in simplified form in Figure 7. This equation shows that the steady-state frequency stability is a function of (1) the stability factor of the reference oscillator, (2) the stability factor of the VCO divided by the open-loop gain, (3) a disturbance term resulting from imperfect limiting that causes the discriminator zero drift to affect the stability (this factor is reduced by the down conversion ratio), and (4) a disturbance term caused by clamping inaccuracy, varactor bias voltage drift, and sampling error.

$$\delta_0 = \delta_R + \frac{\delta_V}{K_0} + \frac{\delta_L}{5} (\delta_D - \delta_R) + \frac{1}{K_0} [K_C \delta_C + K_B \delta_B + K_S \delta_S]$$

$K_0$  - Open Loop Gain ( $K_0 \gg 1$ )

$\delta_R$  - Reference Oscillator Stability Factor

$\delta_V$  - VCO Stability Factor

$\delta_L$  - Limiting Error Factor

$\delta_D$  - Discriminator Stability Factor

$K_C \delta_C$  - Clamping Error Factor

$K_B \delta_B$  - Varactor Bias Drift Factor

$K_S \delta_S$  - Sampling Error Factor

Figure 7. Output frequency stability factor.

The curves of Figure 8 were computed by substituting typical values for the stability factors in the equation. The design limit of 0.01-percent frequency stability is readily achievable with an open-loop gain of 100 to 200 for a VCO frequency stability factor from 0.1 to 0.5 percent.

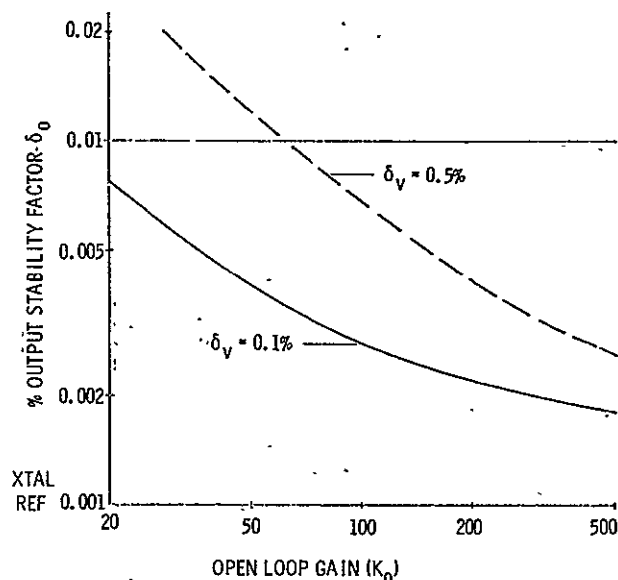


Figure 8. Output frequency stability factor  $\delta_0$  versus open-loop gain  $K_0$  ( $\delta_v$  is VCO frequency stability factor).

A long term frequency stability measurement was made over a temperature range of  $-20$  to  $+85^\circ\text{C}$  by connecting the 225-MHz output of the VCO to a digital frequency counter with a printing readout. The measurement was made by disconnecting the video waveform from the modulation input of the VCO and taking a counter reading of the unmodulated output frequency of the VCO as a function of temperature. Figure 9 shows the results obtained. The measured frequency stability factor of less than  $\pm 0.001$  percent is more than an order of magnitude better than the required stability factor of  $\pm 0.01$  percent. This result was unexpected because the stability factor of the crystal oscillator in developmental form was measured to be  $\pm 0.0008$  percent.

The closed-loop output frequency of the transmitter may be set to the reference frequency, or set above or below the reference frequency, by tuning a capacitor in the VCO circuit. The hold-in range at  $20^\circ\text{C}$  is approximately  $+0.02$  percent and  $-0.04$  percent.

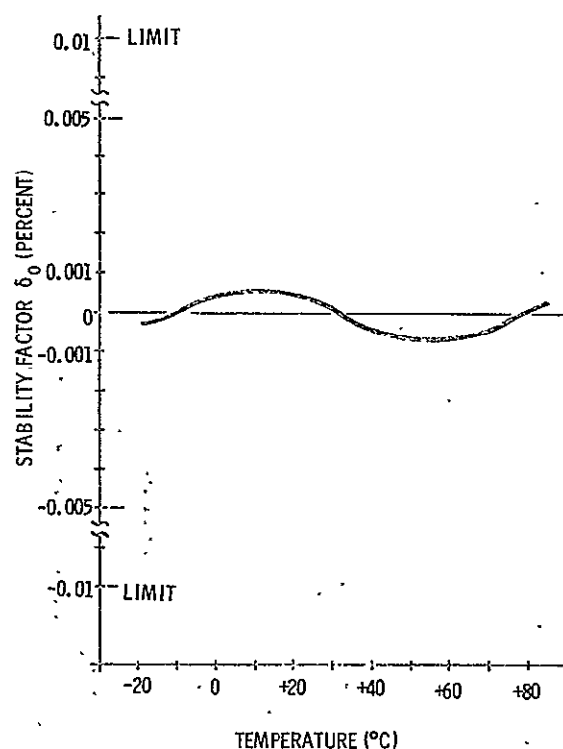


Figure 9. Measured frequency stability.

## CONCLUSIONS

Four models of the sampled AFC FM TV transmitter have been fabricated. All models displayed good frequency locking and holding characteristics under video modulation conditions. A frequency measuring system is being developed to measure the backporch frequency of the transmitters under dynamic modulation conditions.

It is believed that most of the circuits in the transmitter may be duplicated in integrated and microcircuit form. The success of the design is strongly dependent on the use of clean switches and thorough interstage and power supply filtering.

If a clocking pulse is made available, the transmitter may be used for wide-band telemetry purposes by making modifications in the switching logic section.

The possibility of incorporating a phase detector to phase lock the VCO frequency with the reference frequency is now under investigation.

## BIBLIOGRAPHY

Honnell, M. A., et al.: S-Band FM Television Transmitter Exciter Unit Instruction Manual. 24th Quarterly Report, NAS8-11184, Auburn Research Foundation, March 1970.

Honnell, M. A.; and Faust, W. E.: The Development and Analysis of a Sampled-Data Automatic Frequency Control for a Frequency Modulated Transmitter. Final Report, NAS8-11184, Auburn Research Foundation, September 1970.

# SPACE STATION RF HAZARDS

By

R. A. Inman

N71-29325

## SUMMARY

Harmful biological effects that may be caused by exposure to microwave radiation are discussed. Typical values of radio-frequency (rf) power density in the vicinity of space station antennas are calculated and compared to existing microwave exposure standards. It is shown that the currently accepted limit for exposure to rf radiation can be exceeded easily in the near field of high gain antennas on the space station.

permitted for situations in which the time of exposure is controlled. For power densities from 10 to 100 mW/cm<sup>2</sup>, the allowable time of exposure is given by the formula

$$T = 6000/W^2 \quad (1)$$

where 'T' is the allowable exposure time in min/hr and 'W' is the power density expressed in mW/cm<sup>2</sup> [2]. Examples of allowable exposure times are given in Table 1.

## INTRODUCTION

There is currently much controversy and uncertainty concerning the possible effects on the human body of exposure to electromagnetic energy in the microwave frequency range. The maximum safe level of radiation for all-day exposure is currently accepted in the United States as 10 mW/cm<sup>2</sup>. However, there is some pressure for the adoption of a more stringent limit on exposure levels [1].

It is not the purpose of this document to enter the controversy concerning microwave radiation exposure standards. This is a matter for much further study. The purpose is to point out the possible biological effects, including the more controversial effects, of overexposure to microwaves and to examine the possible levels of rf radiation to which personnel on the space station and similar spacecraft might be exposed. Because of the lack of a firm design for the space station, definite calculations cannot be made at this time. However, some typical situations that might be encountered are examined for the possibility of radiation hazards.

## RF EXPOSURE STANDARDS

In the United States, the currently accepted permissible level of rf radiation is 10 mW/cm<sup>2</sup> for continuous exposure. Higher power densities are

TABLE 1. EXAMPLES OF ALLOWABLE EXPOSURE TIMES

Power Density (mW/cm <sup>2</sup> )	Exposure Time (min/hr)
10	60
15	26.7
20	15
25	9.6
30	6.7
40	3.7
50	2.4

Other countries, such as Sweden, have adopted a more conservative standard of 1.0 mW/cm<sup>2</sup>. The Soviet Union enforces a very stringent maximum of 0.01 mW/cm<sup>2</sup> for all-day exposure. For exposures of 15 to 20 min/day, a power density of 1.0 mW/cm<sup>2</sup> is allowed [3]. In many locations in the United States, the power densities resulting from conventional television broadcasts would exceed the Soviet standard.

These widely differing standards have been one source of the controversy that has arisen. Another

area of controversy is that of the biological effects caused by exposure to rf radiation. Some effects, however, have been conclusively proven. The most widely accepted are thermal effects resulting from the heat produced by the excitation of atoms exposed to rf radiation.

## BIOLOGICAL EFFECTS

When the human body is exposed to microwave energy, the body reflects part of the energy, absorbs part of it, and transmits the remainder. At frequencies from 150 to 1000 MHz, about 40 percent of the energy is absorbed. At frequencies above 3000 MHz, 40 percent is also absorbed. In the frequency range from 1000 to 3000 MHz, the percentage of energy absorbed is determined by the composition of the body, in particular the thickness of the skin and fat layers and the moisture content. From 20 to 100 percent of the incident energy may be absorbed.

The depth of penetration into the body also depends on the frequency of the radiation. Below 1000 MHz, penetration is deep and vital organs are heated. Above 3000 MHz, most of the heating occurs in the skin layers. In the range from 1000 to 3000 MHz, a combination of these effects occurs, again depending on frequency and body composition. Fat absorbs microwave energy poorly, while tissues with a high water content are the best absorbers. These include muscle tissue and internal organs [4].

Formation of cataracts in the eyes is another effect of microwave radiation that has been demonstrated in both humans and experimental animals. This has been widely accepted as a thermal effect, but there are researchers who disagree that heat is the basic cause of these cataracts.

There have been some alleged cases of death resulting from exposure to very high microwave power densities. Some people can hear a buzz when exposed to microwave radiation. People who are otherwise deaf have experienced this effect. A sense of warmth may also be experienced by those exposed to microwave radiation, especially in the frequency range from 8 to 26 GHz. Stomach distress and nausea have occurred in cases of exposure to radar at power densities as low as 5 to 10

mW/cm<sup>2</sup>. This effect is usually associated with the frequency range from 8 to 12 GHz.

There are other, more controversial, effects of exposure to microwave radiation. These effects are referred to as "athermal" effects, because they apparently are not caused by heat. In most cases, the mechanism by which these effects are produced remains unexplained. Many of these athermal effects have been reported by researchers in the Soviet Union and are not widely accepted in this country. However, there has been some work in the United States that supports the existence of athermal effects, and it is considered worthwhile to mention some of these effects.

One of these reported effects is a decrease in the rate of contraction of the heart muscle caused by prolonged exposure to low level microwave energy. This may be accompanied by low blood pressure and changes in the composition of the blood. An increase in the histamine content of the blood signifies that the body is reacting to an outside influence.

Enlargement and increased activity of the thyroid gland have also been reported. Hormone imbalances and changes in the central nervous system are other nonthermal effects of exposure to microwave radiation, even at low power densities.

Other symptoms have also been reported, but because of the nature of these symptoms, causes and effects are not easily measured. Extreme tiredness, headaches, disruption of sleep, loss of appetite, fainting, and memory difficulties are reported to be among the effects of exposure to low level microwave energy. The Soviet researchers have also reported behavioral alterations following long periods of exposure to low level microwave energy. These behavioral alterations are reported to appear in the form of unstable mood, anxiety, irritability, and hypochondriac reactions. All of these reported low level effects are apparently reversible, although some may take up to 2 months to disappear.

Even though these athermal effects may not be accepted widely, the possibility of their occurrence, along with the other more accepted effects, is sufficient to demonstrate the need for protecting personnel from such exposure.

## POWER DENSITY CALCULATIONS

### Far Field

The far field of an antenna begins, by definition, at a distance  $R$  meters, where

$$R = 2d^2/\lambda \text{ meters} \quad (2)$$

In this expression,  $d$  is the largest linear dimension of the antenna [5] and  $\lambda$  is the wavelength of the radiation. Beyond this range, the only significant field mode existing is that containing the outwardly radiated power, so that power density varies as  $1/R^2$ . At ranges in the near field, however, a significant part of the power exists in complex modes that do not contribute to the radiated power. In the near field, therefore, the power density no longer varies as  $1/R^2$ .

### Low Gain Antennas

The power density in  $W/m^2$  at a distance  $R$  meters from a lossless isotropic antenna is given by the formula

$$W/m^2 = P_{\text{rad}}/4\pi R^2 \quad (3)$$

in which  $P_{\text{rad}}$  is the power in watts radiated from the antenna. If the antenna is not isotropic but has a directivity  $D$ , the expression for maximum power density becomes

$$W_{\text{max}}/m^2 = P_{\text{rad}} D/4\pi R^2 \quad (4)$$

The maximum power density would exist only in the direction of maximum radiation, or the direction of the peak of the antenna pattern. For the general case of an antenna having both directivity and losses, the expression becomes

$$W_{\text{max}}/m^2 = P_{\text{rad}} D\eta/4\pi R^2 \quad (5)$$

where  $\eta$  is the efficiency of the antenna. Since the gain of the antenna is given by

$$G = D\eta \quad (6)$$

the expression for maximum power density becomes

$$W_{\text{max}}/m^2 = P_{\text{rad}} G/4\pi R^2 \quad (7)$$

### High Gain Parabolic Antennas

Formulas and curves of axial power density for parabolic antennas are given in Reference 6, pages 186 and 187. The axial power density in  $mW/cm^2$  at a distance  $2d^2/\lambda$  meters from the antenna is given in Reference 6 in the form

$$mW/cm^2 = 14.64 P_{\text{kw}}/d^2 \quad (8)$$

where  $d$  is the antenna diameter in meters and  $P_{\text{kw}}$  is the radiated power in kW. The curve on page 187 of Reference 6 shows the axial power density variation in the near field. It can be seen that the axial power density in the near field can be as much as 41 times as great as the axial power density existing at the  $2d^2/\lambda$  distance. This maximum occurs at approximately one-tenth of the far field distance.

Using these curves and the equations that have been given, some possible radiation levels on the space station have been calculated and are shown in Tables 2 and 3. For low gain antennas, equation (7) has been used to calculate power density. For the high gain parabolic antennas, the equations and curves given in Reference 6 have been used.

## POWER DENSITY VERSUS PARABOLIC ANTENNA PARAMETERS

For constant frequency and radiated power, the power density at the far field distance decreases as the antenna gain increases. This variation is inversely proportional and also applies to the maximum power density point at one-tenth of the far field distance. It should be remembered, however, that these distances increase in direct proportion to antenna gain.

If antenna size and transmitted power are the parameters held constant and if the frequency is

TABLE 2. EXAMPLES OF LOW GAIN ANTENNA RADIATION LEVELS AT 20 W POWER

	Distance from Antenna (m)	Maximum Power Density (mW/cm <sup>2</sup> )
<u>Case I</u>		
0 dB antenna gain (G = 1)	1	0.159
	5	0.0064
	10	0.0016
	50	0.00006
<u>Case II</u>		
6 dB antenna gain (G = 4)	1	0.637
	5	0.025
	10	0.0064
	50	0.00025

TABLE 3. EXAMPLES OF HIGH GAIN PARABOLIC ANTENNA RADIATION LEVELS AT 20 W POWER<sup>a</sup>

	Frequency (MHz)	Antenna Diameter [m (ft)]	Near Field Distance (m)	Maximum Axial Power Density at $2d^2/\lambda$ (mW/cm <sup>2</sup> )	Maximum Axial Power Density at One-Tenth of $2d^2/\lambda$ (mW/cm <sup>2</sup> )
<u>Case III</u>					
20 dB antenna gain (G = 100)	250	5.17 (17)	44.1	0.011	0.451 at 4.41 m
	1 000	1.28 (4.2)	10.7	0.18	7.38 at 1.07 m
	2 200	0.58 (1.9)	4.87	0.88	36.1 at 0.487 m
<u>Case IV</u>					
30 dB antenna gain (G = 1000)	1 000	3.96 (13)	104	0.0188	0.77 at 10.4
	2 200	1.82 (6)	48.7	0.088	3.61 at 4.87 m
	6 000	0.67 (2.2)	17.6	0.655	26.85 at 1.76 m
<u>Case V</u>					
45 dB antenna gain (G = 32 000)	4 000	5.78 (19)	882	0.0088	0.361 at 88.2 m
	10 000	2.28 (7.5)	335	0.057	2.32 at 33.5 m
	15 000	1.52 (5)	228	0.127	5.21 at 22.8 m

a. Power densities for transmitted powers other than 20 W may be found by multiplying the given power densities by  $P/20$ , where  $P$  is the desired power in watts. When the beams of two or more antennas overlap, the power density should be considered as the sum of the individual power densities.



varied, it is found that the power density at the far field distance remains constant. However, the far field distance is dependent on the frequency, since it is proportional to it.

If antenna gain and radiated power are kept constant, the far field power density increases as the square of the frequency. However, the distance to the far field decreases as the frequency increases in this case. These same statements apply to the maximum power density point occurring at one-tenth of the far field distance.

## SHIELDING FROM RF RADIATION

Various materials may be used to shield personnel from rf radiation. A very thin sheet of metal that is a good conductor will provide nearly total protection from direct radiation. This material need be only a few skin depths thick at the frequency of the radiation. In the frequency range from 1 to 12 GHz, 60-by-60 mesh screen will allow only about 1 percent of the incident radiation to pass. Window screening material (32-by-32 mesh) will pass less than 2 percent in the same frequency range; 6.35-mm mesh will pass less than 2 percent at 1 GHz,

but it allows 10-percent transmission at 12 GHz. Glass will allow 40- to 65-percent transmission, depending upon the frequency of the incident energy.

When shielding an area against microwave energy, one should consider the possibility of reflected or refracted waves. The path of least attenuation should always be considered.

## CONCLUSIONS

Power densities were calculated here for low-gain antennas and high gain parabolic antennas. In general, the power density in the field of an antenna will depend on the radiated power and the radiation pattern of the antenna.

It can be seen that a possible rf radiation exposure hazard exists for space station personnel exposed to the main beam of high gain antennas. The greatest hazard exists in the near field region of the high gain antennas, where power densities may easily exceed 10 mW/cm<sup>2</sup>. Care should be taken to properly shield personnel against microwave radiation and to keep unshielded personnel out of the main beam and the near field of high gain antennas.

## REFERENCES

1. Hardeman, Lyman J.: Microwave Oven Leakage: Federal Regulations Soon. *Microwaves*, February 1970, pp. 17-24.
2. Control of Hazards to Health from Microwave Radiation. Technical Bulletin No. Med 270, Air Force Manual No. 161-70, Departments of the Army and the Air Force, Washington, D. C., December 6, 1965.
3. Soviet Health Standards on Microwave Exposure. *Microwaves*, April 1969, p. 26.
4. Aaronson, Terri: Mystery. *Environment*, May 1970, pp. 2-10.
5. Jasik, Henry: *Antenna Engineering Handbook*. McGraw-Hill Book Company, New York, 1961, pp. 2-13 through 2-15.
6. Hansen, R. C.: *The Microwave Engineer's Handbook and Buyer's Guide*. Horizon House, Dedham, Mass., 1966, pp. 186-187.

PRECEDING PAGE BLANK NOT FILMED  
TELEVISION RESEARCH

By

C. T. Huggins

N71-29326

## SUMMARY

A solid-state television camera that has no imaging tube and has characteristics of a vidicon camera with resolution greater than the home TV receiver is discussed. A brief theory of operation is given along with changes to the structure and improvements in the response characteristics during the last 4 years of development. The addressing problems and their solution for monolithic mosaics of greater than 50 000 photo-transistors are discussed. A system for testing and evaluating the mosaics with 200 000 elements is described. An ultimate model projection of the solid-state camera is given.

## INTRODUCTION

In the 4 years since the last report on this project in this Research Achievement Review series [1], great strides have been made by many groups in the area of image sensors. This is particularly true in the areas of solid-state image converters and peripheral video and digital-data-handling circuits using large scale integration. This paper discusses the final phases of the development contract with Westinghouse [2] for an all solid-state television camera using a mosaic of photo-transistors.

The mosaic produced 4 years ago contained 2500 npn photo-transistors on a single wafer of silicon 1.25 cm on a side and arranged in a 50-by-50 square array spaced on 0.25 mm centers. Since that time, three other generations of mosaic arrays have been developed. The first of these contained 12 800 photo-transistors on a wafer approximately 1.6 cm on a side. The second series contained 51 200 photo-transistors on a wafer approximately 1.9 cm on a side. The final generation contains 200 000 photo-transistors on a single silicon wafer approximately 2.5 cm on a side.

## ELECTRICAL CHARACTERISTICS OF PHOTO-TRANSISTOR ARRAY

The photo-transistor elements have a rectangular geometry with discrete emitter and base regions, but with collector regions common to a column of 500 elements (Fig. 1). No electrical access is provided to the individual photo-transistor base regions. The emitters are interconnected with evaporated aluminum strips in 400 isolated rows.

Unique access to any individual element of the XY mosaic is available through one of the X and one of the Y external leads. Only the single element that lies at the intersection of these XY interconnections is interrogated.

The 50-by-50 mosaic was operated in the static mode, which meant the signal output current from each photo-transistor in the array was only that current produced by the photon conversion during the sampling period for that element. It has since been found that the output can be increased considerably if the elements of the image converter system operate on a pulsed readout basis, which is an integrated or storage mode of operation. Storage-mode operation has been shown to be the result of sampling the total discharge of the collector-base junctions' depletion layer capacitance. This charge-monitoring process is also aided by the impedance transformation afforded by the photo-transistors current gain,  $\beta$ . Optimum imaging conditions are achieved by maximizing the charge in the junction and tailoring this maximization to appropriate frame rates and light levels. In the current system, which operates at 30 frames per second, a 200 000 element mosaic gives the following input-output values from the first video amplifier: 40 mV output for  $2 \mu\text{W}/\text{cm}^2$  radiant energy on the mosaic and 275 mV at  $7 \mu\text{W}/\text{cm}^2$ . The output voltage is relatively linear between these two values.

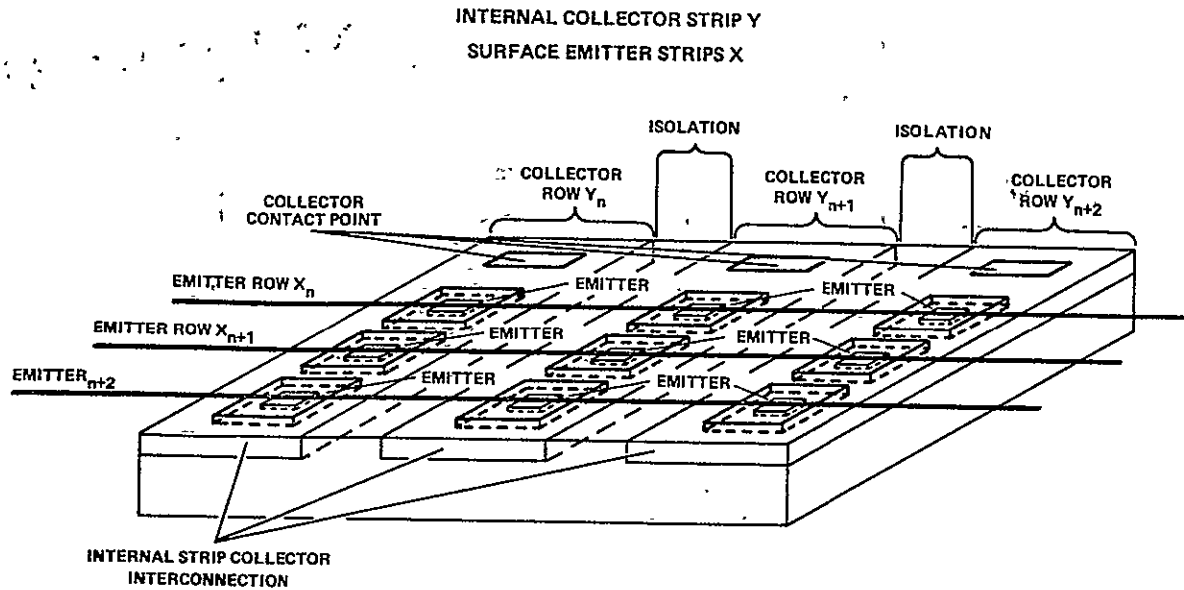


Figure 1. Section of mosaic with XY interconnections.

## REAL TIME INTELLIGENCE ACQUISITION

From the beginning of this program up through the 200-by-256 element arrays, the standard accessing technique that has been employed is called emitter sequenced-emitter read (ESER). Its major limiting factor for extension to still larger sensor arrays is that very high speed metal-oxide-semiconductor (MOS) or J-FET switches with moderate drive capabilities and very low  $R_{ON}$  resistance are required. In particular, for a 400-by-500 element system, it is found that if

$$C_{CB} \approx 0.1 \text{ pF (collector to base capacity);}$$

$$C_{ES} \approx 60 \text{ pF (emitter line to ground line capacity),}$$

$$\beta \approx 30 (\beta \text{ of photo-transistor}),$$

and

$$\tau_{EL} \approx 160 \text{ ns (period of master clock),}$$

then

$$(C_{ES} + \beta C_{CB}) (R_{ON} + R_{LOAD}) \lesssim 1/3 \tau_{ELEMENT}$$

and

$$(R_{ON} + R_{LOAD}) \lesssim [160/3 (60 + 3)] \times 10^{-9} \times 10^{12}$$

$$\lesssim (160/189) \times 10^{+3}$$

$$\lesssim 1 \text{ k}\Omega$$

However, the  $R_{ON}$  resistance of the switching devices alone will be of this magnitude (for any device of acceptable size) and will vary by up to 20 percent from unit to unit. From this observation, it was concluded that the recharge time constant was so short that it precluded using this scheme in the 200 000 (400 by 500) element readout system. After an extensive analysis of other methods of addressing, it was concluded that the most practical way to address the high order array would be to use multiplexed accessing. By extending and overlapping the recharge intervals for successive elements, this modification to the basic ESER accessing approach permits it to be extended to handle extremely high data rates. In particular, the speed requirement of  $R_{ON}$  of the

per-line FET switching devices can be relaxed to nearly any level desired by increasing the degree of multiplexing employed. There are practical limits to this process, however, and the least degree of multiplexing consistent with trade-off between performance and the high cost of additional system complexity is desirable.

The normal per-element recharge interval for the 400-by-500 element system, which is 160 ns, can be increased to 640 ns by using fourth-order multiplexing. When this is done, the limit on total resistance can be raised by a factor of four so that  $R_{TOTAL}$  now becomes 4 k $\Omega$ . If this value is split evenly between  $R_{ON}$  and  $R_L$ , then the "ON" resistance of the per-line switching devices is increased to 2 k $\Omega$ . Switching devices with this  $R_{ON}$  value can be manufactured relatively easy and with good consistency using currently available silicon technology.

Fourth-order multiplexing can be explained in the following manner. Consider the photo-transistors lying along a row "Y" (Fig. 1). Each photo-transistor is normally switched on and off by applying a voltage pulse of one-clock-period duration to each of the "X" row connector strips. The row connections are arranged with all the odd-numbered connections at the top and the even-numbered connections at the bottom. The "Y" column connections are also divided with the odd connections on one side and the even connections on the other side (Fig. 2).

For fourth-order multiplexing, four video information channels are provided for the odd-side emitter connections and four for the even-side emitter connections. The odd and even emitter connections are switched to these eight channels in groups of four.

To consecutively sample the photo-transistors along a column, the switching pulses required are not coincident. Their leading edges are delayed from each other by one clock period and are four clock periods wide instead of the usual one clock period, thus causing them to overlap in a consecutive manner. However, the current that flows at the instant a photo-transistor is connected to a video information channel is proportional to the total light flux incident on the photo-transistor since its previous sampling, or approximately one frame time of the array, 1/30 second for the current system.

After an isolation and buffer stage of amplification, each of these groups of four video information channels is sampled by the two first-level multiplexers giving a serial analog data stream at a frequency of 4.725 MHz. These two serial data streams are sampled by the second-level multiplexer, which puts out a 9.45 MHz data stream with an information bandwidth of 4.725 MHz.

To scan each row of photo-transistors, the collector column voltage has also been switched, but, since each collector gate stays on while 500 emitters are sampled, the required switching can be done in a normal non-overlapped manner. To provide an interlaced scan, all the odd collector columns are consecutively addressed for one field and then the even collector columns are addressed for the other field.

Concluding stages consist of buffers, summing, and shaping circuitry to combine the composite sync, blanking, and video into a fully compatible Electronic Industries Association (EIA) television format signal suitable for all commercial TV applications (Fig. 3).

## MOSAIC EVALUATION SYSTEM

The emitter and collector connections of the photo-transistor mosaic are arranged in two rows on each of the four sides. The 200 odd collector connections are arranged in 2 rows on 1 side, every other odd connection in 1 row (100 in all) and the other 100 odd connections in another row, while the 200 even collector connections are arranged likewise in 2 rows on the opposite side.

The emitter connections are similarly arranged with the odds in 2 rows of 125 each at the top and the evens in two rows of 125 each at the bottom of the mosaic.

Since there are now 900 connections to deal with between the mosaic and the peripheral electronics, it is no longer practical to bond the mosaic into a test camera to check its electrical characteristics. Therefore, a test set has been devised that will allow the operation of the mosaic without mechanical bonding (Fig. 4). The mosaic is shown mounted in the center of the round holder in the lower center of Figure 4. The vertical post with the two white wires contains a vacuum chuck to hold the mosaic frame. This column is positioned underneath the center of the black frame (Fig. 5). On the sides of the frame are mounted four three-axis micromanipulators to which are attached four probe cards. Two cards each contain 100 probes and 2 cards each contain 125 probes.

Since the column and row connection pads are arranged in two ranks on each of the four sides as already described, access to every other connection of each rank will be obtained by these probes (Fig. 6).



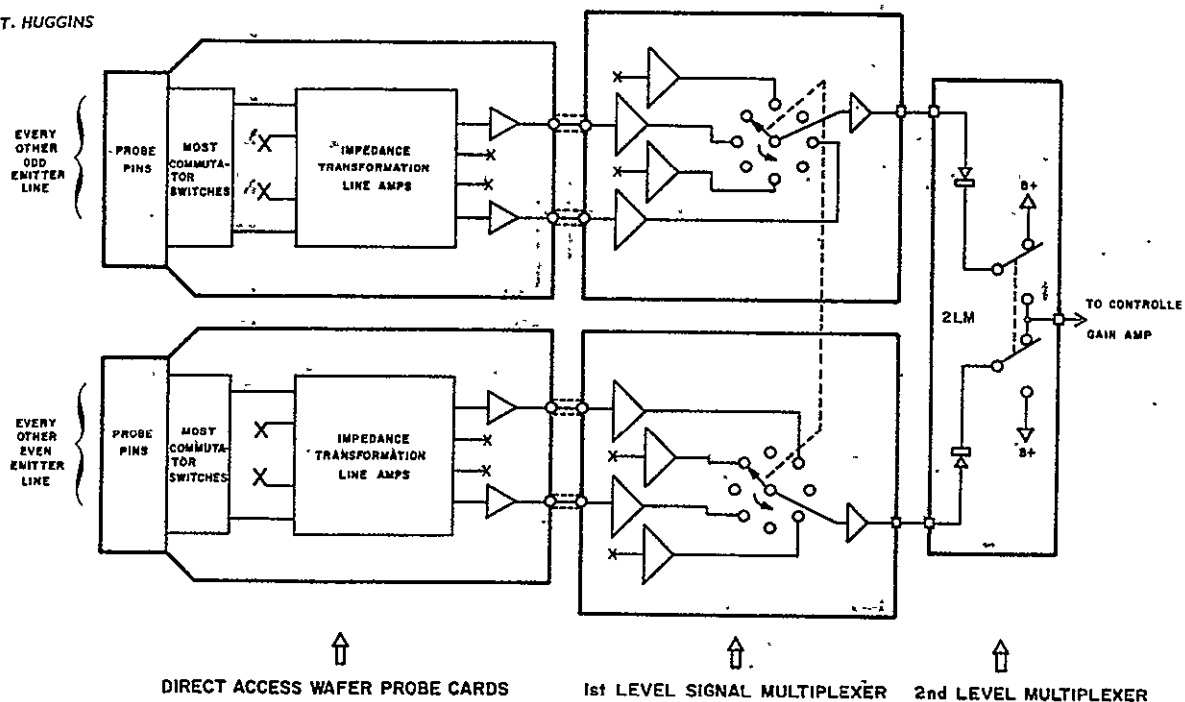


Figure 2. Simplified block diagram of analog signal chain.

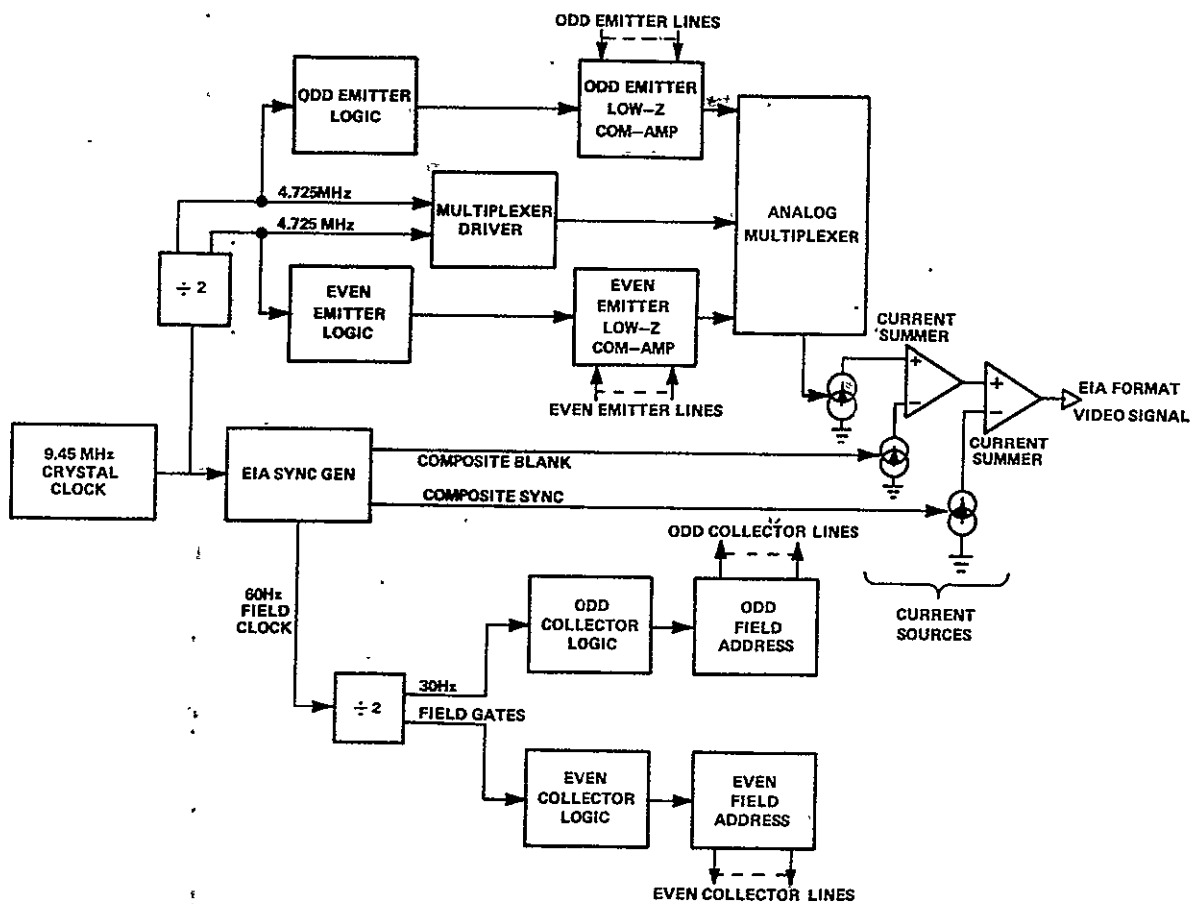


Figure 3. Block diagram of 400-by-500 element solid-state television camera.

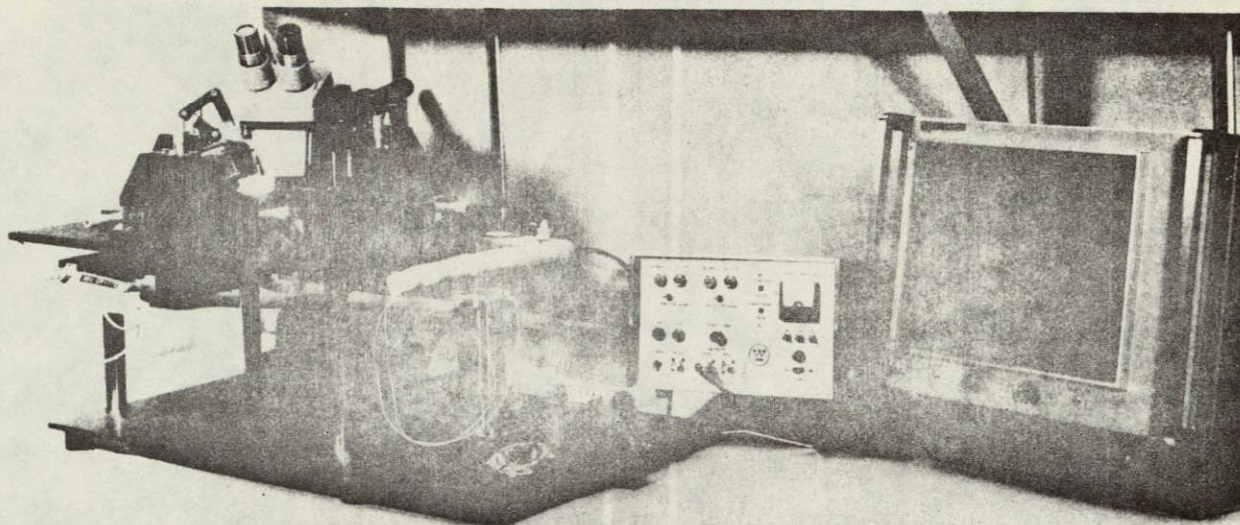


Figure 4. 400-by-500 element mosaic evaluation system.

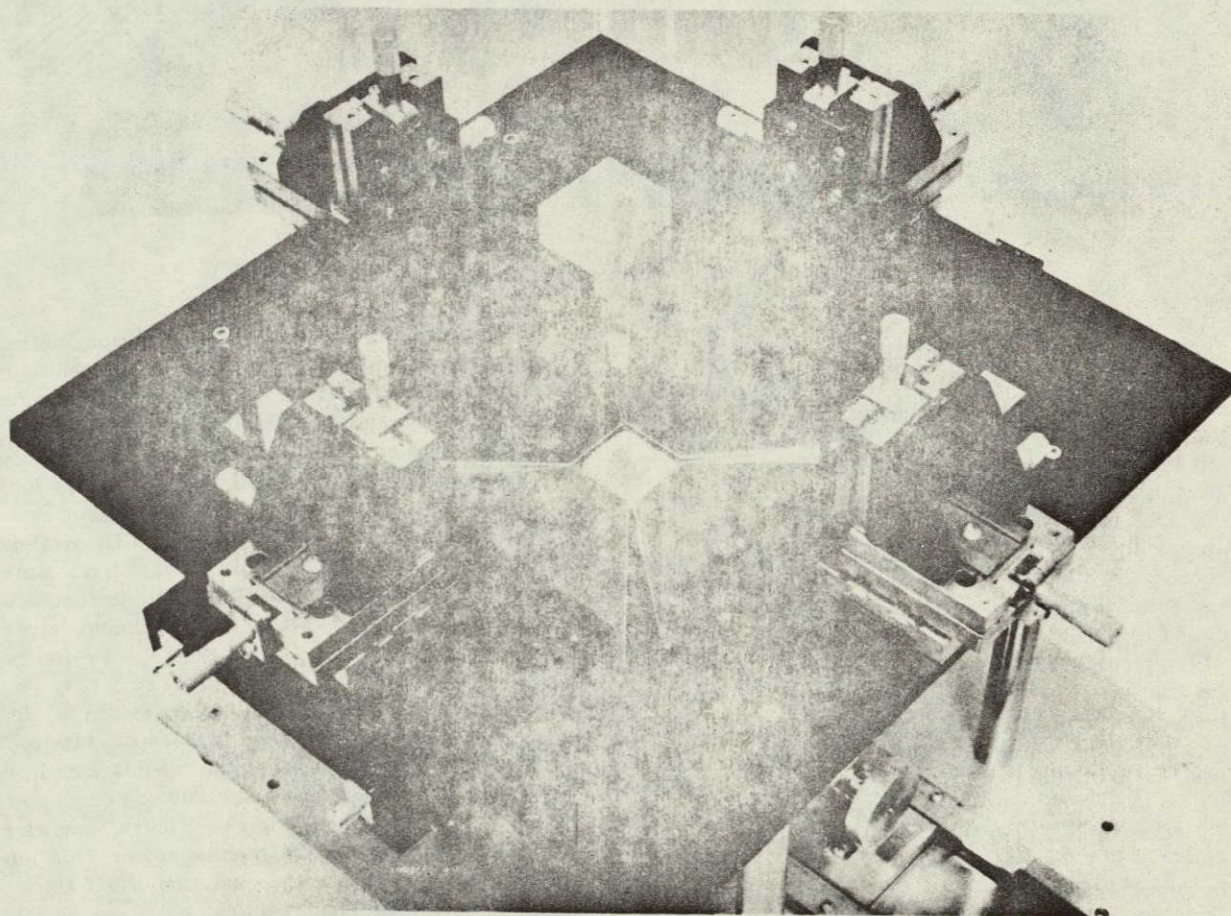


Figure 5. Probe test stand for mosaic.



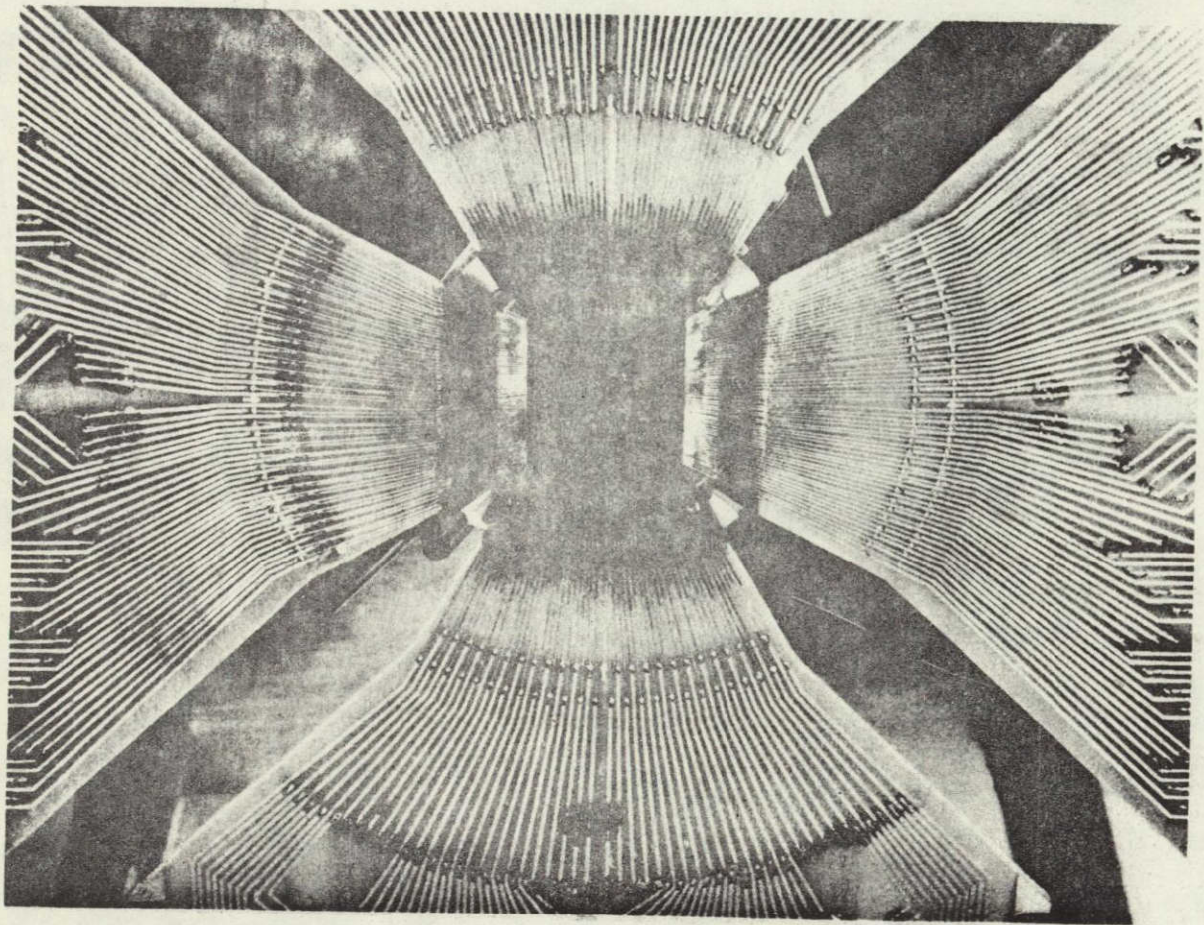


Figure 6. Probe cards in position on mosaic.

If every other odd and every other even emitter line are addressed along with every other odd collector line, all the A photo-transistors shown in Figure 7 will be scanned. If the same emitter lines are retained and every other even collector line is used, all the A' photo-transistors will be scanned. The sum of these two scans gives an image of the whole picture, but the image contains only one-fourth of the picture elements. If the emitter probes are now moved so as to contact the omitted lines and the collector probes are not moved, photo-transistors B and B' will be scanned, giving another one-fourth of the picture. Moving the collector probes to the omitted collector lines and repeating the two emitter probe positions will scan areas C, C' and D, D', giving the remaining one-half of the picture.

If each of the quarters is photographed from the TV monitor and all four images are superimposed, a very close approximation of the image produced by an entire camera system will be obtained.

With this test device now in operation, data are being gathered on the operational characteristics of the mosaic. Work has also begun on the packaging of a complete camera using the 200 000 element mosaic as the sensor. Because of the essentially two-dimensional nature of all of the circuitry including the sensor in this camera, the form factor of the finished camera is almost unlimited. The easiest one to implement was selected for this first camera to prove operational feasibility and to demonstrate the effectiveness of the bare-chip technique in packaging design.

The camera will be rectangular in shape, approximately 5.08 cm (2 in.) thick by 25.4 cm (10 in.) wide by 30.28 cm (12 in.) high with a 50-mm lens in the center of the large side. Some 600 odd chips go together to make up this camera. Figure 8 shows an artist's drawing of the finished camera. This television camera will have a resolution of 500 lines horizontal and 400 lines vertical.



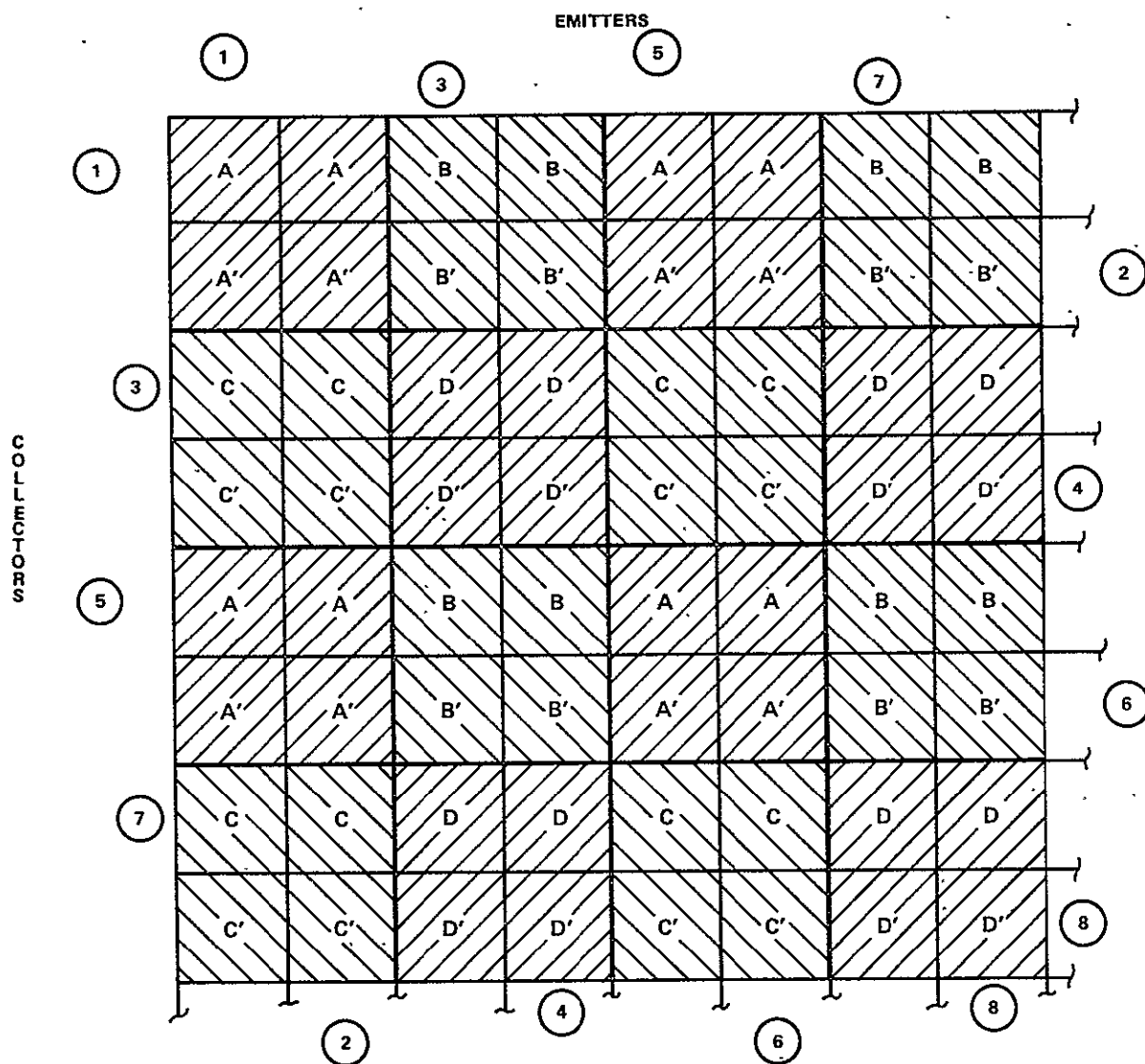


Figure 7. Scanning pattern of 400-by-500 element photo-transistor test set.

The camera's completely solid-state construction gives it the usual potential advantages attributed to integrated circuit systems; i. e., reduced weight, volume, and power consumption plus greatly increased reliability and environmental immunity. In addition, the photo-transistor mosaic performs the functions of a vidicon without the necessity for high voltages, magnetic fields, vacuum envelopes, filament power, and protection against mechanical shock. The elimination of the high voltage requirement is a particularly salient advantage for space environments. The fact that the image plane of the sensor consists of discrete sensor elements geometrically precise in

position eliminates the problem of beam deflection errors of a tube. These errors are important in optical processing systems such as stereo imaging, motion detection, and scene correlation, where it is important to return to an exactly known segment of the image over relatively long periods of time. The electrical accessing of the image area could also facilitate random scanning in these applications.

Because of its low power and small size, this television camera can have a number of excellent applications in space. Figure 9 shows four such uses.



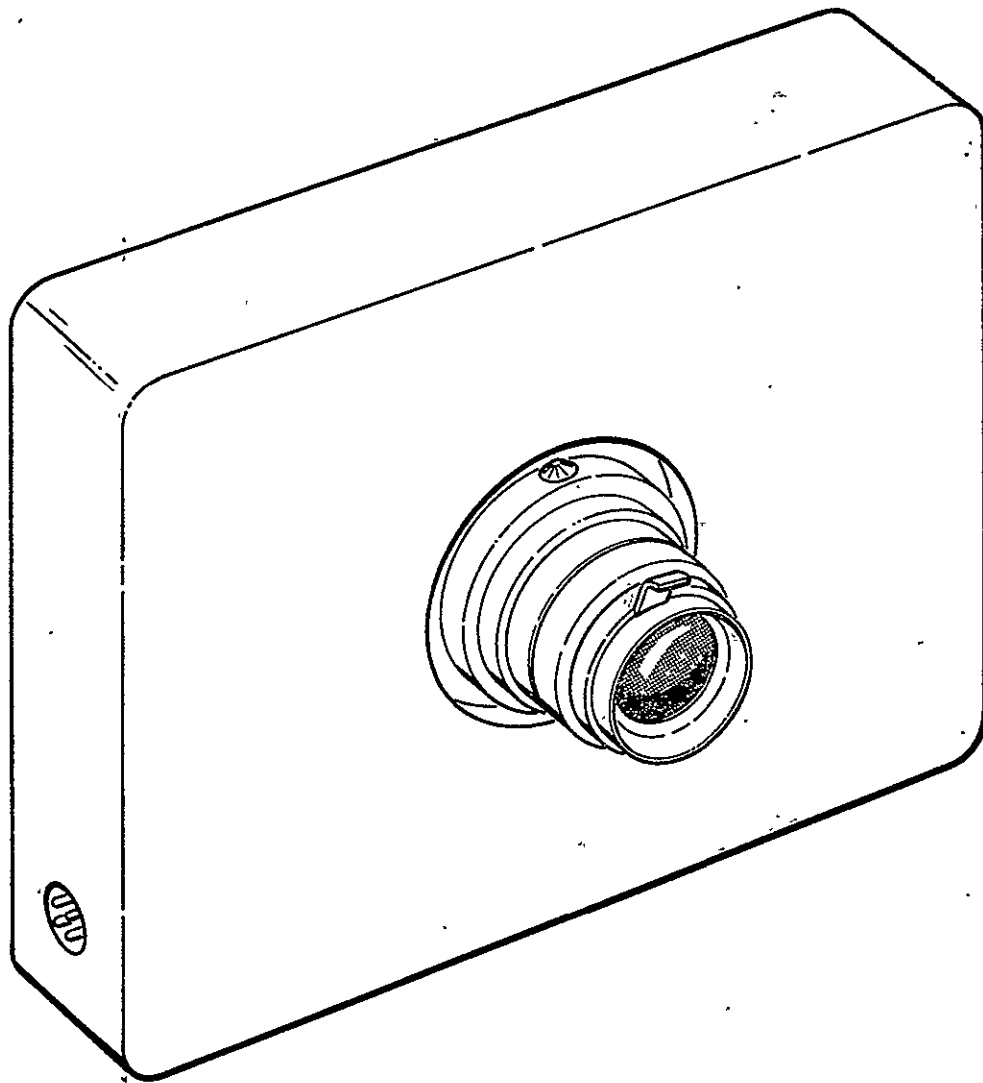


Figure 8. Miniature solid-state television camera.

## CONCLUSIONS

The photo-transistor mosaics are being used as cathode-ray-tube, analog-to-digital converters in the assessment of nuclear blasts. The mosaic itself and the readout techniques developed under the NASA program have been directly applicable to this work.

The Air Force now has work underway that is based on this program but is designed to obtain mosaics of germanium. A readout system very similar to the silicon readout has been developed for germanium.

Currently, very similar mosaics are being evaluated for use as star mapping sensors. Another quite unique application is the use of the mosaic to report the real-time variance in particle generation during nuclear reactions. Quite specialized mosaic interrogation techniques are required in this application, but the basic sensor is the photo-transistor mosaic. Several other applications involving the use of image intensifiers with the mosaic have evolved. The essential contribution of the mosaic has been the analog-to-digital conversion inherent in mosaic operation.

As important a contribution as that of the mosaic itself has been the development of the technology that

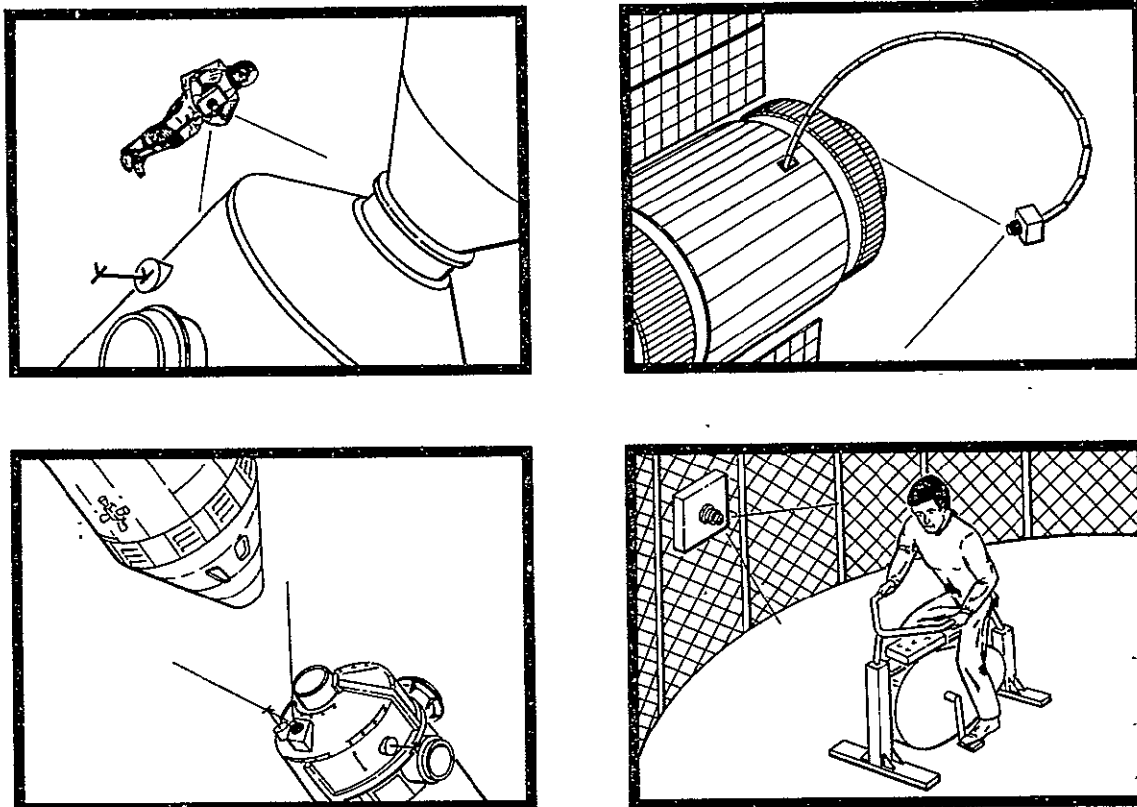


Figure 9. Space usage of solid-state television camera.

allows the grouping of 200 000 photo-transistors in  $6.452 \text{ cm}^2$  ( $1 \text{ in.}^2$ ). The requirements imposed by the mosaic have led to the development of processes and techniques that have found very wide application particularly in areas of large scale integration. The process controls that have been established to insure capable execution of the various operations have helped to increase the yield and quality of all circuits being processed.

Active applications of the basic mosaic have been made and several other applications are being considered. Furthermore, the processing skills and techniques developed for this camera have materially aided in other programs, programs that would have been delayed had it not been for the experience gained on this program. The application of this camera and techniques is limited only by the imagination.

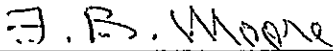
## REFERENCES

1. Communication Systems Research at MSFC. Research Achievements Review, Series No. 18, NASA TM X-53535, 1966.
2. A Solid-State Image Converter of Radical Design. Contract No. NAS8-5112, Westinghouse Electric Corp., Systems Development Division, Baltimore, Maryland.

RESEARCH ACHIEVEMENTS REVIEW  
VOLUME IV REPORT NO. 3

The information in these reports has been reviewed for security classification. Review of any information concerning Department of Defense or Atomic Energy Commission programs has been made by the MSFC Security Classification Officer. These reports, in their entirety, have been determined to be unclassified.

These reports have also been reviewed and approved for technical accuracy.



---

F. B. MOORE  
Director, Astrionics Laboratory

1. Report No. <b>NASA TM X-64572</b>		2. Government Accession No.		3. Recipient's Catalog No.	
4. Title and Subtitle <b>RESEARCH ACHIEVEMENTS REVIEW, VOL. IV, REPORT NO. 3</b>  <b>Instrumentation and Communication Research at MSFC</b>				5. Report Date <b>May, 1971</b>	
				6. Performing Organization Code	
7. Author(s) <b>C. T. Paludan, C. T. Jones, H. S. Harman, W. E. Maynard, J. J. Clubb, M. A. Honnell, R. A. Inman, and C. T. Huggins</b>				8. Performing Organization Report No.	
9. Performing Organization Name and Address <b>George C. Marshall Space Flight Center Marshall Space Flight Center, Alabama 35812</b>				10. Work Unit No.	
				11. Contract or Grant No.	
12. Sponsoring Agency Name and Address. <b>National Aeronautics and Space Administration Washington, D. C. 20546</b>				13. Type of Report and Period Covered <b>Technical Memorandum</b>	
				14. Sponsoring Agency Code	
15. Supplementary Notes  <b>Prepared by Astrionics Laboratory, Science and Engineering</b>					
16. Abstract  Instrumentation and communication achievements applicable to the problems of sensing, tracking, and communication for the Space Station and Space Shuttle are presented. The sequence and contents of the seven papers are:  1. Design, development, proving, and application of an X-ray source for the Apollo Telescope Mount X-ray telescope experiment.  2. Development and capabilities of a digital output pressure transducer capable of replacing analog transducers in ground and flight testing.  3. Comparative evaluation, including advantages and disadvantages, of five data compression techniques.  4. Design techniques and circuits underlying a highly flexible, SSB/DSB/CBW-compatible telemetry system.  5. Description and discussion of an improved TV transmitter featuring S-band and FM.  6. Possible biological effects of microwave radiation assessed in terms of current microwave exposure standards.  7. Solution of solid-state TV (SSTV) camera addressing problems, and a system for testing and evaluating SSTV mosaics.					
17. Key Words (Suggested by Author(s)) X-ray source      FM TV transmitter ATM X-ray telescope      S-band Digital pressure transducer      Microwave radiation Data Compression      Solid-state television SSB/DSB/CBW      Camera addressing Telemetry system      SSTV mosaics				18. Distribution Statement  Unclassified-Unlimited  See Document Release Form	
19. Security Classif. (of this report)  <b>Unclassified</b>		20. Security Classif. (of this page)  <b>Unclassified</b>		21. No. of Pages  <b>76</b>	22. Price*  <b>\$3.00</b>



## CALENDAR OF REVIEWS

### FIRST SERIES (VOLUME I)

REVIEW	DATE	RESEARCH AREA	REVIEW	DATE	RESEARCH AREA	REVIEW	DATE	RESEARCH AREA
1	2/25/65	RADIATION PHYSICS	9	6/24/65	GROUND TESTING	16	10/28/65	ASTRODYNAMICS
2	2/25/65	THERMOPHYSICS	10	6/24/65	QUALITY ASSURANCE AND CHECKOUT	17	1/27/66	ADVANCED TRACKING SYSTEMS
3	3/25/65	CRYOGENIC TECHNOLOGY	11	9/16/65	TERRESTRIAL AND SPACE ENVIRONMENT	18	1/27/66	COMMUNICATIONS SYSTEMS
4*	3/25/65	CHEMICAL PROPULSION	12	9/16/65	AERODYNAMICS	19	1/6/66	STRUCTURES
5	4/29/65	ELECTRONICS	13	9/30/65	INSTRUMENTATION	20	1/6/66	MATHEMATICS AND COMPUTATION
6	4/29/65	CONTROL SYSTEMS	14	9/30/65	POWER SYSTEMS	21	2/24/66	ADVANCED PROPULSION
7	5/27/65	MATERIALS	15	10/28/65	GUIDANCE CONCEPTS	22	2/24/66	LUNAR AND METEOROID PHYSICS
8	5/27/65	MANUFACTURING						

### SECOND SERIES (VOLUME II)

REVIEW	DATE	RESEARCH AREA	REVIEW	DATE	RESEARCH AREA	REVIEW	DATE	RESEARCH AREA
1	3/31/66	RADIATION PHYSICS	6	1/26/67	CHEMICAL PROPULSION	10	9/28/67	TERRESTRIAL AND SPACE ENVIRONMENT
2	3/31/66	THERMOPHYSICS	7	3/30/67	CRYOGENIC TECHNOLOGY	11	11/30/67	MANUFACTURING
3	5/26/66	ELECTRONICS	8**	5/25/67	COMPUTATION	12	1/25/68	INSTRUMENTATION RESEARCH FOR GROUND TESTING
4	7/28/66	MATERIALS	9	7/27/67	POWER SYSTEMS			
5	9/29/66	QUALITY AND RELIABILITY ASSURANCE						

### THIRD SERIES (VOLUME III)

REVIEW	DATE	RESEARCH AREA	REVIEW	DATE	RESEARCH AREA	REVIEW	DATE	RESEARCH AREA
1	3/28/68	AIRBORNE INSTRUMENTATION AND DATA TRANSMISSION	5	11/21/68	COMMUNICATION AND TRACKING	10	12/18/69	MATERIALS RESEARCH FOR SHUTTLE AND SPACE STATION
2	5/22/68	ASTRODYNAMICS, GUIDANCE AND OPTIMIZATION	6	1/30/69	THERMOPHYSICS	11	1/29/70	MICROELECTRONICS RESEARCH FOR SHUTTLE AND SPACE STATION
3	7/25/68	CONTROL SYSTEMS	7	3/27/69	RADIATION PHYSICS	12	3/26/70	COMPUTATION RESEARCH (PART II)
4	9/26/68	AEROPHYSICS	8	6/26/69	METEOROID PHYSICS			
			9	9/25/69	COMPUTATION RESEARCH (PART I)			

### FOURTH SERIES (VOLUME IV)

REVIEW	DATE	RESEARCH AREA	REVIEW	DATE	RESEARCH AREA	
1	5/28/70	STRUCTURES	4	3/25/71	ELECTRICAL POWER SYSTEMS	
2	10/29/70	CRYOGENICS	5	5/27/71	QUALITY AND RELIABILITY ASSURANCE	
3	11/19/70	INSTRUMENTATION				

\*Classified Proceedings not published

\*\*Proceedings summarized only.

Correspondence concerning the Research Achievements Review Series should be addressed to:  
Research Planning Office, S&E-R, Marshall Space Flight Center, Alabama 35812